



HAL
open science

Study of PVDF derivatives for actuation purpose

Pierre Lheritier

► **To cite this version:**

Pierre Lheritier. Study of PVDF derivatives for actuation purpose. Polymers. Université Grenoble Alpes, 2018. English. NNT : 2018GREAI070 . tel-02963638

HAL Id: tel-02963638

<https://theses.hal.science/tel-02963638>

Submitted on 11 Oct 2020

HAL is a multi-disciplinary open access archive for the deposit and dissemination of scientific research documents, whether they are published or not. The documents may come from teaching and research institutions in France or abroad, or from public or private research centers.

L'archive ouverte pluridisciplinaire **HAL**, est destinée au dépôt et à la diffusion de documents scientifiques de niveau recherche, publiés ou non, émanant des établissements d'enseignement et de recherche français ou étrangers, des laboratoires publics ou privés.

THÈSE

Pour obtenir le grade de

DOCTEUR DE LA COMMUNAUTÉ UNIVERSITÉ GRENOBLE ALPES

Spécialité : MEP : Mécanique des fluides Energétique, Procédés

Arrêté ministériel : 25 mai 2016

Présentée par

Pierre LHERITIER

Thèse dirigée par **Gérard GEBEL**, Ingénieur CEA

préparée au sein du **Laboratoire CEA LITEN
Grenoble/DTNM/SENCI/LCEI**
dans l'**École Doctorale I-MEP2 - Ingénierie - Matériaux,
Mécanique, Environnement, Energétique, Procédés,
Production**

Etude des dérivés du PVDF pour l'actuation

Study of Polyvinylidene Fluoride Derivatives for Actuation

Thèse soutenue publiquement le **9 octobre 2018**,
devant le jury composé de :

Monsieur GERARD GEBEL

DIRECTEUR DE RECHERCHE, CEA GRENOBLE, Directeur de thèse

Monsieur LIONEL PETIT

PROFESSEUR, INSA LYON, Rapporteur

Monsieur DANICK BRIAND

MAITRE DE RECHERCHE ET D'ENSEIGNEMENT, EPFL SUISSE,
Rapporteur

Monsieur SKANDAR BASROUR

PROFESSEUR, UNIVERSITE GRENOBLE ALPES, Président

Monsieur EMMANUEL DEFAY

INGENIEUR DE RECHERCHE, LUXEMBOURG INSTITUTE OF
SCIENCE & TECH., Co-directeur de thèse

Monsieur PAOLO BONDAVALLI

INGENIEUR DE RECHERCHE, THALES RECHERCHE ET TECH. A
PALAISEAU, Examineur



Contents

1	PVDF based polymers and their applications	9
1.1	PVDF	10
1.2	Electroactive materials	12
1.3	PVDF in the scientific landscape	14
1.4	Applications	19
1.5	Conclusion	23
2	Performances as actuators	27
2.1	State of the art	28
2.1.1	Electromechanical formalism	28
2.1.2	Copolymer	30
2.1.3	Terpolymer	31
2.2	Experimental	34
2.2.1	Preparation	34
2.2.2	Characterization	36
2.2.3	First experiments	38
2.3	Impact of the CTFE content	42
2.3.1	Electrical evolution	43
2.3.2	Mechanical evolution	46
2.4	Performances as actuator	47
2.4.1	Mechanical performances	47
2.4.2	Electrical energy and coupling efficiency	53
2.4.3	Scope of the comparative study	56
2.5	Conclusion	58
3	Origin of strain in P(VDF-TrFE) and P(VDF-TrFE-CTFE)	63
3.1	Polymers under low electrical field	64
3.1.1	Leakage measurements	64
3.1.2	Permittivity and dielectric losses	66
3.1.3	Making use of the raw data	69

3.2	Transition to high electrical fields	73
3.2.1	Copolymer	73
3.2.2	Terpolymer	75
3.3	Strain	82
3.3.1	In terpolymers	83
3.3.2	Copolymer and ferroelectric terpolymers	89
3.3.3	Origin of butterfly shape in copolymer	93
3.3.4	Isolated domain hypothesis	95
3.3.5	Combined descriptions	98
3.4	Conclusion	99
4	In-situ structural study	105
4.1	Experiments	106
4.2	In-situ study of P(VDF-TrFE)	108
4.2.1	State of the art: structure and XRD characterization	108
4.3	Copolymer	113
4.3.1	Results	113
4.3.2	Discussion	114
4.4	P(VDF-TrFE-CTFE) in-situ study	119
4.4.1	State of the art	119
4.5	Terpolymers	122
4.5.1	Ambient temperature	122
4.5.2	At higher temperatures	128
4.6	Conclusion	133
5	Discussion	137
5.1	Follow up work on P(VDF-TrFE-CTFE)	138
5.1.1	Φ scans	138
5.1.2	Clamping effect	139
5.1.3	Macroscopic approach	140
5.2	Other polymers	143
5.3	Conclusion	144

List of Abbreviations

DHL Double hysteresis loop

EAP Electroactive polymers

FE Ferroelectric

FT Ferroelectric terpolymer ($< 7:8\%$ CTFE)

P(VDF-TrFE) Poly(vinylidene fluoride-trifluoroethylene)

P(VDF-TrFE-CFE) Poly(vinylidene fluoride-trifluoroethylene-chlorofluoroethylene)

P(VDF-TrFE-CTFE) Poly(vinylidene fluoride-trifluoroethylene-chlorotrifluoroethylene)

PE Paraelectric

PEDOT:PSS poly(3,4-ethylenedioxythiophene) polystyrene sulfonate

PEN Polyethylene naphthalate

PVDF Polyvinylidene fluoride

PZT Lead zirconate titanate ceramic

RFE Relaxor Ferroelectric

RT Relaxor terpolymer ($> 7:8\%$ CTFE)

XRD X-ray diffraction

Acknowledgments

First I want to thank my supervisor Emmanuel Defay for his guidance over these past years. It is thanks to our numerous discussions that I have been able to train my critical mind and grasp what it means to be a scientist. Then, I want to thank Nicolas Vaxelaire for the all work he did with me on the XRD study. For all the knowledge I got from him but also for his endless patience and enthusiasm.

I would also like to thank Fabrice Domingues Dos Santos of Piezotech for providing the materials studied, for his support and his pragmatic advice along the way. Thanks to Sylvie Giraut and Francois Bargain of Arkema for their help and the fruitful discussions about polymers.

Thank you to all the people who helped me at any point during the thesis, whether by lending me a hand or giving insightful remarks: Sebastien Noel, Amelie Revaux, Julien Routin, Marine Galliari, Antoine Latour, Magalie Gasiglia, Mickael Charbonneau. For the good times and the memories we made in the laboratory I want to thank Clara Haddad, Alexandre gaitis, Julie Euvrard, Tamara Nunes-Domschke, Smail Amari, Jamal Tallal, Michael Bouvier and Alexandra Cantarano.

I am very grateful to you, Aurore, for having bore with me and supported me during both good and bad times. You made these past years so much happier and I cannot thank you enough. And finally I want thank my beloved parents, to whom I owe everything.

Introduction

With the advent of new technologies, organic electronic is becoming an increasingly attractive research field. It is already exploited to make OLED TVs as well as various sensors and actuators. Due to the general enthusiasm for these applications, a lot of prototypes and patents are presented every day. Yet, it is difficult to discern how organic materials fare against one another or even against 'traditional' ceramics. To this day the main advantage of polymeric materials is considered to be the possibility to produce flexible devices, with cheaper fabrication processes based on printing techniques.

In partnership with Piezotech who provides the electroactive polymers, our laboratory at CEA-LITEN is focused on the development of fully printed organic devices, like sensors and actuators. Functional prototypes are developed as part of European projects or to meet the requests of industrial partners. Besides proofs of concept for new applications, the underlying objective of our research is to further improve the devices performances. There are several possible approaches to achieve that goal and among them, the selection of the most suitable polymer as active layer. As part of this project, our first objective is to evaluate which materials and compositions are best suited for the production of fully printed devices. The following step is trying to understand the physical strain mechanisms in our polymers, and thus provide directions for the development of new electroactive materials.

Chapter I is a general introduction to electroactive properties, their origin and their use in commercial applications. Different types of materials are presented and among them the focus of our study, polyvinylidene fluoride (PVDF) derivatives. The comparison with ceramics provides a good opportunity to determine how polymers can be attractive in a market overwhelmingly dominated by inorganic materials. We identified poly(vinylidene fluoride-trifluoroethylene) P(VDF-TrFE) and poly(vinylidene fluoride-trifluoroethylene-chlorotrifluoroethylene) P(VDF-TrFE-CTFE) as polymers of particular interest for actuation based applications.

Chapter II is a comparative study of polymers performances once embedded in thin films actuators. The influence of CTFE content on the behavior of polymers is characterized for nine different compositions. The electromechanical responses are evaluated in regard of two figures of

merit: cantilever deflection and energy cost. As it turns out, there is no ideal composition and the suitability of a given polymer depends on the prioritizing order between performance and energy consumption.

This study highlights the difficulty of comparing polymers because of their differences in electromechanical responses. To understand the origin of these disparities, Chapter III is focused on their strain-polarization relationship. Deviations from the standard electrostrictive formalism are approached as opportunities to isolate the physical mechanisms at hand. Based on the results, a phenomenological description of strain mechanisms is proposed for both copolymers and terpolymers. In order to strengthen the terpolymer strain model, the following chapter is focused on experimental validation, mostly with the help of in-situ XRD measurements.

In chapter 4 we start the study with copolymer, where the impacts of field-induced phase transition and electrostriction can be observed separately. The case of terpolymers proved to be more complex with several effects taking place simultaneously. This study evidenced the link between the structural changes in the crystalline phase and the nonlinear response of terpolymers. Confronting the XRD data to existent models from the literature, we proposed an improved description of the dipolar order inside the polymer chains.

In order to go further and build on the results presented here, chapter 5 discusses different paths of interest. The study on P(VDF-TrFE-CTFE) can be continued with both XRD and electromechanical follow-up measurements. We also present the results of preliminary measurements made on another class of polymers: P(VDF-TrFE-CFE). By relying on the framework laid out here, it would be possible to produce similar results on these polymers and further extend the comparison.

Chapter 1

PVDF based polymers and their applications

This first chapter aims at explaining the interest for polyvinylidene-fluoride (PVDF) and its derivatives. This introduction is a mere overview of the polymers nature and applications, their properties will be detailed in the following chapters.

1.1 PVDF

PVDF is a semi-crystalline polymer of formula $(C_2F_2H_2)_n$. It possesses remarkable properties such as a strong resistance to corrosion, low reactivity to most chemical products and a high mechanical resistance. For those reasons, it is commonly found in industry to coat chemical tanks and pipes. The pie chart displayed below is taken from [1] and represents the annual production of fluorine based polymer as of year 2012.

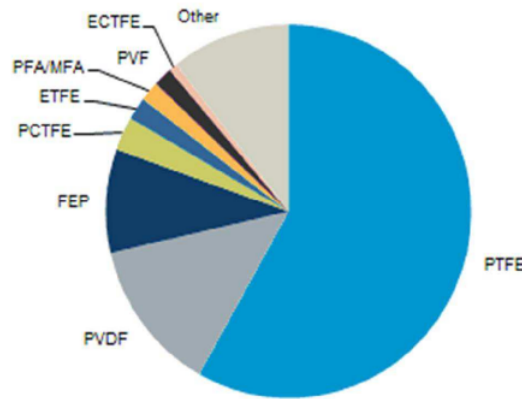


Figure 1.1: Production of fluorinated polymers in 2012 [1]

PTFE, often know as TEFLON is by far the most commercialized fluorinated polymer. PVDF comes in second and its production volume is expected to double by the year 2022. PVDF mechanical and chemical features are the main reasons behind these numbers but its electroactive properties are what we are interested in here. Indeed, PVDF can be ferroelectric depending on which phase it crystallizes on. Whether PVDF possesses electroactive properties or not is entirely dependent on the polymer chains conformation inside the crystalline phase. The three most common phases, called α , β and γ are pictured in figure 1.2. This is taken from a review on the different PVDF fabrication and characterization methods, [2]. There exists a fourth phase called δ that is not represented in figure 1.2, most likely because it is the less common form of PVDF.

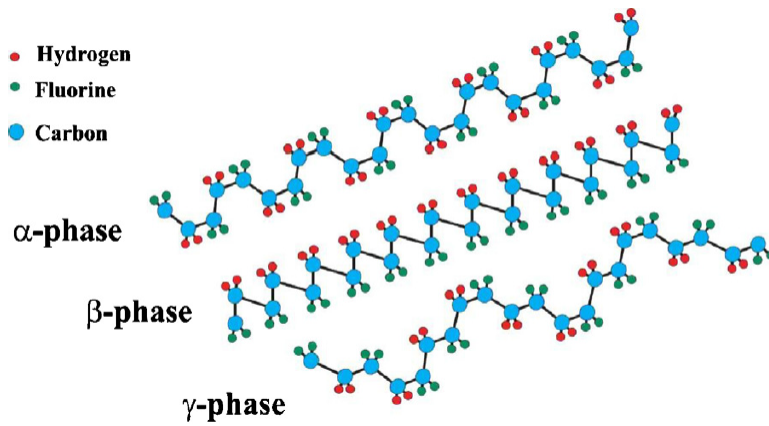


Figure 1.2: Representation of the α , β and γ phases of PVDF [2]

The α phase is the most stable one when the polymer is processed at ambient pressure. Unfortunately, this is the one phase that does not possess ferroelectric properties. This can be inferred from figure 1.2 by looking at the positioning of carbon and fluorine atoms. The CF_2 strong dipolar moments cancel each other in the α chain because of their opposite orientations. In other phases, these moments add up and grant its ferroelectric properties to PVDF. This effect is maximized in the β phase which is the phase sought after in electroactive devices.

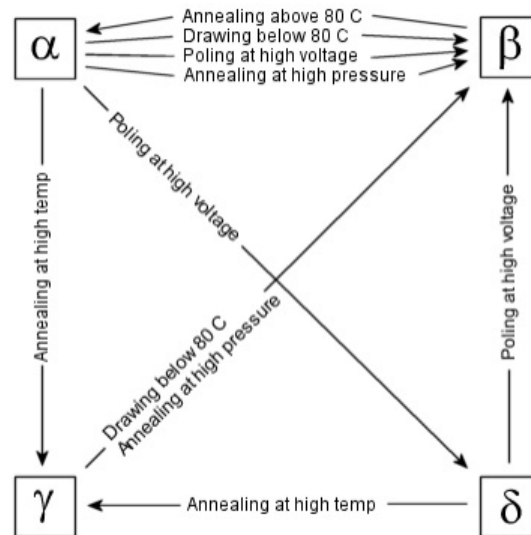


Figure 1.3: Experimental process to obtain the different phases of PVDF []

Figure 1.3 displays the available paths to obtain the different phases of PVDF. Among the possibilities, the most common way is the mechanical drawing of the PVDF film, several times its initial length. The major drawback of this technique is its incompatibility with thin film tech-

nologies due to the presence of a substrate. A solution to that particular issue is to copolymerise PVDF with trifluoroethylene (TrFE) to favour the β form directly. The structure of this polymer will be detailed in chapter 4 and before anything else we need to understand why obtaining ferroelectric properties is worth the effort.

1.2 Electroactive materials

Figure 1.4 illustrates the categories of electroactive materials and their links to one another.

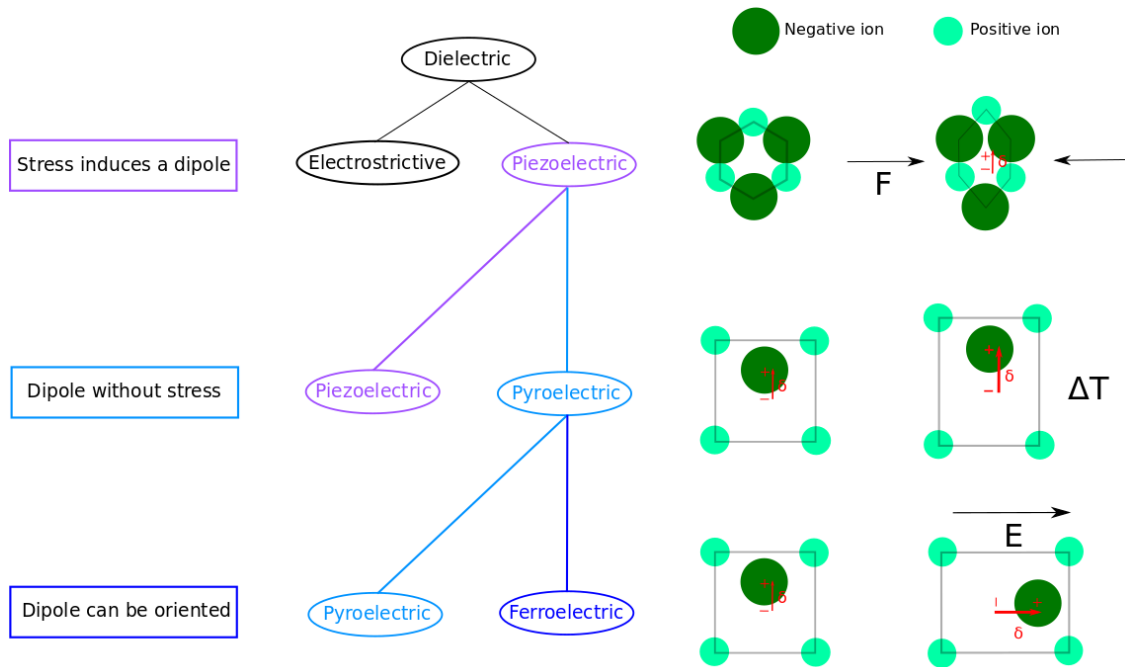


Figure 1.4: Schematic representation of the electroactive materials categories.

A dielectric material is an insulator, its quality as a dielectric depends on its insulation properties but also on its polarizability. Electrically speaking, this means a good dielectric makes a capacitor with a high capacitance value and no leakage current.

As charges are displaced with the application of an electrical field, the material will be strained ever so slightly; this property is referred to as electrostriction. Electrostriction is negligible in the vast majority of dielectrics with a few exceptions such as $Pb(Mn_{1/3}Nb_{2/3})O_3$ or poly(vinylidene fluoride-trifluoroethylene-chlorotrifluoroethylene) P(VDF-TrFE-CTFE).

Among the different materials, a few ones such as quartz display piezoelectric properties. The piezoelectric effect arises from the crystalline lattice symmetry and its occurrence can be inferred based on the crystal classes [3]. In these particular structures, the application of a stress will sep-

arate the positive and negative charge centroids and therefore generate a dipolar moment. The apparition of those dipoles in the crystal will result in the generation of charges at the electrode and this mechanism is called the direct piezoelectric effect. The opposite mechanism, referred to as converse effect corresponds to a lattice strain induced by the application of an electrical field.

There are twenty crystal classes with piezoelectric properties and half of them are also pyroelectric. A pyroelectric material possesses a dipolar moment even before the application of any electrical bias or mechanical stress. As a consequence, a temperature variation will result in the generation of electrical charges, the so-called pyroelectric effect. This is represented in fig 1.4 with an example where the cation is not located in the lattice centre and thus is separated from the negative charge centroid. Such material is also piezoelectric because the application of a mechanical stress will necessarily change the dipole amplitude and therefore induce a charge displacement.

With a pyroelectric material, the dipolar moments might be oriented through the application of an electrical field. This is not always the case because dipoles are not isolated but constrained in a crystalline structure. If they can align with the electrical field, the material is referred to as ferroelectric. Naturally, a ferroelectric material will possess both piezoelectric and pyroelectric properties.

There are two main categories of materials falling into the classification described in figure 1.4. The first family is comprised of ceramics which are inorganic compounds and often contain heavy metals. The other category is that of electroactive polymers (EAP), separated into two sub-classes: the ionic and the electronic families. We summed up in table 1.1 some key properties in each category.

	Ceramics	EAP	
		Ionic	Electronic
Advantages	Low actuation voltage	Low actuation voltage	Fabrication process
	High stress	High strain	Medium stress
Drawbacks	Brittle	Low stress	High actuation voltage
	High acoustic impedance	Slow response	
Material	PZT	Polyacrylonitrile	PVDF

Table 1.1: Advantages and drawbacks of the different electroactive materials categories.

The ceramics are capable of producing the highest levels stress when submitted to an electrical field. The ionic EAPs can reach the highest levels of strain, often at the cost of a very low rigidity. The electronic family to which PVDF belongs, does not reach the highest strain nor stress values and their main advantage is the fabrication process. They can be printed quickly and cheaply, onto large surfaces and on flexible substrates. These are just a few elements of comparison, a thorough analysis between different EAPs can be found in [4].

Besides strain and stress, other parameters such as the time response or acoustic impedance can be determining factors in the choice of a given electroactive material. In that regard, their respective features can be seen as complementary, each material being better suited to one particular application. This is a recurring argument in most comparative studies found in the literature. Yet, the industrial market for actuators is overwhelmingly dominated by piezoceramics despite the promising potential of EAPs in general, and PVDF in particular. In order to assess if PVDF is still a "promising" material 50 years after its discovery [5], we conducted a bibliometric study on the last three decades.

1.3 PVDF in the scientific landscape

Interest over the years

Figure 1.5 displays the results to the query 'PZT' and 'PVDF' in the scopus database. It is presented as the number of annual publications between the year 1990 and 2017.

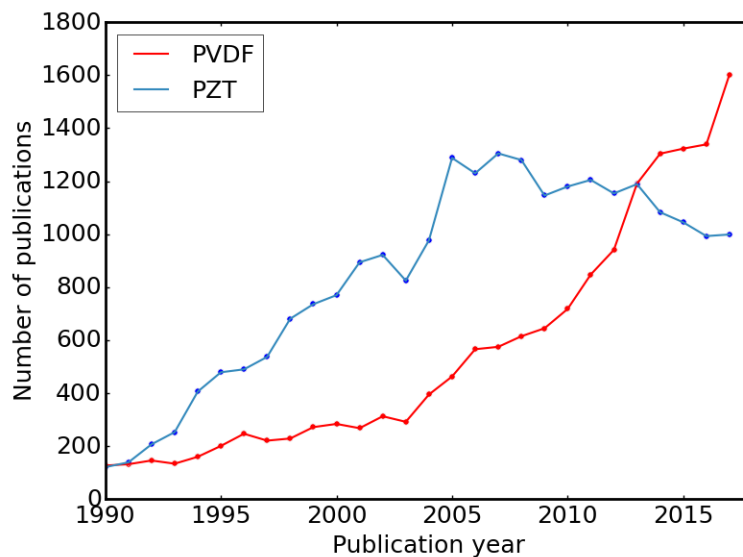


Figure 1.5: Number of publications per year containing the key-word PZT and PVDF. Source: scopus

The publication volume on PVDF increased dramatically over the past 30 years and this trend is still in the ascending phase. To put this evolution into perspective, we represented the number of annual publications on PZT, the most common piezoceramics in industry. If we just consider these data, there seems to be a real paradigm shift, with PVDF potentially revealing itself as the piezoelectric material of the future. However as mentioned before, PVDF also has remarkable chemical properties which could also be the reason behind that renewed interest. To uncover the actual motivations, 4000 publications between 2016 and 2018 were analyzed with VOSviewer. This software analyses results from a scientific database and forms clusters to highlight the different topics of interest. The resulting graph is displayed in figure 1.6.

It appears that PVDF has three main areas of interest with few links to one another. The red cluster corresponds to publications focused on the use of PVDF as a membrane, it is the most prolific topic at the moment. The main application is water treatment and the key properties are chemical resistance and mechanical strength [6].

The green cluster corresponds to the use of PVDF in batteries. For that application, PVDF is used as a solid electrolyte and the key property is its ionic conductivity. To improve its efficiency, PVDF is often copolymerized with hexafluoropropylene to form P(VDF-HFP).

The third cluster is divided into two sub-clusters: yellow and blue. The yellow one corresponds to PVDF electrical properties and the related applications. For an organic material PVDF has a high permittivity, which makes it an interesting candidate for organic capacitors and transistors.

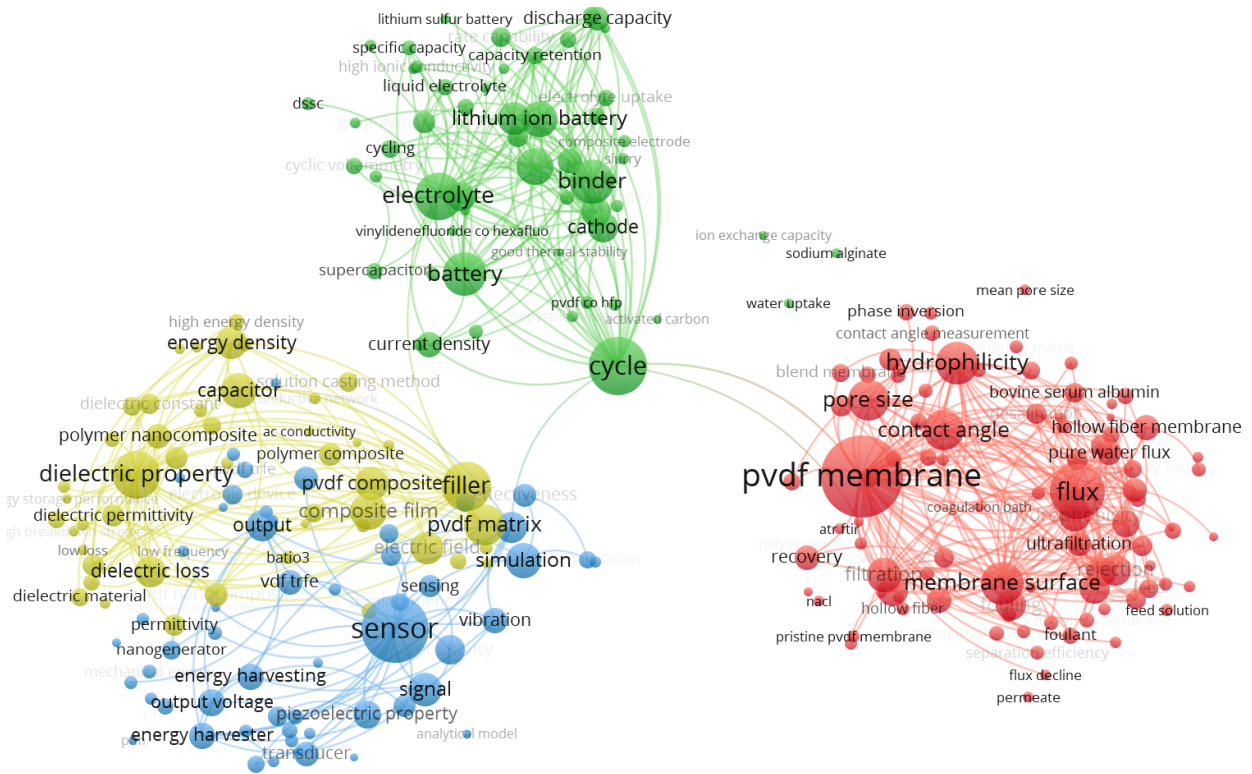


Figure 1.6: VOSviewer analysis of the publication on PVDF for the years 2016, 2017 and 2018. The algorithm displays clusters based on occurrence of terms in title and abstract

The notions of fillers, matrix and composite materials occur frequently in that cluster because the inclusion of conducting particles in a PVDF matrix is a promising road towards organic materials with a high dielectric constant.

The blue cluster corresponds to the piezoelectric properties and their applications, such as sensor, transducer, or energy harvester. It is close to the yellow cluster because piezoelectricity is intrinsically linked to the material electrical properties. This is the area of interest for us but, as displayed in fig 1.6, only a minor topic among the different fields of application.

It turns out the infatuation over PVDF is largely driven by its use as a membrane and not its electroactive properties. In order to make the comparison with PZT more relevant we narrowed down the query to P(VDF-TrFE). The advantage of P(VDF-TrFE) over the pristine PVDF is that it is ferroelectric without the need for mechanical stretching. It is more expensive than PVDF and not of any use in membranes or batteries. The only reason to use it is as a ferroelectric material in thin films devices. Figure 1.7 displays the corresponding publication volumes.

The amount of publications on P(VDF-TrFE) is about 10% that of PVDF and the increase

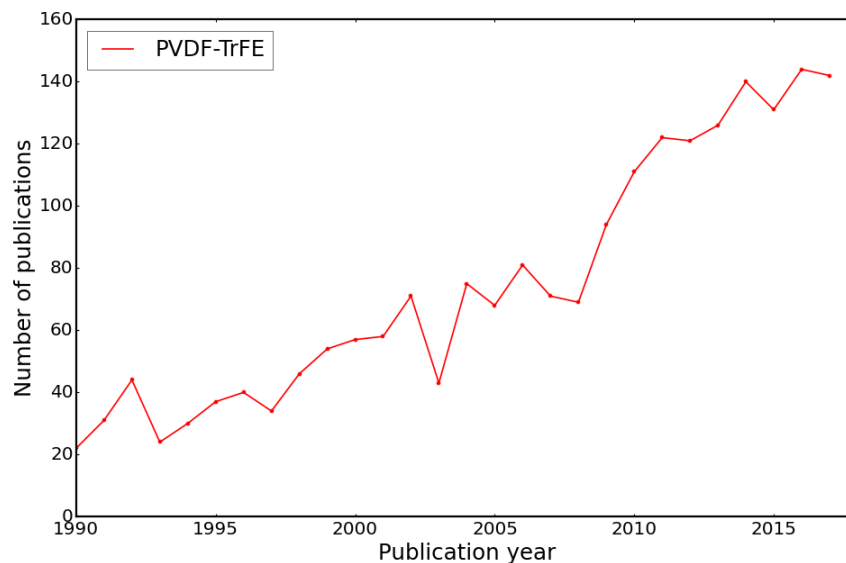


Figure 1.7: Number of publications per year containing the keyword PVDF-TrFE. Source: scopus

over time is milder. However, there is also a growing interest for this material and therefore the use of PVDF electroactive properties. This is not the piezoelectric revolution hinted by the trend in figure 1.5 but it most likely means that PVDF can be used in applications where the current piezoceramics have found their limits. A few possibilities regarding the advantages of polymers over ceramics are listed below.

The first one is on the side of environment and health issues as PZT contains toxic metals such as lead. Over the last few years, lead-free ceramics have been the focus of several scientific studies and PVDF is even more environmentally friendly than most of the other alternatives. This trend in eco-friendly materials grew during the mid-00's, suggesting that it is a possible factor behind the renewed interest in P(VDF-TrFE).

The second edge PVDF based device have over ceramics is the possibility of making fully printed flexible devices. The corresponding fabrication processes are usually quick and cheap [7]. Furthermore, the flexibility of the overall device can help generate strains that could not be achieved on rigid substrates such as glass or silicon. The need for flexible devices is also related to the emergence of new technologies such as 'smart' textiles [8] or artificial muscles [9].

These advantages can help P(VDF-TrFE) finding markets in the future, but in order to increase those odds the main drawback of copolymers must also be addressed. This issue is, as displayed in table 1.1, the lower levels of stress polymers can generate compared to ceramics. In attempts to bridge that gap, new polymers have been developed over the past two decades.

Most of these polymers are P(VDF-TrFE) derivatives and they appear as promising candidates to replace the copolymer but their electromechanical properties are still largely undocumented.

P(VDF-TrFE) derivatives

The first copolymer derivative to be studied was an irradiated sample [10]. After receiving the proper dosage, P(VDF-TrFE) exhibits a large electrostrictive strain although it comes at the cost of its ferroelectric properties [11]. In order to reach similar levels of strain but without the need to irradiate polymers, a third monomer was introduced in the polymer chain. This third monomer can be either chlorofluoroethylene (CFE) [12] or chlorotrifluoroethylene (CTFE) [13]. Other attempts with different monomers proved to be unsuccessful [14].

The raw formula of P(VDF-TrFE-CTFE) is represented fig 1.8. This is just a brief introduction on these terpolymers, and their properties will be detailed in the following chapters.

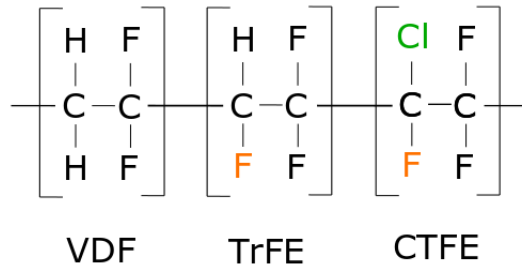


Figure 1.8: Structural formula of P(VDF-TrFE-CTFE)

With this additional compound the polymer loses its ferroelectric nature, and consequently its piezoelectric and pyroelectric properties. Like irradiated copolymers, terpolymers exhibit very large deformations, up to several times that of copolymer.

Terpolymers date back to 2001 but more recently they have been used as a base to form new electrostrictive materials. For example, Capsal & al added a DEHP plasticizer and significantly enhanced the electromechanical performances at low frequencies [15]. P(VDF-TrFE-CFE) has also been blended with P(VDF-CTFE) [16] or used as a matrix for carbon black nanocomposite [17]. Overall, there are several proofs of concept and theoretical models promising new improved performances for electroactive polymers. However, their interest once embedded in an actual device is still unclear, mostly because their high strain comes with a lower rigidity. Besides questions about their performances, the physical understanding of strain mechanisms in these polymers is lacking and it seems unlikely that the behaviour of blends or nanocomposites can be fully explained

if the polymer matrix itself remains a mystery. For that reason we chose P(VDF-TrFE-CTFE) as the focus of this work. The other polymer family P(VDF-TrFE-CFE) also deserves its own study but we focused our efforts on CTFE because its fabrication process is less expensive, making it a potentially better material from an industrial perspective.

1.4 Applications

In this section we present a few examples to illustrate the different uses of thin film PVDF based devices.

Sensors

With the ability to generate charges under stress, a piezoelectric material can be used as strain gauge or pressure sensor. If it is pyroelectric, it can also be used to detect temperature variations. Figure 1.9 displays two functional sensor prototypes exploiting these properties.

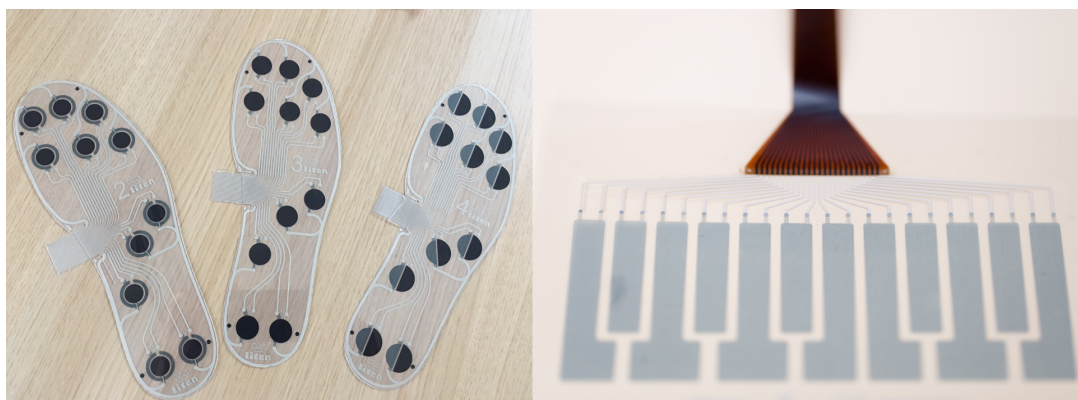


Figure 1.9: Left: soles with embedded piezoelectric and piezoresistive sensors. Right: prototype for an electric piano keyboard

The two devices in fig 1.9 were fabricated using a screen printing technique (fig 2.4) and P(VDF-TrFE) as active layer. The white lines are made of conducting silver ink and the blue color is due to poly(3,4-ethylenedioxythiophene) polystyrene sulfonate (PEDOT:PSS), a conducting polymer used to make the electrodes. The left picture prototypes are soles with piezoelectric and piezoresistive captors, to detect and quantify the distribution of weight inside a foot. The right picture device was designed to reproduce a piano keyboard pattern. When pressing a key, charges will be generated and detected by an electronic circuit that will play the corresponding sound. This sensor exploits both the piezoelectric and the pyroelectric effect with the combined heat and pressure of the user's finger. The pyroelectric properties of PVDF and copolymers also allow for the detection of heat sources without direct contact and they can be used as infrared

sensors [18].

This application of electroactive polymers as sensors is only accessible to PVDF and P(VDFTrFE) copolymers. Terpolymers are not ferroelectric nor do they possess piezoelectric properties, this makes them unable to gather charges in a similar fashion.

Energy harvesting

The piezoelectric effect can also be used for energy harvesting. The aim is to exploit mechanical motions such as vibrations to convert them into electrical energy.

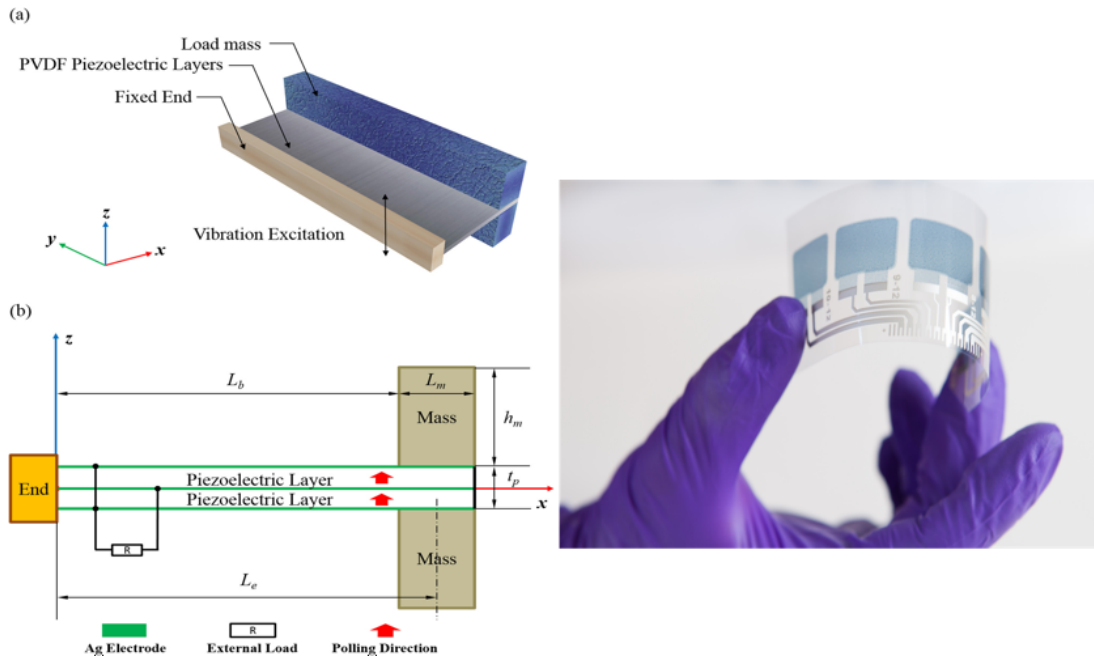


Figure 1.10: Left: Structure developed for a PVDF based piezoelectric harvester, taken from [19]. Right: illustration of a simple yet effective way to generate large strains inside the polymer

The left picture in figure 1.11 is taken from [19], recently published. The structure was designed to use PVDF as the active layer to harvest energy. In that domain, PVDF could hope to compete with piezoceramics because large strains can be easily reached in the active layer. This is illustrated with the picture of one of our samples displayed in the right panel. A large strain of the entire device can be achieved with a mild movement of the two fingers. This is a much more efficient approach than applying pressure vertically, as we should have done had the substrate been made of silicon.

Despite the lack of piezoelectricity, it is also possible to harvest energy with terpolymers. The sample must be stressed electrically and mechanically according to the following cycle, taken from

[20].

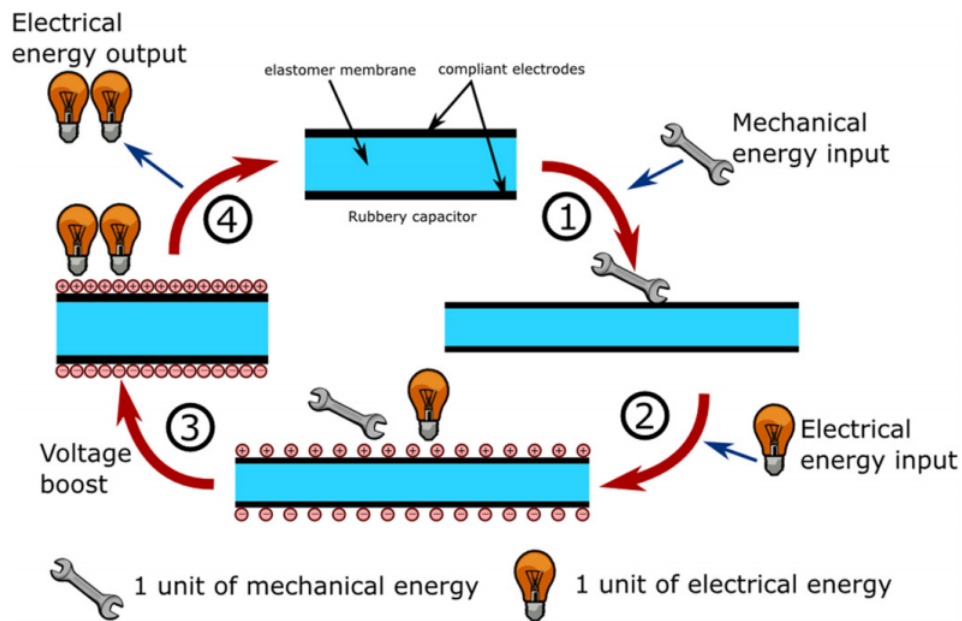


Figure 1.11: Electromechanical cycle required to harvest energy with an elastomer [20]

Figure 1.11 displays the cycle required to harvest energy with a non piezoelectric material. P(VDF-TrFE-CFE) terpolymers can be used that way and have proven to be good candidates for such applications [21]. The theoretical figures of merit of these generators are higher than those of piezoelectric materials, but the need to function with an applied bias can be a significant drawback. Because of the mechanical stretch step, terpolymers cannot be deposited onto a substrate and this application is not compatible with thin film devices.

Actuation

Actuation uses the converse piezoelectric effect or the electrostrictive effect. The strain responses are different but in both cases it comes down to an electric potential changing the polymer dimensions. If the layer is deposited onto a substrate, the entire device will be bent, as displayed in figure 1.12.

The device on the right part of figure 1.12 is a 1.3 cm long cantilever under an electric potential of 100V. The substrate is $125\mu\text{m}$ thick and the active layer is $2\mu\text{m}$ thick. To maximize the deflection, up to 20 capacitors (40 layers) were stacked and the resulting deflection is visible with the naked eye.

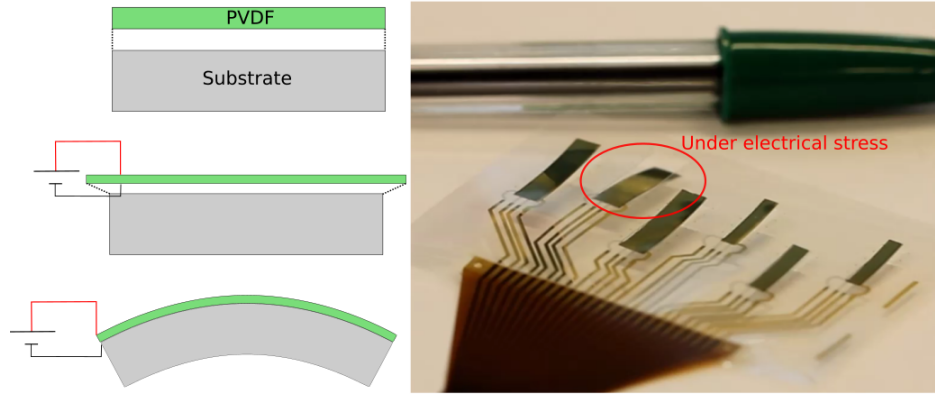


Figure 1.12: Left: Principle of an actuator. Right: fully printed actuator, with and without electrical bias

Among the three domains of applications presented above, actuation is the only one where copolymers and terpolymers can be compared directly. For this reason, actuation was chosen as the application of reference in the following study.

Other applications

The P(VDF-TrFE) based terpolymers can also be employed in others applications with no link to their electrostrictive properties. Two main domains of applications fall into that category, their use as gate dielectric in organic transistors [22] and as electrocaloric material in cooling devices.

In 2008, Neese & al discovered the large electrocaloric effect (ECE) of PVDF-TrFE-CFE near room temperature [23]. From an engineering point of view, ECE is the opposite of the pyroelectric effect. It is the ability to generate a change in temperature with the application of an electrical field. From a physical point of view, ECE and pyroelectricity are not two sides of the same coin and the large ECE of P(VDF-TrFE-CFE) has no pyroelectric counterpart. Figure 1.13 is an example of what the electrocaloric effect of terpolymers can achieve.

The variations of temperature in this polymer can reach 12K for an electrical field of $300MV.m^{-1}$. Recently a functional device using ECE has been fabricated with P(VDF-TrFE-CFE) as active material. Fig 1.13 taken from [24], displays an experiment in which the test battery was cooled by $8^{\circ}C$ under an applied electrical field of $68MV.m^{-1}$. In the future, terpolymers might very well find their use as electrocaloric materials and not for what they were invented for in the first place.

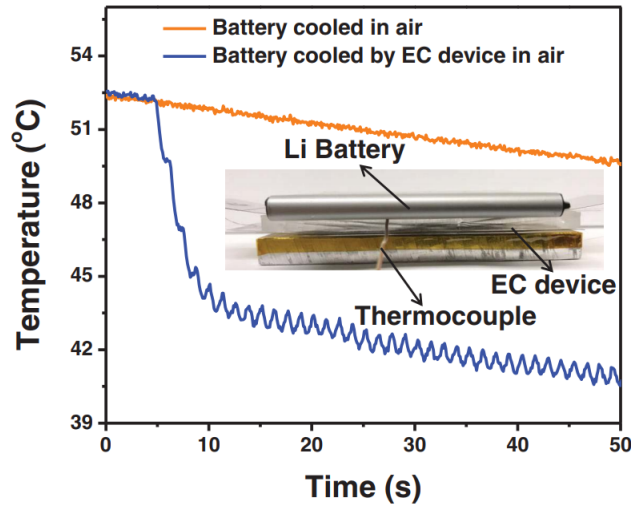


Figure 1.13: Demonstration of a functioning electrocaloric cooler using PVDF-TrFE-CFE as active material. Taken from [24]

1.5 Conclusion

PVDF is a ferroelectric polymer and therefore possesses piezoelectric and pyroelectric properties. The ferroelectric order is not occurring naturally and the polymer films need to be stretched. This is not compatible with thin film devices and fully printed technologies. The most practical way around this limitation is the addition of TrFE in the polymer chain. This makes of P(VDFTrFE) the ideal material for thin film applications such as sensors, energy harvesters or actuators.

The ferroelectric properties of PVDF have been known since 1969 but ceramics have supplanted electroactive polymers in industry ever since. Interestingly, PVDF is now the focus of more academic research than PZT, the most common piezoceramic. It turns out that most of the activity in this field is focused on the use of PVDF as a membrane for water treatment. Still, the interest for electroactive applications is also growing. The most likely explanation for this new-found enthusiasm is the search for lead-free alternative to PZT as well as the possibility of printing flexible devices.

The main issue with polymers remains their lower intrinsic performances compared to piezoceramics. In efforts to reduce that gap, new formulations have been developed such as P(VDFTrFE-CTFE) terpolymers. These materials lose their ferroelectric properties with the addition of the third monomer but becomes significantly more electrostrictive in return. There are several proofs of concepts and even derivated formulations making this material potentially interesting. Yet, it is still unclear whether terpolymers are more suited than P(VDF-TrFE) for practical purposes.

Actuation is the one application where the polymers performances can be directly compared to one another. The following chapter is a comparative study between P(VDF-TrFE) and P(VDF-TrFE-CTFE) based devices, to assess the interest of using terpolymers in thin film actuators. The emphasis will be put on the influence of CTFE content on the actuator response.

Bibliography

- [1] Ameduri Bruno Michel. Fluoropolymers: the right material for the right applications. *Chemistry - A European Journal*, 0(ja), 2018.
- [2] P. Martins, A. C. Lopes, and S. Lanceros-Mendez. Electroactive phases of poly(vinylidene fluoride): Determination, processing and applications. *Progress in Polymer Science*, 39(4):683–706, April 2014.
- [3] E.Defay. Integration of Ferroelectric and Piezoelectric thin films. In *Integration of Ferroelectric and Piezoelectric thin films*. WILEY, 2011.
- [4] Claire Jean Mistral. *Recuperation d'energie mecanique par polymeres electroactifs pour microsystemes autonomes*. Thesis, INSA Lyon, January 2009.
- [5] Heiji Kawai. The piezoelectricity of poly (vinylidene fluoride). *Japanese Journal of Applied Physics*, 8(7):975, 1969.
- [6] Fu Liu, N. Awanis Hashim, Yutie Liu, M.R. Moghareh Abed, and K. Li. Progress in the production and modification of pvdf membranes. *Journal of Membrane Science*, 375(1):1 – 27, 2011.
- [7] S. Khan, L. Lorenzelli, and R. S. Dahiya. Technologies for printing sensors and electronics over large flexible substrates: A review. *IEEE Sensors Journal*, 15(6):3164–3185, June 2015.
- [8] C.A. Hewitt, A.B. Kaiser, S. Roth, M. Craps, R. Czerw, and D.L. Carroll. Multilayered carbon nanotube/polymer composite based thermoelectric fabrics. *Nano Letters*, 12(3):1307–1310, 2012. cited By 162.
- [9] Jun Lu, Sang-Gyun Kim, Sunwoo Lee, and Il-Kwon Oh. A biomimetic actuator based on an ionic networking membrane of poly(styrene-alt-maleimide)-incorporated poly(vinylidene fluoride). *Advanced Functional Materials*, 18(8):1290–1298, 2018.
- [10] Q. M. Zhang, Vivek Bharti, and X. Zhao. Giant Electrostriction and Relaxor Ferroelectric Behavior in Electron-Irradiated Poly(vinylidene fluoride-trifluoroethylene) Copolymer. *Science*, 280(5372):2101–2104, June 1998.

- [11] C. Huang, R. Klein, Feng Xia, H. Li, Q.M. Zhang, F. Bauer, and Z.Y. Cheng. Poly(vinylidene fluoride-trifluoroethylene) based high performance electroactive polymers. *IEEE Transactions on Dielectrics and Electrical Insulation*, 11(2):299–311, April 2004.
- [12] F. Bauer, E. Fousson, and Q.M. Zhang. Recent advances in highly electrostrictive P(VDF-TrFE-CFE) terpolymers. *IEEE Transactions on Dielectrics and Electrical Insulation*, 13(5):1149–1154, October 2006.
- [13] Haisheng Xu, Z.-Y. Cheng, Dana Olson, T. Mai, Q. M. Zhang, and G. Kavarnos. Ferroelectric and electromechanical properties of poly(vinylidene-fluoride–trifluoroethylene–chlorotrifluoroethylene) terpolymer. *Applied Physics Letters*, 78(16):2360–2362, April 2001.
- [14] François Bargain, Thibaut Soulestin, Fabrice Domingues Dos Santos, Vincent Ladmiral, Bruno Améduri, and Sylvie Tencé-Girault. Semicrystalline organization of vdf- and trfe-based electroactive terpolymers: Impact of the trans-1,3,3,3-tetrafluoropropene termonomer. *Macromolecules*, 50(8):3313–3322, 2017.
- [15] Jean-Fabien Capsal, Jeremy Galineau, Minh-Quyen Le, Fabrice Domingues Dos Santos, and Pierre-Jean Cottinet. Enhanced electrostriction based on plasticized relaxor ferroelectric P(VDF-TrFE-CFE/CTFE) blends. *Journal of Polymer Science Part B: Polymer Physics*, 53(19):1368–1379, October 2015.
- [16] L.J. Gorny, Sheng-Guo Lu, Sheng Liu, and Minren Lin. Electromechanical properties of relaxor ferroelectric P(VDF-TrFE-CFE)-P(VDF-CTFE) blends. *IEEE Transactions on Ultrasonics, Ferroelectrics, and Frequency Control*, 60(3):441–445, March 2013.
- [17] Xunqian Yin, Jean-Fabien Capsal, and Daniel Guyomar. A comprehensive investigation of poly(vinylidene fluoride-trifluoroethylene-chlorofluoroethylene) terpolymer nanocomposites with carbon black for electrostrictive applications. *Applied Physics Letters*, 104(5):052913, February 2014.
- [18] Reinhard Köhler, Norbert Neumann, and Günter Hofmann. Pyroelectric single-element and linear-array sensors based on p(vdf/trfe) thin films. *Sensors and Actuators A: Physical*, 45(3):209 – 218, 1994.
- [19] Jundong Song, Guanxing Zhao, Bo Li, and Jin Wang. Design optimization of pvdf-based piezoelectric energy harvesters. *Heliyon*, 3(9):e00377, 2017.
- [20] T G McKay, S Rosset, I A Anderson, and H Shea. Dielectric elastomer generators that stack up. *Smart Materials and Structures*, 24(1):015014, 2015.
- [21] Pierre-Jean Cottinet. *Actionnement et récupération d'énergie à l'aide de polymères électro-actifs*. Thesis, INSA Lyon, November 2010.

- [22] Vincenzo Pecunia, Mark Nikolka, Antony Sou, Iyad Nasrallah, Atefeh Y. Amin, Iain McCulloch, and Henning Sirringhaus. Trap healing for high-performance low-voltage polymer transistors and solution-based analog amplifiers on foil. *Advanced Materials*, 29(23):1606938, 2017.
- [23] Bret Neese, Baojin Chu, Sheng-Guo Lu, Yong Wang, E. Furman, and Q. M. Zhang. Large electrocaloric effect in ferroelectric polymers near room temperature. *Science*, 321(5890):821–823, 2008.
- [24] Rujun Ma, Ziyang Zhang, Kwing Tong, David Huber, Roy Kornbluh, Yongho Sungtaek Ju, and Qibing Pei. Highly efficient electrocaloric cooling with electrostatic actuation. *Science*, 357(6356):1130–1134, 2017.

Chapter 2

Performances as actuators

2.1 State of the art

In this chapter we will study different types of P(VDF-TrFE-CTFE) terpolymers and assess their interest as active material in thin film actuators.

2.1.1 Electromechanical formalism

The constitutive equations of electroactive materials link the electrical displacement and field to other physical quantities such as stress, strain or temperature. Their notation and units are regrouped in table 2.1.

Physical quantity	Notation	Units
Strain	S_{ij}	
Stress	T_{ij}	Pa
Electrical field	E_i	$V.m^{-1}$
Electrical displacement	D_i	$C.m^{-2}$
Polarization	P_i	$C.m^{-2}$

Table 2.1: Physical quantities of the electroactive material

The physical quantities in table 2.1 have subscripts because they are tensors and not scalar values. i and j are Einstein notations and correspond to the different directions of space. These quantities are interdependent and are linked to one another by the electromechanical coefficients referenced in table 2.2.

Coefficient	Notation	Units
Permittivity	ϵ_{ij}	$F.m_{-1}$
Rigidity	c_{ijkl}	Pa
Compliance	s_{ijkl}	Pa^{-1}
Young's modulus	Y	Pa
Poisson coefficient	ν	
Piezoelectric coefficients (T,E)	d_{ijk}	$m.V^{-1}$
Piezoelectric coefficients (T,D)	g_{ijk}	$m^2.C^{-1}$
Electrostrictive coefficients (T,E)	M_{ijkl}	$m^2.V^{-2}$
Electrostrictive coefficients (T,D)	Q_{ijkl}	$m^4.C^{-2}$

Table 2.2: Electromechanical coefficients

The constitutive equations of an electroactive materials are the following:

$$\begin{aligned}
 S_{ij} &= s_{ijkl}.T_{ij} + d_{kij}.E_k + M_{kl ij}.E_k E_l \\
 D_{ij} &= \epsilon_{ij}.E_j + d_{ij}.T_j
 \end{aligned}
 \tag{2.1}$$

$$\begin{aligned} S_i &= s_{ij} \cdot T_j + g_{ij} \cdot D_j + Q_{klj} \cdot D_k D_l \\ E_i &= \beta_{ij} \cdot D_j - g_{ij} \cdot T_j \end{aligned} \quad (2.2)$$

The first terms of each equation in 2.1 and 2.2 are used to describe all dielectric materials. The strain-stress relationship made with the s_{ij} coefficients is nothing more than Hooke's law for elastic materials. The relationship between electrical displacement and electrical field is made using permittivity (ϵ_{ij}), which is the description of a linear dielectric. In the case of electroactive materials, other coefficients are added to account for the interdependence of mechanical and electrical quantities. That is why equations 2.1 and 2.2 contains the piezoelectric and electrostrictive coefficients d , g , Q and M . The electromechanical equations have several forms depending on which quantity we want to express. We only present here the equations with an explicit strain formulation. The other forms and coefficients are described in [1].

A fourth order tensor such as M or Q contains 81 coefficients but based on symmetry considerations this number can be reduced to 36. Among these 36 coefficients, only a few are actually relevant for practical calculations. Figure 2.1 is a representation of the two strain directions we are interested in, and the coefficients used to characterize those strains.

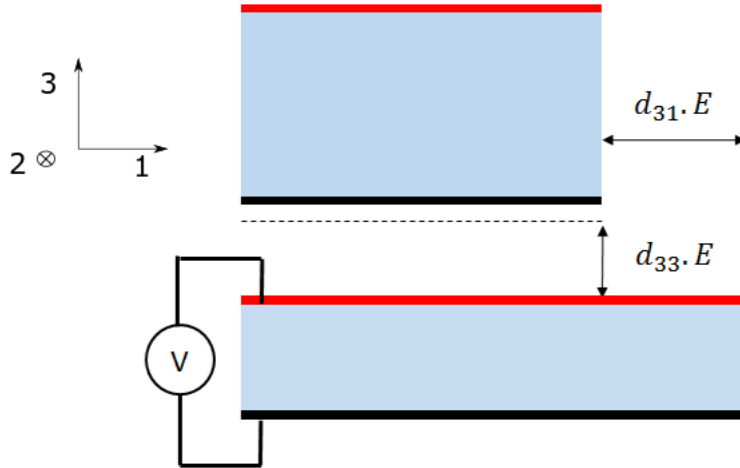


Figure 2.1: Representation of the principal strain directions and the corresponding piezoelectric coefficients

Figure 2.1 is a simplified representation of a dielectric material, with and without an applied electrical bias. d_{33} characterizes the strain in the electrical field direction and d_{31} in the thickness direction. They are the only coefficient lefts once equation 2.1 is applied to the practical case represented in figure 2.1.

We do not apply any external stress to the sample so $T_{ij} = 0$ in equation, additionally the electrical field is applied in the principal direction 3 so $E_1 = E_2 = 0$. If the material is piezoelectric, the second order terms are negligible behind the first order ones. The strains along thickness and

length directions are then expressed with equation 2.3.

$$\begin{aligned} S_1 &= d_{311} \cdot E_3 \\ S_3 &= d_{333} \cdot E_3 \\ &+ M_{3333} \cdot E_3^2 \end{aligned} \quad (2.3)$$

With simplified Einstein notations, d_{3ii} and M_{33ii} become d_{3i} and M_{3i} . A few more coefficients will be used in chapter 4 but these are the most important ones.

Here we conveniently forget about the direction 2. However, in a clamped device blocking one direction (here direction 2) will affect the two others. This issue will be not developed here nor its impact in most studies, but we will keep that in mind when comparing different geometries in chapter 5.

2.1.2 Copolymer

The material to which we will compare P(VDF-TrFE-CTFE) terpolymers is the better-known P(VDF-TrFE) copolymer. Several grades of copolymers are commercially available with different piezoelectric and pyroelectric properties. Fig 2.2 displays the polarization of copolymers with different compositions, ranging between 80/20 and 50/50 VDF/TrFE. This figure was furnished by Piezotech, who also provided the polymers studied in this work.

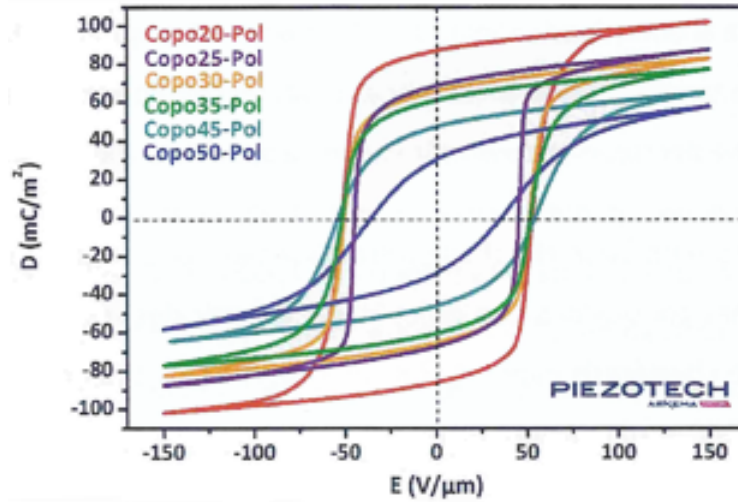


Figure 2.2: Polarization cycles of six different grades of copolymer

As mentioned in the previous section, the insertion of TrFe in the VDF chains favors the ferroelectric phase at ambient pressure. A certain amount of TrFE is required so that all VDF is in the desired polar conformation [2]. However, too much TrFE simply reduces the amount of VDF dipoles forming the ferroelectric domains. This leads to the reduction of remanent polarization (polarization at zero volt) observed in figure 2.2. This ferroelectric response is especially relevant

for actuation because in PVDF and P(VDF-TrFE) the piezoelectric effect is proportional to remanent polarization [3]. Based on these considerations and the compositions available at the time, we chose as our reference the copolymer with 75% VDF and 25 % TrFE.

In terms of processing conditions, several studies have been dedicated to the impact of annealing on copolymers structure and properties [4][5][6][7]. To maximize the piezoelectric performances, copolymer must be annealed between their Curie temperature and their melting point. Based on Piezotech data, we chose an annealing temperature of 130 °C.

The electromechanical performances of copolymers depend on their composition and fabrication process but the values are in the same range throughout the different studies. To give an idea of the typical values for a copolymer we reported a few examples in table 2.3.

	Value	Ref
d_{31} ($pm.V^{-1}$)	12.5, 11	[8],[9]
d_{33} ($pm.V^{-1}$)	-25, -34, -31, -44	[10], [9], [11], [12]
Y (GPa)	2.1, 3.3, 1.4	[8],[9], [12]

Table 2.3: Piezoelectric coefficients and Young’s modulus of P(VDF-TrFE) from different studies

The d coefficients quantify the amount of charges we can get out of a given mechanical stress (eq 2.1). For reference, the PZT ceramics commercially available have coefficient $d_{33} > 300 pm.V^{-1}$ [13], ten times superior as the values in table 2.3. Beside their higher d_{33} value, PZT have a Young’s modulus around 60 GPa which is around thirty times more than that of P(VDF-TrFE). The stress output of an actuator is a function of both rigidity and strain so ceramics are overwhelmingly dominant in that regard.

To compensate the discrepancy in d values, a PVDF energy harvester would have to be strained at least ten times more than a PZT one. As we discussed in the previous chapter this might not be an issue and can be achieved with something as simple as folding a plastic sheet (i.e the substrate). This is the same with actuation where a thin flexible substrate can help compensate the lower strain values of PVDF.

2.1.3 Terpolymer

Electrical behaviour

The high strain of terpolymers is associated with their relaxor ferroelectric nature. This denomination of relaxor ferroelectric has been taken from the electrostrictive formalism commonly used with ceramics. The relaxor behaviour is associated to a reduction of the crystalline domains size which in turn leads to a frequency dependent Curie temperature.

In figure 2.3 left panel displays the permittivity versus temperature at different frequencies. The peak position defines the Curie temperature and its frequency dependence is a characteristic

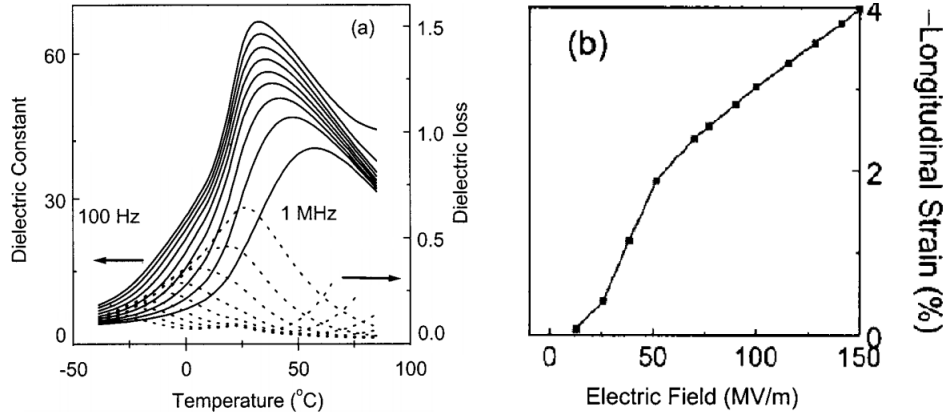


Figure 2.3: Left: permittivity versus temperature and frequency of a P(VDF-TrFE-CTFE) terpolymer. Right: strain versus electrical field [14]

feature of relaxor ferroelectric materials. The curve in the right panel is the first report of the important strain in P(VDF-TrFE-CTFE).

To achieve this transition from ferroelectric to relaxor ferroelectric and improve the strain response, a certain amount of CTFE has to be introduced. The influence of composition on terpolymers electrical properties was mostly investigated by Z.Zhang [15] [16]. The permittivity and also the polarization response were measured for more than twenty terpolymers with different compositions and fabrication processes. The polymers were evaluated on their viability as dielectric material for high permittivity capacitors and no electromechanical data were collected.

Mechanical

Published data are scarce on the mechanical performances of terpolymers. In terms of rigidity, terpolymers are softer than copolymers and this value is heavily dependent on their composition, ranging from 0.1 to 0.6 GPa [17]. To compare the terpolymers strain and stress to that of copolymers we regrouped in table 2.4 values of Y and M found in different reports. The terpolymers in these studies contain between 7 and 9 of% CTFE.

	Value	Ref
M_{31} ($nm^2.V^{-2}$)	3, 2.3, 2.4	[18], [19]
Y (GPa)	0.4, 0.1, 0.16	[20], [18], [19]

Table 2.4: Electrostrictive coefficient M_{31} and Young's modulus of terpolymers found in different studies.

Using table 2.3 and 2.4 we can estimate the order of magnitude for the stress and strain of co- and ter-polymers at $20 V.\mu m^{-1}$. Strain is calculated with equation 2.1 and stress is the product of strain and Young's modulus (Hooke's law).

	Copolymers	Terpolymers
Strain	0.02 %	0.1 %
Stress (Pa)	5.10^5	2.10^5

Table 2.5: Estimation of the strain and stress achieved in polymers at $20 V.\mu m^{-1}$, assuming that equation 2.1 is valid at that electrical field value.

We can see that while the strain is superior in terpolymers, the stress is twice smaller. This is for an electrical field of $20 V.\mu m^{-1}$ and terpolymers are likely to be more efficient at higher electrical fields where they can reach strain up to 4 %, as shown in figure 2.3. Because of non linearities in the strain-electrical field relationship (fig 2.3, [21]), the electrostrictive coefficients are never used at high electrical fields and it becomes impossible to reproduce the comparison in table 2.5.

From the overall lack of data it is impossible to conclude properly on the interest of terpolymers over copolymers and even more so on the influence of CTFE. In particular, there are almost no reports on terpolymers with a low CTFE content, below 7% [17]. It is likely that these polymers have been dismissed as promising materials because of their incomplete transition toward relaxor materials. Nevertheless, this lack of interest seems unwarranted and they will be incorporated in our study.

Despite these uncertainties on their performances, terpolymers are used in demonstrators at both low [22] and high electrical fields [23], or in patented devices [24][25].

Conclusion 1: State of the art

The P(VDF-TrFE) copolymers have been studied extensively but data on P(VDF-TrFE-CTFE) terpolymers are much scarcer. It is especially true regarding the terpolymer strain response and its dependence to CTFE content.

2.2 Experimental**2.2.1 Preparation****Product**

The polymers constituting the active layer were provided by Piezotech as powders. They were dissolved in cyclopentanone and stirred at 90°C for 24h to form solutions with either 12 or 15% polymer mass ratio. Nine terpolymer compositions have been studied with increased CTFE content from 0 to 9.7%, as referenced in table 2.1.

Sample #	PVDF (%)	TrFE (%)	CTFE (%)
1	80	20	0
2	69	28.8	2.2
3	62.6	33.4	4
4	64.5	30	5.5
5	67.8	24.7	7.5
6	61.8	30.4	7.8
7	61.4	30.3	8.3
8	60.6	30.9	8.5
9	60	30.3	9.7

Table 2.6: Mass ratio in percentage of PVDF, TrFE and CTFE in each polymer

Top and bottom electrodes were made of poly(3,4-ethylenedioxythiophene) polystyrene sulfonate (PEDOT:PSS) purchased from Hereaus and stirred 15 min at room temperature before use. The 125 μm -thick substrate of the unimorph cantilevers is made of polyethylene naphthalate (PEN) from Dupont Teijin (ref Q65). A thinner substrate would give an increased actuator deflection but below 100 μm the films become harder to manipulate.

Printing

The first tryouts were spin coated polymers with sputtered gold electrodes, but too few devices were functional after the process. It could be the consequence of manually positioning the electrodes masks or the gold deposition itself. Either way we chose to use a different process and more specifically a screen printing technique. A survey of the other possible methods (slot-dye,

inkjet, engraving...) and their features can be found in [26]. Screen printing fits our needs and is quite easy to use, making it an adapted technique for the following study. The principle is similar to that of a stencil but the hole is replaced by a thin mesh. The paste is spread out by a blade with programmed speed and pressure instructions. Fig 2.4 shows graphic representation of a screen printer, taken from [27].

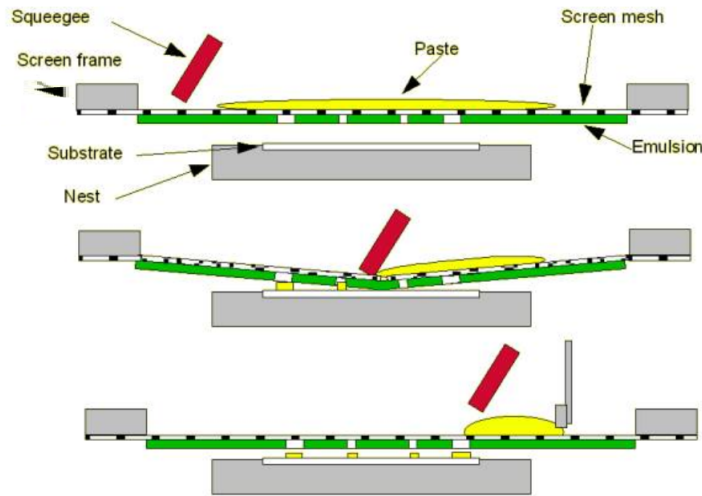


Figure 2.4: Principle of screen printing [27]

There are several parameters that can be tuned to obtain the desired layer thickness: blade rigidity, paste viscosity, speed, pressure and mesh dimensions. Even so, the thickness range we get is quite small and limited, from 0.8 to 2.5 μm thick polymer layers. The difficulty to reach smaller layers is seen as a drawback of this technique for devices such as organic transistors. In this study oriented toward actuation, there are competing interests regarding the ideal thickness. A thick polymer layer requires a very large electrical potential and cannot be actuated at high electrical fields. On the other hand thin devices have higher chances of failure and increased leakage currents. A thickness of 2 μm is a decent compromise given the 200V generator at our disposal.

With screen printing it is possible to deposit different patterns onto a single substrate. Taking advantage of that, we designed a mask with 12 cantilevers and 4 disks of different sizes. The cantilever width is either 2, 4 or 10 mm and the length 5, 10, 15 or 20 mm. A picture of a sample is shown in fig 2.5.

The presence of several geometries makes of a single printed sheet a versatile tool for the different studies. The first objective of this design is to verify if the analytical model explains correctly the experimental deflections so we can use the analytical model to extract electromechanical coefficients. Secondly, it allows to change the substrate, the frequency or any other parameters and always have a few geometries adapted to the new framework. As an example,

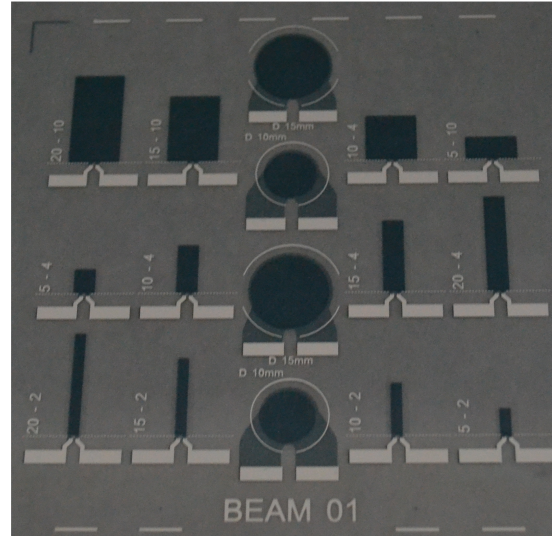


Figure 2.5: Picture of a printed PEN sheet with the 16 actuators. White numbers are the dimensions in mm

long cantilevers have larger deflections but higher vibration modes appear at lower frequencies (annex). Lastly, some devices are not ideally suited for mechanical studies but are appropriate for other experiments. The upper row (10mm width) was principally used for diffraction measurements where a large surface allows for faster acquisition. The disks were supposed to be used for charge generation although this path was not pursued eventually.

2.2.2 Characterization

Once the 3 layers (PEDOT/P(VDF-TrFE-CTFE)/PEDOT) have been printed onto the PEN sheet, the cantilevers are cut out using a laser with programmed pattern in order to have a cut as reproducible as possible. At that point the fabrication process is over and we move on to the electric and mechanical characterization. The polarization cycles are acquired by a Padiant premier precision ferroelectric tester from Radiant inc. The tester is commanded with the dedicated Vision software and the measurement unit is a virtual ground circuit.

The cantilever deflection is measured using a chromatic confocal sensor (STIL Initial) with a resolution of a few hundred nanometers. The radiant tester is linked to the STIL sensor and sends it a trigger when the polarization measurements starts. That way we have the electrical field, the polarization and the strain as a function of time. Unfortunately, the radiant tester does not accept any interaction other than through its dedicated software. Thus, the bench automation was done using a python macro to deal with the laser directly and simulate the user behaviour in the vision software when the radiant tester was needed. This allows for lengthy measurements with different waveforms, frequencies and amplitudes without the presence of an operator. A

picture of the characterization bench is displayed fig 2.6.

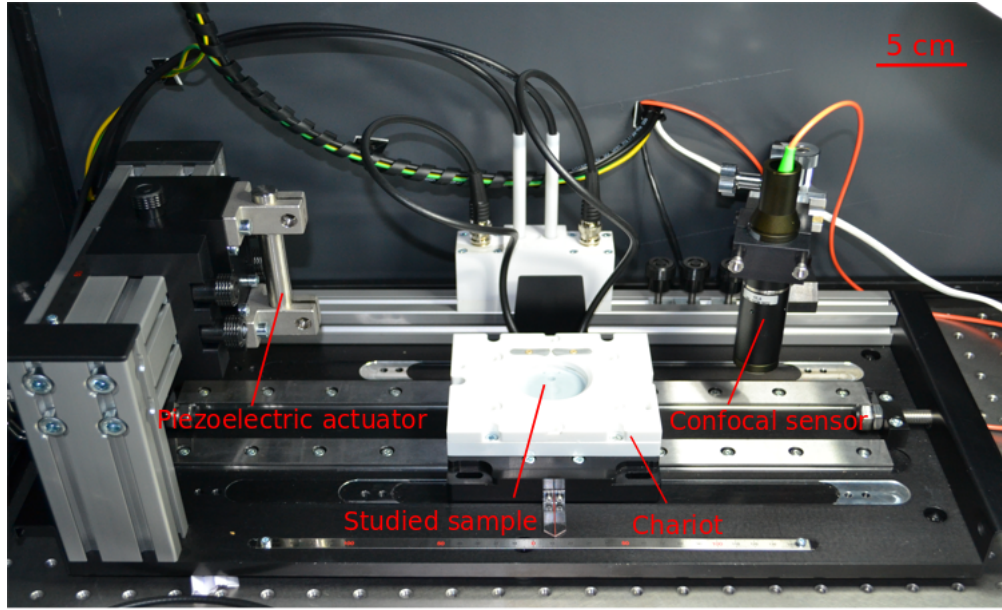


Figure 2.6: Picture of the characterization bench

The clamping of the device as well as the electrical contact are assured by the white block in fig 2.6 in an effort to ensure repeatability of the measurement. This block can move laterally to go under either the deflection measurement unit (right) or a piezoelectric motor for charge generation (left).

The link between measured deflection and polymer properties is made using beam theory. Considering the equilibrium at the layers interface and writing the sum of forces and the sum of moments as null yields the relation 2.4 [1].

$$\delta = \frac{3Y_s Y_p t_s t_p (t_s + t_p) L^2}{Y_s^2 t_s^4 + Y_p^2 t_p^4 + 2Y_s Y_p t_s t_p (2t_p^2 + 3t_s t_p + 2t_s^2)} \cdot S \quad (2.4)$$

- δ : cantilever deflection
- Y_s : substrate Young's modulus
- Y_p : polymer Young's modulus
- t_s : substrate thickness
- t_p : polymer thickness
- S: strain mismatch between the layers
- L: cantilever length

The relevant polymer properties are its rigidity Y_p and its strain S. The issue here is that the polymer rigidity is intertwined with substrate dependent parameters. A comparative study between polymers would not be of much use as it would only be true for a specific set of substrate

and geometry. However, we are working here with thin films: the printed polymers layers are only $2 \mu m$ thick, against the $125 \mu m$ of the substrate. Moreover, the rigidity of P(VDF-TrFE-CTFE) is highly dependent on the composition but at best it can reach 2-3GPa while the PEN has a Young's modulus of 6GPa. Therefore, we can neglect t_p before t_s in equation 2.4 which gives the much simpler equation 2.5.

$$\begin{aligned}\delta &= \frac{3.t_p L^2}{Y_s t_s^2} Y_p S \\ \delta &= \frac{3.t_p L^2}{Y_s t_s^2} T\end{aligned}\tag{2.5}$$

T : stress inside the polymer layer

In the case of thin films, the cantilever deflection is directly proportional to the polymer strain times its rigidity i.e. its stress. This makes a comparative study actually transferable without the need to measure the polymer Young's modulus beforehand.

In this discussion we neglected the influence of electrodes. Being only a micron thick (against $125 \mu m$ of PEN) and with a Young's modulus of the same order as the substrate, their influence is negligible in the present case. This was verified with a more complete model of the multilayered cantilever that can be found in [28].

2.2.3 First experiments

Cantilever length

Before moving on to the polymers comparative study we checked how our processed samples relates to beam theory (eq 2.5). Fig 2.7 shows the deflection at 120 V of terpolymer based cantilevers with $1.6 \mu m$ thickness, 4mm width and 4 different lengths (0.5-1-1.5-2 cm).

The blue dots are deflections of 4 cantilevers measured experimentally and plotted as a function of their squared length. The measurements follow closely a linear evolution with L^2 , as predicted by equation 2.5. Based on this observation, all the deflections in the following work will be normalized to that of a 1cm long cantilever (eq 2.6).

$$\delta_N = \left(\frac{L_N}{L}\right)^2 \delta\tag{2.6}$$

δ_N : normalized deflection
 δ : measured deflection

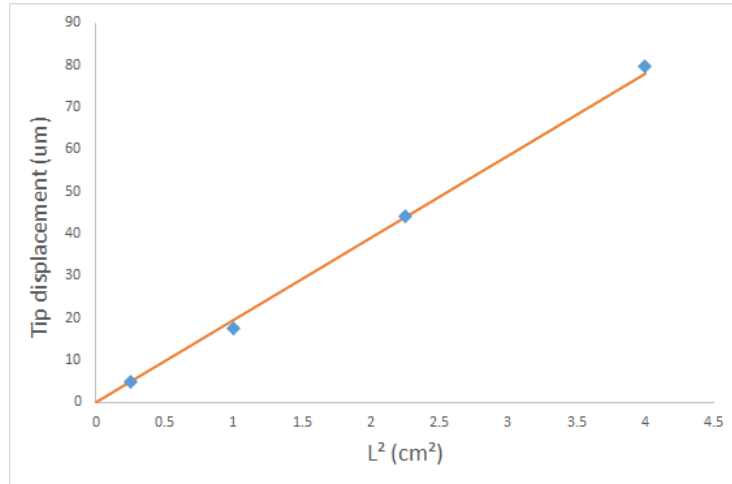


Figure 2.7: Deflection of cantilevers from the same PEN sheet with different lengths

Cantilever width

After the effect of length we study the influence of width. Following cantilever equation 2.4, the devices width should not affect the results. However, this equation obtained analytically supposes that the cantilever length is much larger than its width, a condition hardly respected. We used a finite element software to estimate how this can impact our measurements (fig 2.8).

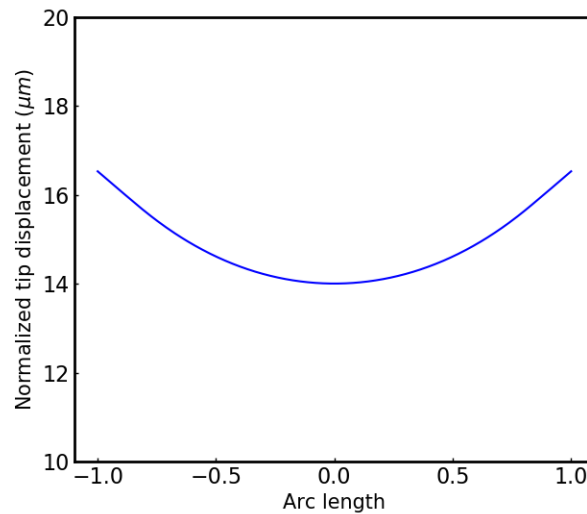


Figure 2.8: Height profile in the width direction of a cantilever end. COMSOL simulation

Fig 2.8 is the height profile of the cantilever end. As we can see, the end is also bent in the width direction. In a 10mm wide cantilever the height variation reaches 20% of the deflection in the length direction. This effect is reduced in narrower polymers as it represents 7% and 3% respectively for a 4mm and 2mm wide cantilevers. In order to stay as close as possible to the

theory we should use the narrowest cantilevers.

However, this is not the only place where we deviate from beam theory. The other and more problematic difference with an ideal beam is the presence of additional substrate around the cantilever after the cut. Fig 2.9 is a picture of a device edge taken with an optical microscope.

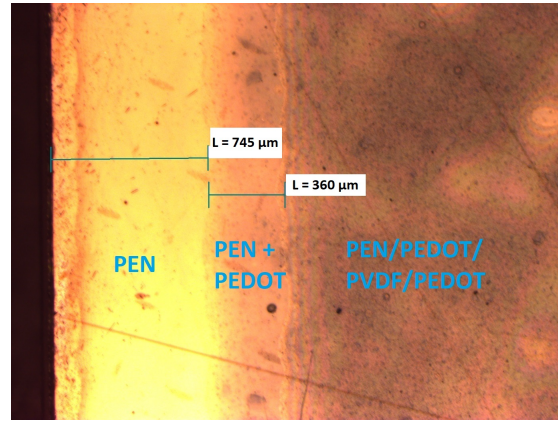


Figure 2.9: Picture of a cantilever edge after the laser cut. The dark part is the entire stack and the lightest part is consists of PEN alone

There is about 1mm of PEN on each side which is not covered by the active stack and is likely to hinder the cantilever deflection. To estimate the deviation induced by the additional substrate we can take a look at the ratio of the actual stack width over the total width. The deflection of an ideally cut device and the deflection measured experimentally are linked through equation 2.7.

$$\delta = \frac{w_{PVDF}}{w_{PVDF} + w_{PEN}} \delta_{th} \quad (2.7)$$

δ_{th} : estimated deflection of an ideally processed device.

w_{PVDF} : active layer width

w_{PEN} : total width

δ : measured deflection

As an other way to characterize the 'dead' width influence we used COMSOL, a finite element based software. Using equation 2.7 or finite element simulations we are able to estimate δ_{th} , the deflection of an ideally processed device. This theoretical deflection is the value to be used in equation 2.5 if we want to extract the polymers physical constants.

In order to estimate the influence of width on deflection, cantilevers taken from the same sheet but with 3 different widths are submitted to a 100 V bias. The deflections are measured and displayed fig 2.10 as the three green dots.



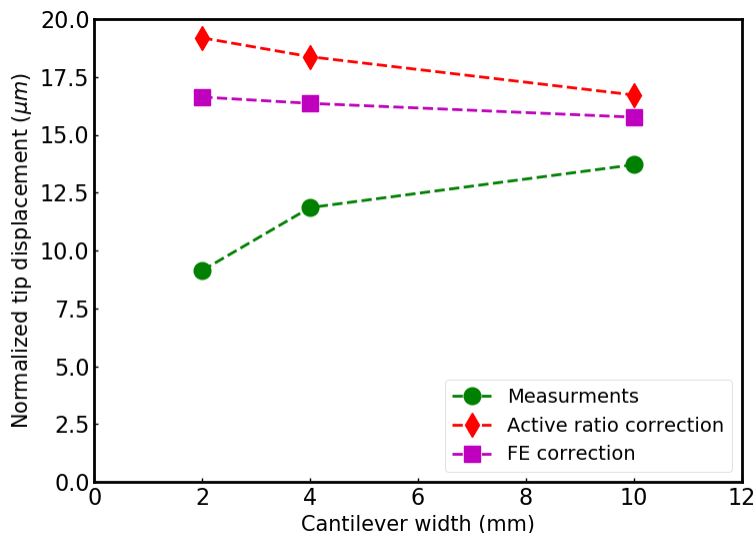


Figure 2.10: Deflection of cantilevers from the same print with identical lengths but different widths. Green dots are the deflection measurements. Red and purple dots are the estimated deflection of the device without surrounding PEN substrate. Red from equation 2.5, purple from COMSOL

The 10mm large cantilevers have a displacement 50% higher than 2mm ones. The red and purple curves are the two aforementioned corrections to estimate how an ideal device would deflect. This gives an estimation of the substrate impact. However it is hard to pinpoint an exact value for the corrections because the two approaches do not yield the same results. Therefore, we chose to work with only 4mm wide cantilever so there is no need to normalize the deflection with respect to their width.

Conclusion 2: Devices geometry

The screen printing technique allows for the processing of different geometries in a single run. Using this feature the printed PEN sheets have cantilevers with 14 different geometries. The following study is done on 4mm wide cantilevers and the deflections are normalized to that of an equivalent 1cm long cantilever.

2.3 Impact of the CTFE content

In this section we will study the impact of the CTFE content on the electromechanical response of the terpolymer.

2.3.1 Electrical evolution

Leakage currents

First, we take a look at the leakage currents in polymers because it can affect our polarization measurements. The leakage currents are the charge flowing through the sample and a net loss from an energetic standpoint. It is not an intrinsic response of the material and these charge movements do not participate to the polymer strain. Leakage currents could indirectly bend the cantilever with the heat they generate but we dismissed this phenomenon by monitoring the temperature with an IR cam. Figure 2.11 is the leakage measurement of two devices with the same thickness measured with an impedance meter (agilent 4156C).

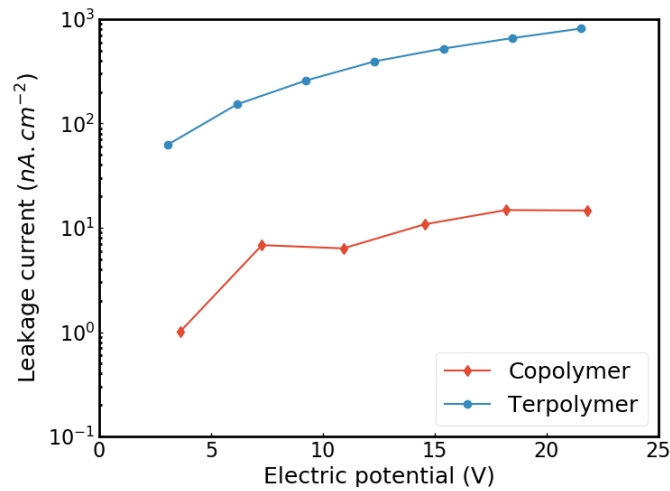


Figure 2.11: Leakage measurements of a copolymer and a terpolymer

The leakage currents depend strongly on the fabrication process and the device itself. The choice of electrodes alone can lead to decades of difference in the amount of leaked charges [29]. However, through these important variations, identically processed copolymers and terpolymers will not have the same conductivity. Overall, terpolymers turn out to be much more leaky than copolymers. The distortion of polarization measurement due to leakage can be monitored by equation 2.8.

$$Q_l = \frac{1}{2} \int_0^{T/2} i_l(t) dt \quad (2.8)$$

Q_l : increase in the remanent polarization due to leakage
 i_l : leakage current

In equation 2.8 $t = \frac{T}{2}$ corresponds to the first point where $V=0$, i.e the value in the polarization cycle that we read as the remanent polarization. Using equation 2.8 we can assess how much we overestimate the remanent polarization of polymers.

$$Q_l = \frac{GU_0}{2\omega} \quad (2.9)$$

G: Device conductance
 ω : sinusoid pulsation
 U_0 : sinusoid amplitude

The increase in a copolymer remanent polarization is around $0.01\mu C.cm^{-2}$ at 1 Hz, 100V and with leakage currents taken from fig 2.11. In terpolymers the remanent polarization is overestimated by $0.3\mu C.cm^{-2}$, the same order of magnitude as the actual value. These overestimations correspond to an error of 0.1% in copolymer and 100% in terpolymer, which is problematic in the latter. At 20 Hz however, this deviation is about 20 times lower and the error represents only 5% of the measured value in terpolymers. For this reason the following polarization cycles are acquired at 20Hz.

Polarization

The polarization cycles of the nine compositions are displayed in fig 2.12. The radiant tester allows for different types of cycles and we measured here the bipolar ($-100 V\mu m^{-1}$ to $100 V\mu m^{-1}$) and the unipolar (0 to $100 V\mu m^{-1}$) response to a triangle waveform.

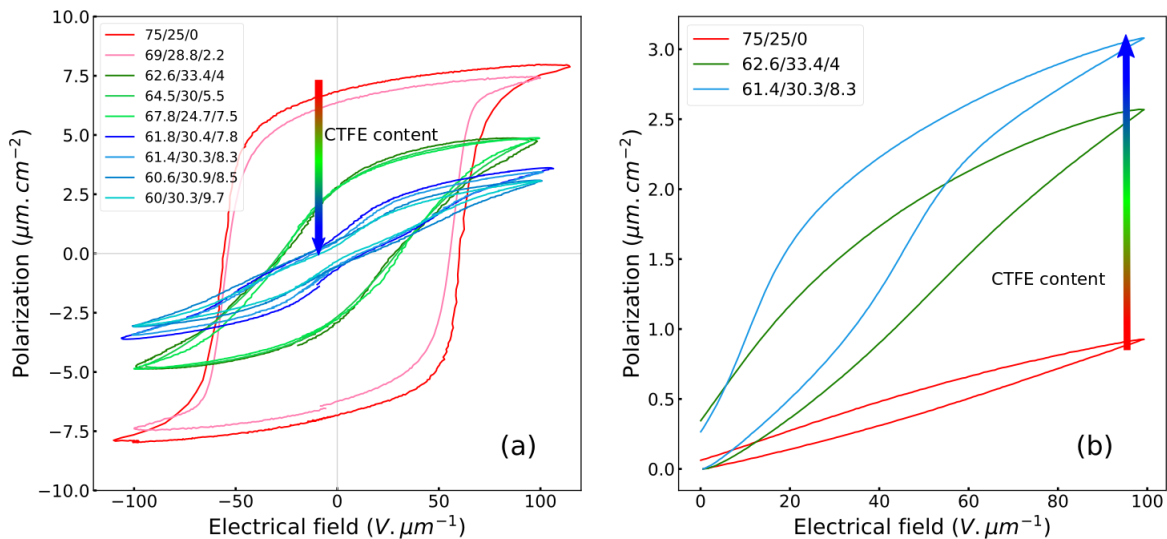


Figure 2.12: Polarization response of the nine polymer compositions. Fig b: bipolar solicitation. Fig a: Unipolar solicitation

In figure 2.12, the bipolar cycles are on the left and the unipolar cycles on the right. The first thing we observe is that instead of a continuous change with the addition of CTFE, there is an abrupt transition. As a visual aid we use a color code for each family: red for the copolymer and the 2% CTFE terpolymer, green for terpolymers with a CTFE content between 4 and 7.5% and blue above. The 3 categories will be hereafter referred to as copolymer, ferroelectric terpolymers

(FT) and relaxor terpolymers (RT). It makes things easier as we can focus qualitative studies on one representative of each class (0%, 4% and 8.3% CTFE) instead of the nine compositions.

The copolymer is ferroelectric with a remanent polarization of $7 \mu C.cm^{-2}$ which is expected for this kind of VDF/TrFE ratio (fig 2.2). Its unipolar response (red cycle on the right panel) is much smaller and only reaches $1 \mu C.cm^{-2}$ at $100 V\mu m^{-1}$. Provided that the ferroelectric domains are already aligned adequately, there is no ferroelectric switching during the unipolar cycle. Therefore the difference between fig 2.12 a. and b. is the contribution of ferroelectric domains and we can monitor its evolution with the CTFE content.

The FT have a remanent polarization value near $2.5 \mu C.cm^{-2}$ and their unipolar response reaches the same value. Compared to copolymers, they have a lower ferroelectric response but an otherwise higher polarization. This trends is accentuated with RT polarization cycles (in blue) which are not ferroelectric anymore but possess an even higher unipolar response.

Permittivity

The polymer permittivity was measured with an impedance meter at 0V and 20Hz. It characterizes the polarization response when submitted to a small electrical signal. The link between the capacitance and the full polarization cycle of polymers will be discussed in the following chapter. The aim here is to monitor how the amount of CTFE impacts the permittivity in terpolymers. The results are displayed fig 2.13.

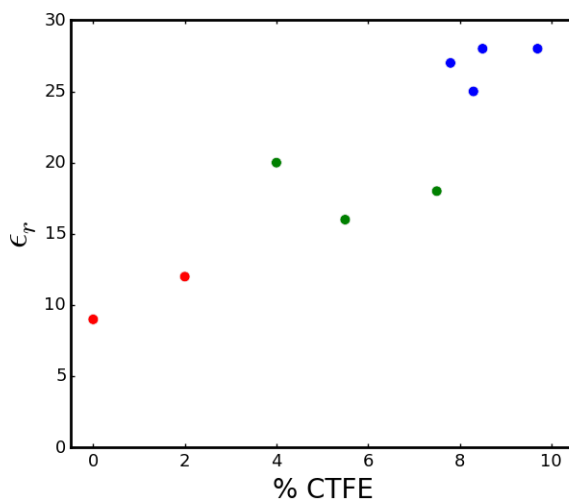


Figure 2.13: Permittivity of the terpolymer as a function of the CTFE content

We have two separate families of terpolymers once again: RT with $\epsilon \approx 27$ and FT with $\epsilon \approx 17$ while the copolymer is around 9. There are few reports on FT but the permittivity of copolymer

and RT are consistent with values found in the literature [30] [21].

Conclusion 3: Impact of CTFE on electrical properties

The impact of CTFE on the electrical response is a reduction of the ferroelectricity, an increase of permittivity and leakage currents. Instead of a continuous transition from copolymer to relaxor (RT), the terpolymers between 4 and 7.5% (FT) are almost identical with an abrupt change of permittivity and ferroelectricity around 8% CTFE.

2.3.2 Mechanical evolution

The cantilever equations have been detailed above, and the deflection is an image of the polymer strain (eq 2.4). In order to observe how strain evolves with composition, we measured the deflection of cantilevers with different amount of CTFE and displayed the results in fig 2.14, with one representative of each polymer type.

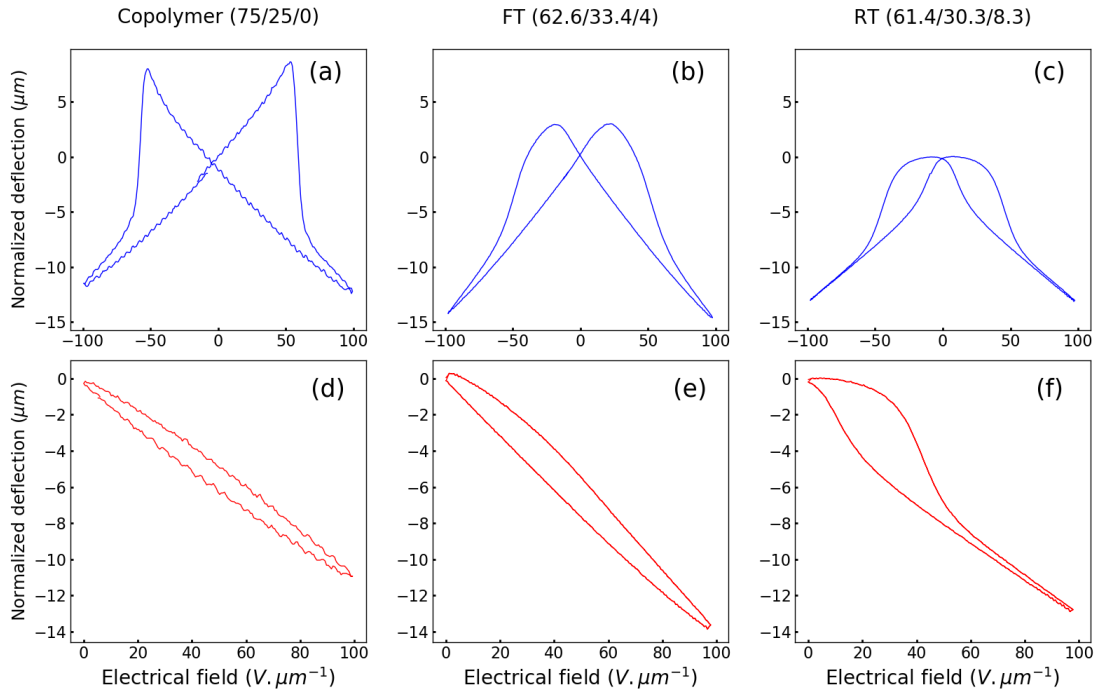


Figure 2.14: Displacement of three polymers, one for each behaviour identified above. a: copolymer; b: ferroelectric terpolymer; c: relaxor terpolymer. The upper row is the bipolar cycle and the lower one the unipolar cycle.

Figure 2.14 shows the normalized cantilever deflection for the three different categories of polymers, when a bipolar or a unipolar electrical field waveform are applied. First, P(VDF-TrFE) exhibits a butterfly shape in bipolar regime and a piezoelectric linear response in unipolar

regime (Fig. 3a and 3d). In the case of the ferroelectric ter-polymer (Fig 2.14 b and e), the smaller difference between bipolar and unipolar cycles is consistent with a reduced ferroelectric contribution. For the relaxor ter-polymer (Fig. 3c and 3f), the unipolar and bipolar cycles superimpose exactly, likely due to an absence of ferroelectricity. Beyond a specific electrical field (around $60 \text{ V}\mu\text{m}^{-1}$), the mechanical response exhibits a linear regime with very little hysteresis.

Conclusion 4: Impact of CTFE on the polymers behaviour

The copolymer has a marked butterfly shape due to its ferroelectric nature. Below 7.5% CTFE the butterfly still exists in terpolymers although strongly reduced and beyond 7.5% CTFE the strain can only be negative but retains an hysteretic shape. The changes in strain behaviour are consistent with the change in ferroelectric properties observed above.

2.4 Performances as actuator

We want to compare the performances of terpolymers as actuators, but the different behaviours make the results dependent on test parameters such as the range of electrical field. For example if we take a bipolar regime, copolymer has a much larger deflection than terpolymers, that cannot reach a positive strain (fig 2.14). However, the ferroelectric domain switching comes at the cost of a huge energy consumption that would not appear otherwise. The results of a comparative study in bipolar regime are opposed to that of a study in unipolar regime in terms of performance and energy cost. The chosen settings are the following:

- Unipolar regime: only positive potential is applied
- Low frequency: 1 Hz
- Established regime: from the 2^{nd} to the ∞ -th cycle

2.4.1 Mechanical performances

Figures of merit

The objective when using an actuator is to generate either a displacement or a force. The force generated by a cantilever is equivalent to the minimum force required to block the deflection.

It is expressed as eq 2.10:

$$F_b = \frac{3t_s l t_p Y_p}{4L} S \quad (2.10)$$

F_b : Blocking force
 t_p : polymer thickness
 t_s : substrate thickness
 l : cantilever width
 L : cantilever length
 Y_p : polymer rigidity
 S : strain of the active layer

Using cantilever equation 2.5 we transform 2.10 into eq 2.11.

$$F_b = \frac{Y_s t_s^3 l}{4L^3} \delta \quad (2.11)$$

δ : displacement of the cantilever free of any load

The blocking force of a cantilever is proportional to its displacement when it is free of any load. Therefore, a comparative study on the cantilevers deflection also communicates their ability to generate a force.

Another way to assess the mechanical performances of a polymer is through its stored elastic energy. In the literature this figure of merit is given for the polymer free of any constraint (equation 2.12) [31][19].

$$E_{mp} = \frac{Y_p}{2} S^2 \quad (2.12)$$

E_{mp} : mechanical energy density of a polymer

This quantity is much larger in a terpolymer than in a copolymer and the terpolymer appears more than 10 times better in this regard [20]. However eq 2.12 is not suited in our case, where the polymer has to drag the substrate along with it. The relevant parameter is then the elastic energy of the whole cantilever and we can calculate it using eq 2.13

$$E_m = \int_0^L YI\delta''(x)^2 dx \quad (2.13)$$

E_m : mechanical energy of a bent cantilever
 I: Moment of inertia of the beam

Considering small deflections, $\delta(x)$ is a parabola and δ is expressed as

$$\delta(x) = \frac{x^2}{L^2}\delta(L) \quad (2.14)$$

$\delta(L)$: deflection measured with our sensor

This gives a simpler form of eq 2.13

$$E_m = \frac{Y_s t_s^3 l}{6L^3} \delta^2 \quad (2.15)$$

This physical value is proportional to δ^2 and once again a simple study on the cantilevers deflection will be enough to compare the different polymers. We will use eq 2.15 to calculate the electromechanical coupling later on but we can already infer the difference with the common figure of merit in the literature. Using equations 2.12, 2.5 and 2.15 we get the ratio between the mechanical energy of the free standing polymer and that of the whole device (eq 2.16).

$$\frac{E_{polymer}}{E_{device}} = \frac{3t_p}{Y_s t_s} Y_p \quad (2.16)$$

This ratio corresponds to the ability of the active layer to transmit its elastic energy to the rest of the device. As we see it is proportional to the polymer rigidity and the terpolymers are likely to lose their overwhelming superiority once embedded into an actual device.

Conclusion 5: Figures of merits of polymers

Measuring the deflection of cantilevers also gives the force they can generate and the elastic energy stored. The energy is that of the entire device and not the usual figure of merit of free standing polymers. As a result this figure of merit is less favourable to terpolymers and their interest for actuation is put into question.

Deflection profiles

The studied terpolymers FT and RT have respectively 4% and 8.3% CTFE content. Their deflection below $20 \text{ V}\mu\text{m}^{-1}$ are compared in fig 2.15.

The copolymer based cantilever (green curve in figure 2.15) deflects more than both terpolymers (purple and yellow curves). At $20 \text{ V}\mu\text{m}^{-1}$ the copolymer reaches $1.4\mu\text{m}$ while the FT is at

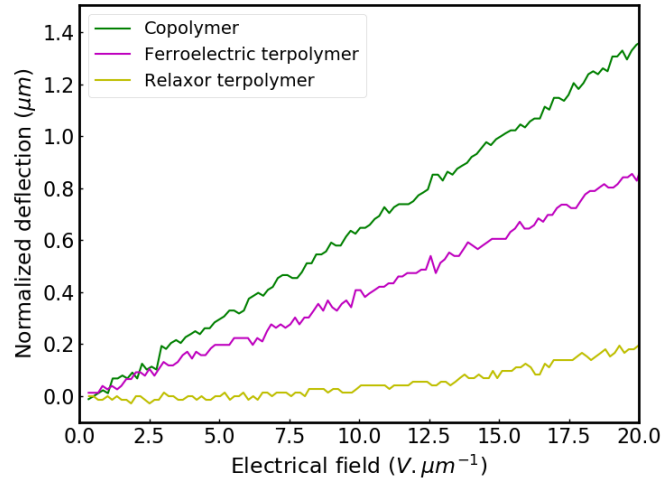


Figure 2.15: Deflection at low electrical field of three cantilevers, one for each type of polymers.

$0.8 \mu m$ and the RT deflection is only $0.2 \mu m$. The difference between RT and copolymer is even higher than what we estimated from the electromechanical coefficients taken in the literature (table 2.5).

Attempts at improving the actuation performances by tuning the fabrication process [21] or mixing the RT with other blends [19] do not seem promising for low electrical field applications. A sevenfold increase of the relaxor terpolymer stress would only allow it to reach the copolymer performances. We increase the electrical field and display the results in figure 2.16 to see how this comparison evolves.

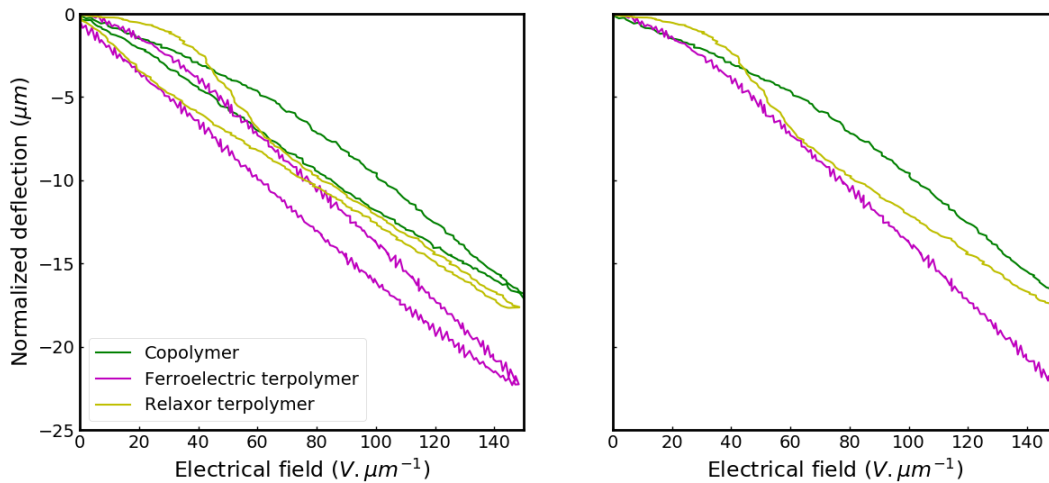


Figure 2.16: Deflection at high electrical field of three cantilevers, one for each type of polymers. Left panel: full cycle. Right panel: forward direction.

The left pannel displays the complete unipolar deflection cycles of the three polymers and the right panel only the forward direction (increasing field) used hereafter to calculate the cantilever elastic energy.

At high electrical fields the copolymer based cantilever has the lowest deflection and even the RT performs slightly better beyond $40 \text{ V}\mu\text{m}^{-1}$. As it turns out, the increased strain of P(VDF-TrFE-CTFE) relaxor terpolymers is almost perfectly balanced by the decrease in Young's modulus reported in different studies [20] [19]. The FT on the other hand diverges from the other polymers with a $6\mu\text{m}$ difference at $140 \text{ V}\mu\text{m}^{-1}$. That is 35 % higher compared to a copolymer and this difference seems to only improve going at higher electrical fields.

In early studies FT have been quickly dismissed as potential candidates for applications, most likely because they were not as ferroelectric as a copolymer and reached lower strains compared to higher CTFE/CFE concentrations [32]. As we can see in figure 2.16 they turn out to outperform both copolymer and relaxor terpolymers. A consequence of the improved deflection is that FT also possess the highest mechanical energy (fig 2.17).

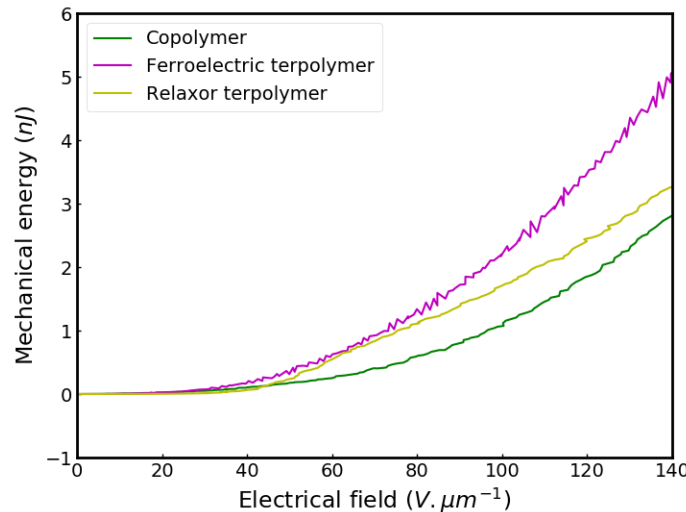


Figure 2.17: Elastic energy stored in the cantilevers as a function of the electrical field.
Calculated from fig 2.16

Figure 2.17 is the elastic energy of cantilevers as a function of the electrical field and will be of use to get the polymers coupling efficiency. It is calculated using the displacement values displayed in fig 2.16 and equation 2.15.

To simplify the reading, the figures presented above only display a single polymer in each category. Although polymers of a given family (copo/FT/RT) have the same kind of response,

the amplitude they reach can vary. Therefore, a similar study was performed on the nine polymer compositions.

Representing the strain curves on the same figure would only make it unreadable so we chose an arbitrary high electrical field value of $100 \text{ V}\mu\text{m}^{-1}$ and compared the nine compositions at that point.

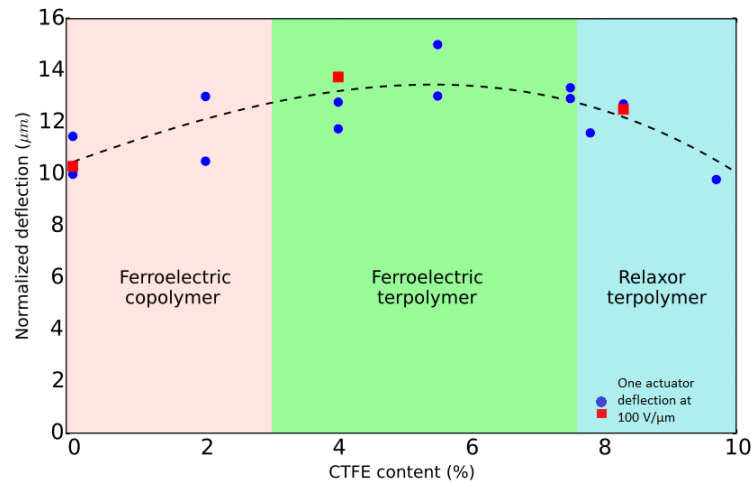


Figure 2.18: Deflection of cantilevers at $100 \text{ V}\mu\text{m}^{-1}$ as a function of the CTFE content. Each dot represents one cantilever and the squares are the 3 cantilevers shown in fig 2.14

Fig 2.18 presents the normalized deflection of cantilevers at $100 \text{ V}\mu\text{m}^{-1}$ as a function of the CTFE content in the polymer. Each dot represents one device and the red squares are the samples whose responses are shown in the section above (fig 2.15-2.16). Because of the different polymers nature, fig 2.18 changes depending on the chosen electrical field value. However the trend (dotted line) is similar for any electrical field above $80 \text{ V}\mu\text{m}^{-1}$. With this figure, we can narrow down the optimal composition of terpolymer to a CTFE content near 5%.

Conclusion 6: Mechanical performances

A higher deflection implies that the cantilevers also possess a higher blocking force and elastic energy. Used at low electrical fields ($< 20 \text{ V}\mu\text{m}^{-1}$) copolymer based cantilevers have the highest deflection. At higher electrical fields the ferroelectric terpolymers are better with a CTFE content around 5-6 %.

2.4.2 Electrical energy and coupling efficiency

Figure of merit

We now focus on the energy cost of these actuators. The electrical energy stored in a device is written as eq 2.17.

$$W_e = \int V(t).i(t)dt \quad (2.17)$$

W_e : electrical energy brought to the cantilever

V: electric potential at the electrodes

i: current in the circuit

An electrical current is the derivative of the charge versus time. Thus eq 2.17 can be reformulated into eq 2.18.

$$W_e = \int_0^{Q_{max}} VdQ \quad (2.18)$$

Q: Charge at the electrodes

A visual representation of the right hand term is shown in fig 2.19

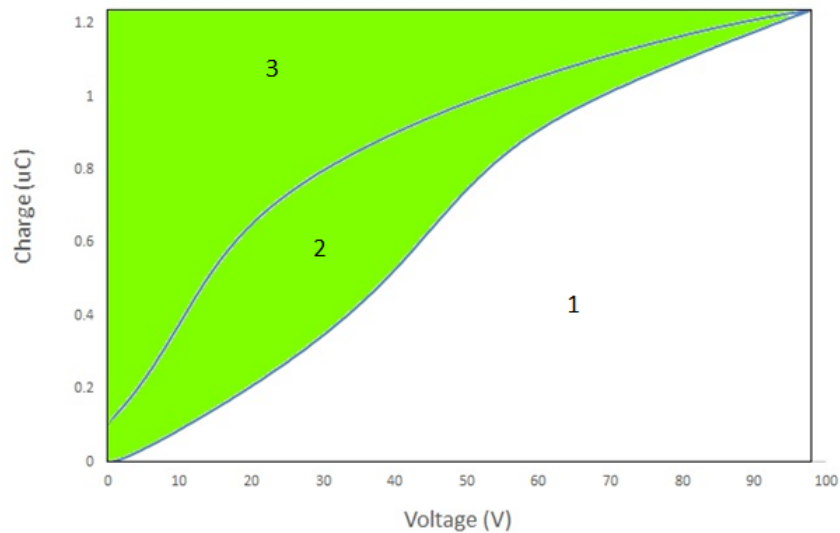


Figure 2.19: Electrical charge as a function of the potential in a device. The green area is the electrical energy consumption during a cycle

By plotting $V(Q)$ instead of $Q(V)$ the electrical energy can be easily integrated. The area 2 and 3 in fig 2.19 both correspond to the energy required by the cantilever to function. However they do not have the same physical significance. Area 2 is the intrinsic loss of the material, the

electrical energy is mostly dissipated as heat and cannot be recovered. Area 3 is the energy sent back in the electrical circuit during the device discharge.

Here we can make a parallel with energy harvesting for which it is interesting to have a high value for 3 and a low one for 2. For its part, actuation needs $2+3$ to be as small as possible to obtain a high coupling efficiency; these objective are not exact opposites but are quite different nonetheless.

Electrical energy and coupling

Applying the principle above to our polymer gives fig 2.20.

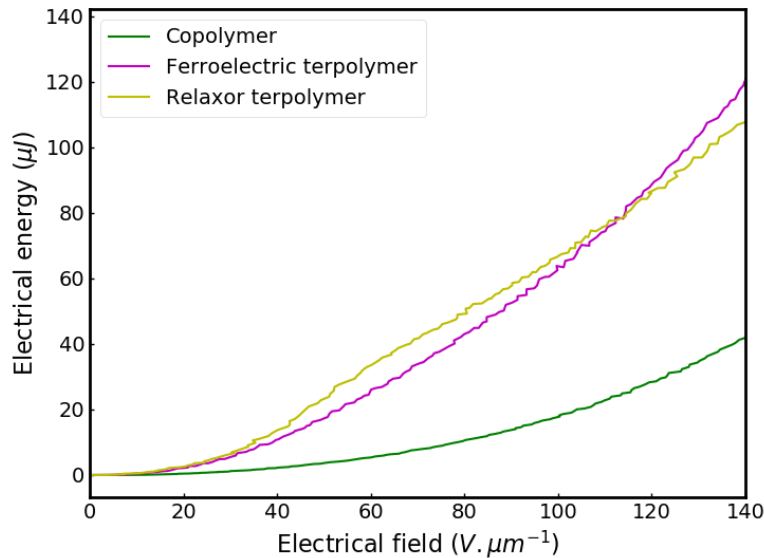


Figure 2.20: Electrical work of three cantilevers, same as fig 2.17

The copolymer requires much less energy than both terpolymers; at $140 V \mu m^{-1}$ the electrical energy stored in the device is $40 \mu J$ around one third the amount stored in the other ones. Now that we have both mechanical and electrical energy we can calculate our second figure of merit, the effective electromechanical coupling coefficient. This coefficient is adimensional and represents the efficiency of the device, it is defined with equation 2.19. Each application requires its own coupling efficiency study.

$$k^2 = \frac{E_{meca}}{W_{elec}} \quad (2.19)$$

k^2 : Coupling coefficient
 E_{meca} : Mechanical energy
 W_{elec} : Electrical work

Using equation 2.19 with the data presented in figure 2.17 and 2.20 gives the coupling coefficient as a function of the electrical field. The results are displayed in fig 2.21

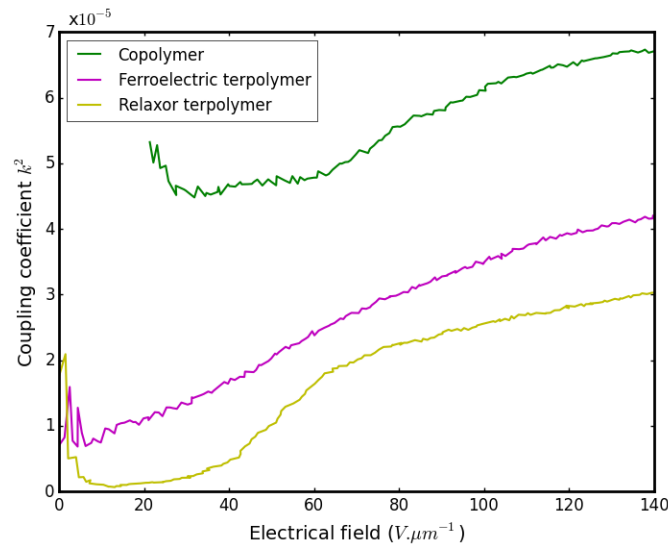


Figure 2.21: Coupling coefficient of the three types of polymers

There is a strong dependence on the electrical field but even at $140 \text{ V}\mu\text{m}^{-1}$ the RT coupling efficiency is half that of the copolymer. The FT are also less cost efficient than copolymers but better than RT. Overall the coupling coefficient is very low, under 0.01% for all polymers. This is due to the nature of our device where only the thin polymer layer receives electrical energy and have to transmit it to the whole device. Based on eq 2.16 the coupling coefficient of a free standing copolymer film would be around 0.8 % at $60 \text{ V}\mu\text{m}^{-1}$ while it would reach 1.5 % for a RT. Applied to an actual device it turns out that the copolymer is by far the most efficient among the different compositions.

Conclusion 7: Electrical energy and coupling efficiency

The electrical work is calculated from the polarization cycles and the terpolymers require several times more energy to reach equivalent deflections. The increase in electrical cost is much larger than the increase in mechanical output. This translates into a coupling coefficient of terpolymers about half that of the copolymer.

2.4.3 Scope of the comparative study

We evaluated the performances of nine different terpolymers processed identically. However, there are countless combinations of compositions and annealing conditions and we want to assess the scope of the results presented above.

Influence of the processing conditions

There are few studies focused on the impact of annealing duration and temperature on terpolymers mechanical performances. Sigamani & al studied the impact of annealing duration, up to 24 hours with no significant increase of the terpolymers strain [33]. While this reassuring, the annealing duration of our process is even lower at only 15 min. We verified on a few compositions that for durations this short the terpolymer behaviour is not dramatically modified. Fig 2.22 shows the difference between annealing a 5.5% CTFE terpolymer for 15mn or 1 hour.

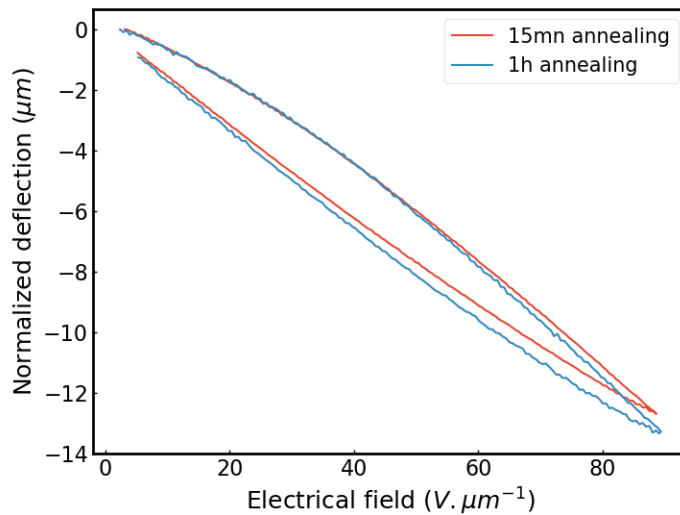


Figure 2.22: Normalized deflection of a FT annealed for 15 and 60mn

The difference is smaller than the statistical variation from supposedly identical samples (fig 2.18). The second annealing parameter is the temperature. Annealing below the Curie temperature or above the melting point is detrimental to the actuation performances [21] so we chose a temperature in between at 115°C. We made a few different samples to check if our choice of an identical annealing temperature for all terpolymers could impact the results. Fig 2.23 shows a RT (8.3% CTFE) and a FT (4%) CTFE annealed at 115°C and 125°C for 15 minutes.

Left panel is the RT, there is little to no difference between the two annealing temperatures. Regarding the FT, a slightly different first cycle hints that higher annealing temperatures might favor the ferroelectric behaviour. FT could possibly be slightly enhanced by different annealing

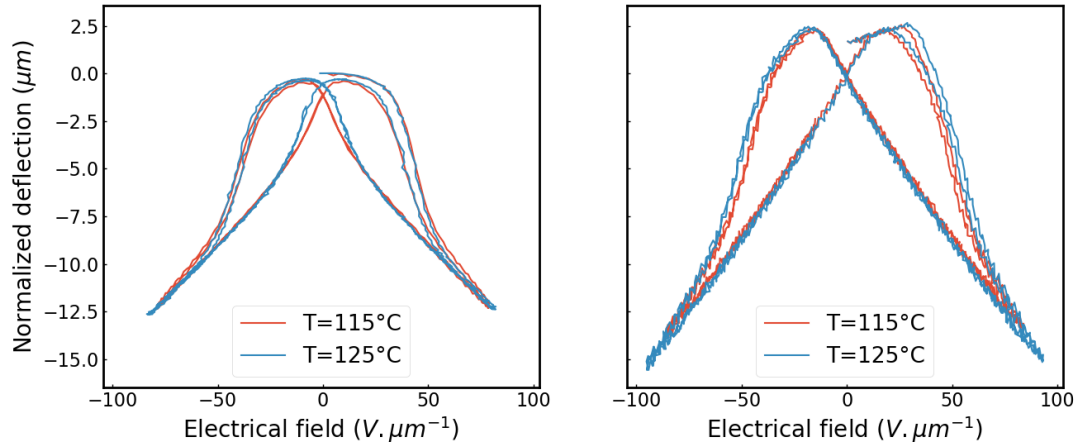


Figure 2.23: Normalized deflection of a RT (left) and a FT (right) annealed at 115° and 125 °

temperatures but the variations are small and would not change the above considerations.

VDF-TrFE ratio

The main difference between our nine terpolymers composition is their CTFE content. However, it is likely the VDF/TrFE ratio also plays an important role in the electromechanical behaviour. Fig 2.24 shows the impedance measurements of two terpolymers with the same CTFE amount but different VDF-TrFE contents, taken from [15].

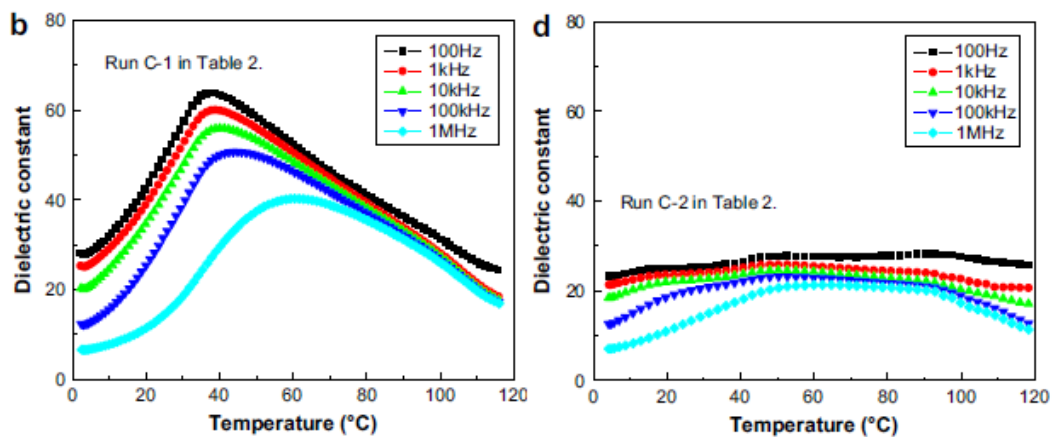


Figure 2.24: Permittivity as a function of temperature of two terpolymers. Left: 65.6/26.7/7.7 VDF/TrFE/CTFE. Right: 80.7/11.6/7.7, taken from [15]

The left panel is the permittivity of a 65.6/26.7/7.7 terpolymer and shows a frequency dependence typical of relaxor ferroelectrics. The right panel is the terpolymer 80.7/11.6/7.7 and its

response is that of a dielectric material, not of a relaxor. This shows how our study only holds for a particular VDF-TrFE ratio around 60/30 in P(VDF-TrFE-CTFE). However, it is easier to perform electrical measurements than mechanical ones and what we showed with this study is that the form to look for is that of a ferroelectric terpolymer.

Conclusion 8: Scope of the comparative study

The results of our comparative study should hold true for different processing conditions such as annealing temperature and duration. However the considerations on the terpolymer nature are very dependent on the VDF-TrFE ratio, a dimension we did not investigate.

2.5 Conclusion

In this chapter we assessed the capability of P(VDF-TrFE-CTFE) terpolymers to act as the active layer of an actuator. The actuators are cantilevers made using screen printing, which allows making different geometries in one run. With different lengths and widths it is possible to verify the match between the thin beam theory and our measurements. The length and thickness have the expected influence on the deflection which allows for a normalization of the data. Mostly because of the additional substrate around the edges, cantilever width also impacts the deflection. For the study presented here we get around this obstacle by only comparing beams with an identical 4mm width.

We studied nine different compositions starting with the copolymer (0% CTFE) up to 9.7 % CTFE content. The addition of CTFE transforms the copolymer into a relaxor but the transition is not gradual and the polymers can be separated into three families. From 2 to 7.5 % the terpolymers are still ferroelectric with a remanent polarization at 2-3 $\mu C.cm^{-2}$. We refer to them as ferroelectric terpolymers or simply FT. Past 7.5% CTFE content there is another change in the electromechanical response and the polymers fully translate into relaxors. Electrically there is no remanent polarization and the permittivity increases from 9 in copolymer to 18 in FT and 28 in RT. Mechanically the butterfly strain cycle disappears although the cycle is still hysteretic. The abrupt changes and the three distinct behaviours allow us to focus on only one composition of each polymers family. We measured the deflection and the polarization as a function of electrical field. Deflection is a figure of merit in itself but it also bears information on the blocking force and the elastic energy of the device. The electrical consumption is obtained with the polarization cycle and coupled with the elastic energy it gives our second figure of merit: electromechanical coupling. The main conclusions of the comparative study are displayed in the following table 2.25.










	Displacement/force		Coupling coefficient
	<i>Low-field</i>	<i>High-field</i>	
Copolymer			
Ferroelectric terpolymer			
Relaxor terpolymer			

Figure 2.25: Ranking of the three categories of polymer. The two figures of merit are the mechanical stress and the electromechanical coupling

For actuation purposes the choice of a polymer depends on the importance given to the stress generated and the energy consumption. In terms of deflection and blocking force the ferroelectric terpolymers turns out to be the best at high electrical fields and copolymer has the highest displacement below $40 \text{ V}\mu\text{m}^{-1}$. Regarding electromechanical coupling efficiency, the copolymer coefficient is about twice that of terpolymers and that is even without considering the increased leakage currents of terpolymers.

The choice in composition was based on the state of the art in the literature. However, there are a lot of other formulations for the VDF/TrFE/CTFE ratio, not to mention recent materials such as terpolymers blends with even more possible combinations. To avoid the tedious characterization of countless new recipes, it seems important to better understand the mechanisms at the origin of terpolymer performance. In the following chapter we will analyse the polarization-strain relationship of co- and ter-polymers in an effort to uncover the strain mechanisms at hand.

Bibliography

- [1] E. Defay, "Integration of Ferroelectric and Piezoelectric thin films," in *Integration of Ferroelectric and Piezoelectric thin films*, WILEY, 2011.
- [2] K. Koga, N. Nakano, T. Hattori, and H. Ohigashi, "Crystallization, field-induced phase transformation, thermally induced phase transition, and piezoelectric activity in p(vinylidene fluoride-trfe) copolymers with high molar content of vinylidene fluoride," *Journal of Applied Physics*, vol. 67, no. 2, pp. 965–974, 1990.
- [3] T. Furukawa and N. Seo, "Electrostriction as the origin of piezoelectricity in ferroelectric polymers," *Japanese Journal of Applied Physics*, vol. 29, no. 4R, p. 675, 1990.
- [4] A. A. Prabu, J. S. Lee, K. J. Kim, and H. S. Lee, "Infrared spectroscopic studies on crystallization and Curie transition behavior of ultrathin films of P(VDF/TrFE) (72/28)," *Vibrational Spectroscopy*, vol. 41, pp. 1–13, May 2006.
- [5] D. Mao, B. E. Gnade, and M. A. Quevedo-Lopez, "Ferroelectric properties and polarization switching kinetic of poly (vinylidene fluoride-trifluoroethylene) copolymer," in *Ferroelectrics* (M. Lallart, ed.), ch. 4, Rijeka: IntechOpen, 2011.
- [6] R. I. Mahdi, W. C. Gan, and W. H. A. Majid, "Hot Plate Annealing at a Low Temperature of a Thin Ferroelectric P(VDF-TrFE) Film with an Improved Crystalline Structure for Sensors and Actuators," *Sensors*, vol. 14, pp. 19115–19127, Oct. 2014.
- [7] O. Fabiane, L. Yves, M. Jan-Anders, S. Olha, N. Antonia, D. Alex, and D. Dragan, "Process influences on the structure, piezoelectric, and gas-barrier properties of pvdF-trfe copolymer," *Journal of Polymer Science Part B: Polymer Physics*, vol. 52, no. 7, pp. 496–506, 2014.
- [8] H. Ohigashi and K. Koga, "Ferroelectric copolymers of vinylidene fluoride and trifluoroethylene with a large electromechanical coupling factor," *Japanese Journal of Applied Physics*, vol. 21, no. 8A, p. L455, 1982.
- [9] H. Wang, Q. M. Zhang, L. E. Cross, and A. O. Sykes, "Piezoelectric, dielectric, and elastic properties of poly(vinylidene fluoride/trifluoroethylene)," *Journal of Applied Physics*, vol. 74, pp. 3394–3398, Sept. 1993.
- [10] W. Xia, Z. Xu, Q. Zhang, Z. Zhang, and Y. Chen, "Dependence of dielectric, ferroelectric, and piezoelectric properties on crystalline properties of p(VDF-co-TrFE) copolymers," *Journal of Polymer Science Part B: Polymer Physics*, vol. 50, pp. 1271–1276, Sept. 2012.
- [11] I. Katsouras, K. Asadi, M. Li, T. B. van Driel, K. S. Kjaer, D. Zhao, T. Lenz, Y. Gu, P. W. M. Blom, D. Damjanovic, M. M. Nielsen, and D. M. de Leeuw, "The negative piezoelectric effect of the ferroelectric polymer poly(vinylidene fluoride)," *nature materials*, 2015.

- [12] V. V. Kochervinskii, "Piezoelectricity in crystallizing ferroelectric polymers: Poly(vinylidene fluoride) and its copolymers (A review)," *Crystallography Reports*, vol. 48, pp. 649–675, July 2003.
- [13] A. Jain, P. K. J., A. K. Sharma, A. Jain, and R. P.n, "Dielectric and piezoelectric properties of PVDF/PZT composites: A review," *Polymer Engineering & Science*, vol. 55, pp. 1589–1616, July 2015.
- [14] H. Xu, Z.-Y. Cheng, D. Olson, T. Mai, Q. M. Zhang, and G. Kavarnos, "Ferroelectric and electromechanical properties of poly(vinylidene-fluoride-trifluoroethylene-chlorotrifluoroethylene) terpolymer," *Applied Physics Letters*, vol. 78, pp. 2360–2362, Apr. 2001.
- [15] Z. Zhang, Q. Meng, and T. C. M. Chung, "Energy storage study of ferroelectric poly(vinylidene fluoride-trifluoroethylene-chlorotrifluoroethylene) terpolymers," *Polymer*, vol. 50, pp. 707–715, Jan. 2009.
- [16] Z. Zhang and T. C. M. Chung, "The structure property relationship of poly(vinylidene difluoride) based polymers with energy storage and loss under applied electric fields," *Macromolecules*, vol. 40, no. 26, pp. 9391–9397, 2007.
- [17] X. Yin, Q. Liu, J. Galineau, P.-J. Cottinet, D. Guyomar, and J.-F. Capsal, "Enhanced electromechanical performances in plasticizer modified electrostrictive polymers," *European Polymer Journal*, vol. 76, pp. 88–98, Mar. 2016.
- [18] F. Ganet, M. Q. Le, J. F. Capsal, J. F. Gérard, S. Pruvost, J. Duchet, S. Livi, P. Lermusiaux, A. Millon, and P. J. Cottinet, "Haptic feedback using an all-organic electroactive polymer composite," *Sensors and Actuators B: Chemical*, vol. 220, pp. 1120–1130, Dec. 2015.
- [19] J.-F. Capsal, J. Galineau, M.-Q. Le, F. Domingues Dos Santos, and P.-J. Cottinet, "Enhanced electrostriction based on plasticized relaxor ferroelectric P(VDF-TrFE-CFE/CTFE) blends," *Journal of Polymer Science Part B: Polymer Physics*, vol. 53, pp. 1368–1379, Oct. 2015.
- [20] C. Huang, R. Klein, F. Xia, H. Li, Q. Zhang, F. Bauer, and Z. Cheng, "Poly(vinylidene fluoride-trifluoroethylene) based high performance electroactive polymers," *IEEE Transactions on Dielectrics and Electrical Insulation*, vol. 11, pp. 299–311, Apr. 2004.
- [21] Q. Liu, C. Richard, and J.-F. Capsal, "Control of crystal morphology and its effect on electromechanical performances of electrostrictive P(VDF-TrFE-CTFE) terpolymer," *European Polymer Journal*, vol. 91, pp. 46–60, June 2017.
- [22] F. Bauer, J. F. Capsal, Q. Larcher, and F. D. D. Santos, "Advances in relaxor ferroelectric terpolymer: New applications," in *2011 International Symposium on Applications of Ferro-*

- electrics (ISAF/PFM) and 2011 International Symposium on Piezoresponse Force Microscopy and Nanoscale Phenomena in Polar Materials*, pp. 1–4, July 2011.
- [23] S. Ahmed, Z. Ounaies, and E. A. F. Arrojado, “Electric field-induced bending and folding of polymer sheets,” *Sensors and Actuators A: Physical*, vol. 260, pp. 68–80, June 2017.
- [24] Ham.Yong-su, “Display device.”
- [25] Ham.Yong-su, “Touch sensitive element, display device comprising the same, and method for manufacturing the same.”
- [26] S. Khan, L. Lorenzelli, and R. S. Dahiya, “Technologies for printing sensors and electronics over large flexible substrates: A review,” *IEEE Sensors Journal*, vol. 15, pp. 3164–3185, June 2015.
- [27] A.Loi, “Inkjet printing: technique and applicationsfor organic electronic devices,” *Thesis manuscript*, 2012.
- [28] C.-H. Hsueh, S. Lee, and T.-H. Chuang, “An alternative method of solving multilayer bending problems,” *Journal of Applied Mechanics*, vol. 70, pp. 151–, 01 2003.
- [29] A. N. Hanna, U. S. Bhansali, M. A. Khan, and H. N. Alshareef, “Characterization of current transport in ferroelectric polymer devices,” *Organic Electronics*, vol. 15, pp. 22–28, Jan. 2014.
- [30] Y. Lu, J. Claude, B. Neese, Q. Zhang, and Q. Wang, “A modular approach to ferroelectric polymers with chemically tunable curie temperatures and dielectric constants,” *Journal of the American Chemical Society*, vol. 128, no. 25, pp. 8120–8121, 2006. PMID: 16787060.
- [31] X.-Z. Zhao, V. Bharti, Q. M. Zhang, T. Romotowski, F. Tito, and R. Ting, “Electromechanical properties of electrostrictive poly(vinylidene fluoride–trifluoroethylene) copolymer,” *Applied Physics Letters*, vol. 73, pp. 2054–2056, Oct. 1998.
- [32] R. J. Klein, F. Xia, Q. M. Zhang, and F. Bauer, “Influence of composition on relaxor ferroelectric and electromechanical properties of poly(vinylidene fluoride-trifluoroethylene- chlorofluoroethylene),” *Journal of Applied Physics*, vol. 97, no. 9, p. 094105, 2005.
- [33] N.Sigamani, “Effect of carbon nanofillers on the microstructure and electromechanical properties of electroactive polymers,” *Thesis manuscript*, 2015.

Chapter 3

Origin of strain in P(VDF-TrFE) and P(VDF-TrFE-CTFE)

3.1 Polymers under low electrical field

In this chapter we will try to understand the PVDF-TrFE copolymer and PVDF-TrFE-CTFE terpolymers behaviour through a study of their polarization-strain relationship.

3.1.1 Leakage measurements

In the previous chapter we got rid of the leakage currents contribution by acquiring at higher frequencies. However, it is likely that other contributions to the polarization cycle are also frequency dependent. Ideally, we want polarization measurements to be done at the actuation frequency and thus we need to isolate and remove the contribution of leakage currents.

The conduction mechanisms are not clearly identified in our polymers. In PVDF derivatives, electrons are injected in at the electrodes and can move through the sample with different regimes and conduction laws [1]. In a first attempt to remove the leakage currents from the polarization data, we performed IV measurements using an Agilent 4156C. The measurement principle as well as the results are displayed in fig 3.1.

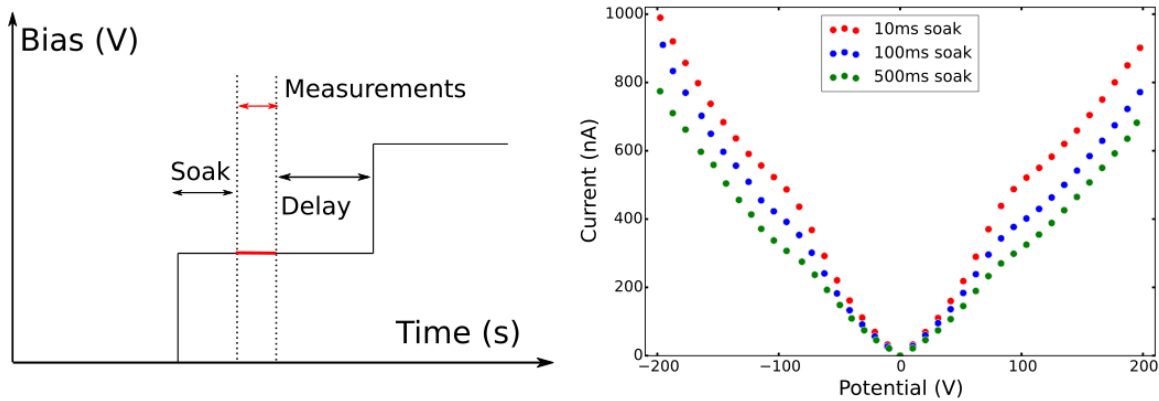


Figure 3.1: Left panel: $I(V)$ measurement principle. Right panel: leakage in a terpolymer with different setup parameters

We measure the static currents as a function of the applied electrical bias as represented in the left part. The soak time is here to avoid measuring capacitive contribution. At each bias step the current is acquired and averaged during 100ms which gives the leakage value at a given electrical bias. The right panel in fig 3.1 shows the leakage of the device with different soak times. The amount of leakage in the sample depends on the measurement parameters and mostly on the soak time. This is likely to be due to slow relaxations processes taking place in the amorphous part of terpolymers [2].

To understand what is the impact of the leakage currents on the measured polarization response we can calculate the cycle of polarization of a purely resistive component using equation 3.1.

$$Q(V) = \int_0^{t_{max}} GV(t)dt \quad (3.1)$$

Q: charge measured at the electrodes
 G: device conductance
 V: electrical waveform

This equation is based on the approximation that the leakage current is linear with respect to the electrical potential. We can now compare the estimated effect of leakage currents to the actual polarization cycle of our terpolymer (fig 3.2).

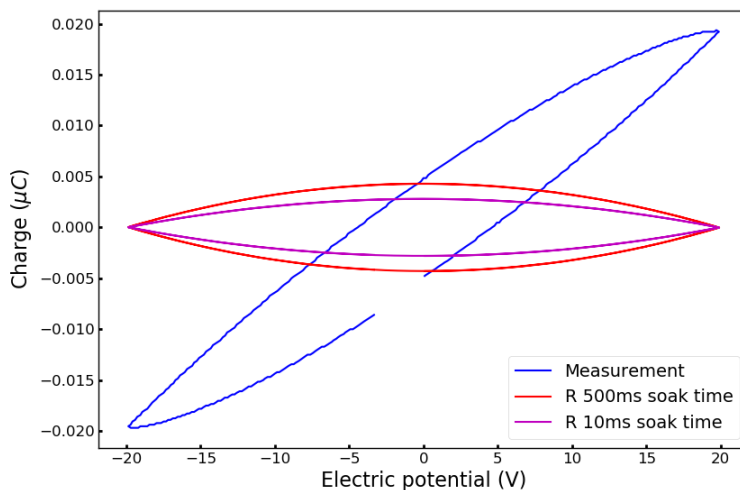


Figure 3.2: Electrical response of the device when submitted to a 1Hz triangular waveform. The red and purple curves are the calculated cycles of a pure resistor whose value is taken from two different soak times in fig 3.1.

Fig 3.2 shows that the leakage currents distort the charge cycle and are responsible for a good portion of its opening. The blue cycle is a standard polarization measurement acquired using the radiant tester, as described in the previous chapter. The red and purple cycles are the calculated cycles of a pure resistor whose resistance value is taken calculated from the red and purple leakage dataset in fig 3.1. The order of magnitude is correct but the uncertainty on the device conductance makes it difficult to make sure that leakage currents alone are responsible for the polarization cycle opening.

3.1.2 Permittivity and dielectric losses

The polymers are dielectric materials and as such can be polarized when an electrical field is applied. From a physical point of view this polarization may come from several contributions as represented in fig 3.3.

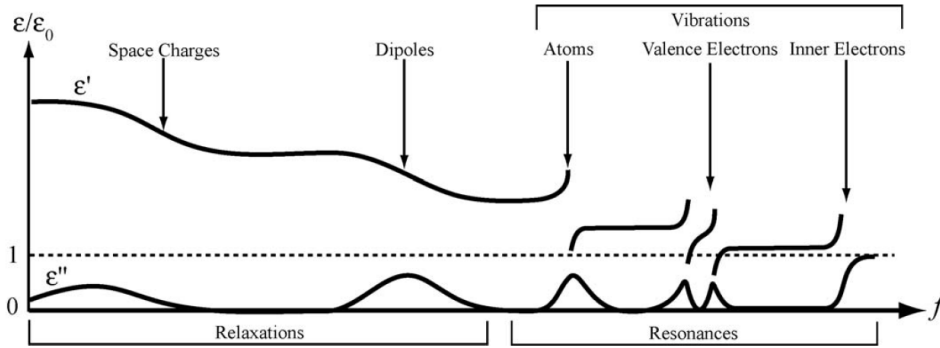


Figure 3.3: Contribution of different mechanisms to the overall permittivity of a material, taken from [3]

The permittivity has been introduced in the previous chapter with equation 2.1. From an electrical circuit point of view, an ideal dielectric with a permittivity ϵ gives an ideal capacitor as shown in equation 3.2

$$\begin{aligned} \frac{D}{S} &= \frac{\epsilon V}{S e} \\ Q &= CV \end{aligned} \quad (3.2)$$

- D: Electrical displacement of an ideal dielectric
- S: device surface
- e: device thickness
- Q: charge measured at the electrodes
- C device capacitance
- V: electrical potential

In equation 3.2 if $\epsilon \gg \epsilon_0$, D can be approximated by the material polarization P . This equations shows why an ideal dielectric material is the electrical equivalent of a pure capacitance. However, a material is never ideal and regardless of their speed the physical mechanisms at the origin of the polarization need some time to reach equilibrium. This translates into a polarization response slightly out of phase with the electrical field and is described by complex permittivity, following equation 3.3.

$$\epsilon = \epsilon' + i\epsilon'' \quad (3.3)$$

ϵ : complex permittivity

ϵ' : real part

ϵ'' : imaginary part

The phase difference experimentally measured is called δ_{elec} and is linked to permittivity through equation 3.4

$$\tan(\delta_{elec}) = \frac{\epsilon''}{\epsilon'} \quad (3.4)$$

δ_{elec} = phase difference between polarization and electrical field

To understand how this phase shift affects the polarization measurements we simulated the polarization cycle of a dielectric with $\epsilon' = 30$ and different values for the dielectric losses (fig 3.4). We switched from a triangular waveform in fig 3.2 to a sinusoidal waveform for the electrical potential. This does not affect the following considerations but is more suited to the complex formalism and easier to manipulate.

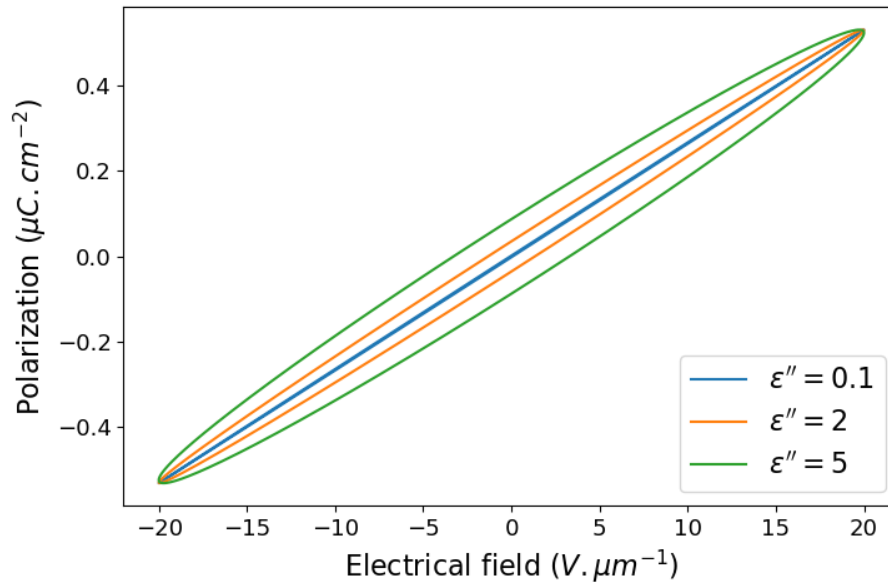


Figure 3.4: Calculated polarization cycle at 1Hz of a dielectric material with a permittivity of 30 and various amounts of dielectric losses.

Figure 3.4 shows how polarization mechanisms lagging behind the electrical field impact the polarization measurements. The effect is similar to that of leakage currents, resulting in an elliptical polarization cycle. To model the lag with an equivalent electrical circuit, a resistor is added in series with the ideal capacitance. A parallel resistance the same as the leakage

contribution also results in a phase shift but only a series resistor introduces a time constant in the system that can model properly the transient response and the relaxation effects. This equivalent R-C series branch is also suited to model the mechanism frequency evolution, as described in the Debye relaxation theory.

In an actual dielectric several mechanisms can contribute to the polarization response, as presented in figure 3.3. Each one has its own time response and adds up to make the total electrical current, which is the value that we actually measure. Electrically, the physical mechanisms correspond to R-C series branches in parallel with one another. Figure 3.5 shows the polarization cycle and equivalent electrical circuit of a theoretical dielectric with two different mechanisms.

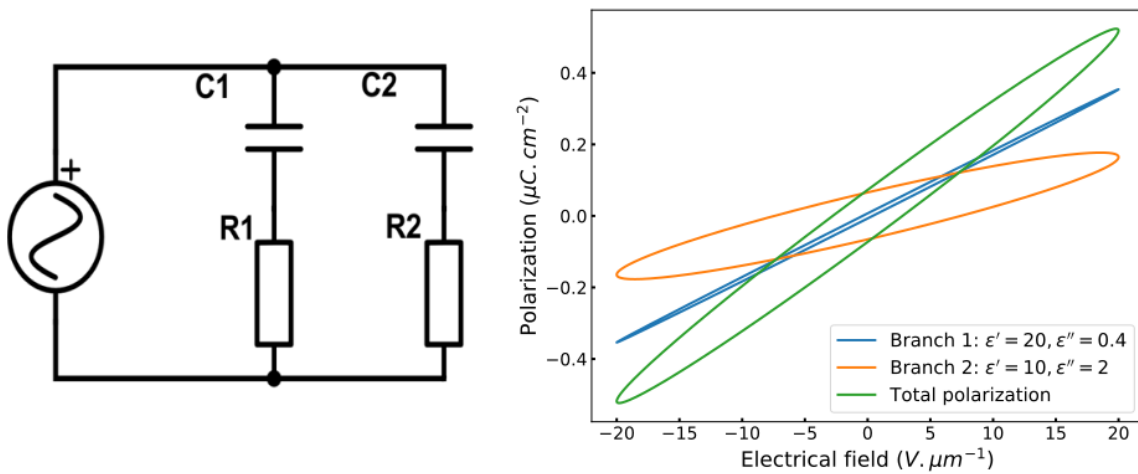


Figure 3.5: Theoretical material with two polarization mechanisms. Left is the equivalent electrical circuit and right the resulting polarization. Only the green cycle is accessible through measurement

Each branch contributes to the overall polarization with its own amplitude and phase shift (orange and blue cycles). What we would measure with our radiant tester is only their sum, i.e. the green cycle. From the tilt and the ellipse opening we could extract a capacitance and a resistor equivalent to the whole circuit but not identify the two contributions. This is pretty much the process done in a LCR meter with the measurement of the current gain and phase.

Conclusion 9: Leakage current permittivity and dielectric losses

Leaked charges are free charges flowing through the sample while dielectric losses are bound charges lagging behind the electrical field. We want to remove the leakage currents from the polarization cycles but their contribution to the charge measurement is mixed to the capacitive response. IV measurements give a good idea of their amplitude but the dynamic relaxations in the material render this approach unsuitable for a quantitative analysis.

3.1.3 Making use of the raw data

The polymers studied here are dielectric materials with possibly several contributions to the polarization response. As we discussed in the section above, each one is electrically equivalent to a RC branch in parallel with the rest. Based on our observations detailed hereafter and on the work in [2], a good electrical equivalent of the polymers is the circuit in fig 3.6.

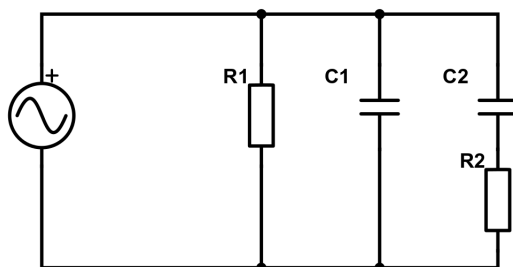


Figure 3.6: Equivalent electrical circuit of a polymer at low frequencies and electrical bias

In figure 3.6, the $R_2 - C_2$ series branch is a 'slow' polarization mechanism that lags noticeably behind the electrical field. The other polarization mechanisms respond much faster and are modelled by an ideal capacitance C_1 and the pure losses are accounted for by the R_1 resistor. As we said before, the different contributions are mixed indistinguishably giving a tilted ellipse as a result of the polarization measurement. However, this only corresponds to the polymer response in established regime and analyzing the transient regime should yield additional information. To better illustrate this consideration we used a breadboard with discrete components to reproduce the circuit in figure 3.6. We can measure the full polarization cycle but also each separate branches in the circuit, as displayed in fig 3.7.

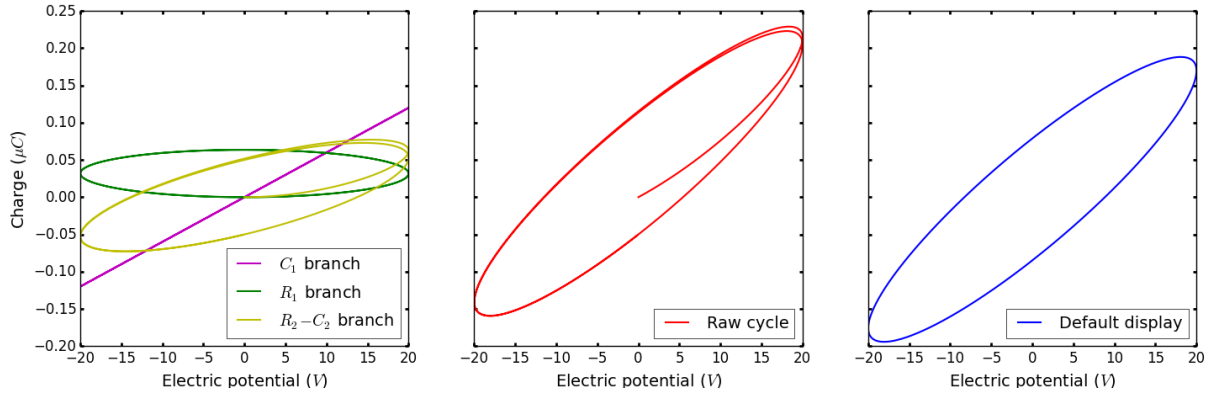


Figure 3.7: Polarization cycle of the electrical circuit in fig 3.6 made with discrete components, at 200Hz. Left: Separate measurement of each branch. Center: polarization cycle of the whole circuit. Left: Polarization cycle actually displayed with default tester settings.

In figure 3.7, the first panel displays the polarization cycles of the three circuit branch in 3.6, measured separately. The second panel is the polarization cycle of the entire circuit. The right panel is the polarization cycle displayed with the radiant default settings. The blue cycle is the reason why we said in the previous examples that the only accessible parameters are the ellipse tilt and opening (or gain and phase in an impedance-meter). There is a post-measurement processing step in the Radiant tester, consisting in a removal of the first polarization cycle and a centering of remaining cycle. This is the default configuration of the tester and also a standard of polarization measurements. In ferroelectric materials the charge state at the electrode is not null at $t=0$, thus the centred cycle is the actual charge value at the electrode. However, in a dielectric material there is no reason to do so and we lose potentially useful information.

1- The transient response is the consequence of polarization lagging behind the electrical field (R_2). Yellow cycle in figure 3.7

2- The offset is only due to the pure losses (R_1). Green cycle in figure 3.7

The first point is pretty straightforward, a pure resistor or capacitance does not have a transient response. To justify the second point we will show that once the transient response is over in an R-C series branch, the positive and negative "remanent polarization" have opposite values. Therefore the higher positive value is only coming from the pure losses.

$$Q_{RC}(t) = Q_1(\sin(\omega t + \delta) - \sin(\delta)e^{-\frac{t}{\tau}}) \quad (3.5)$$

Q_{RC} : charge

Q_1 : amplitude

τ : time constant

ω : pulsation

δ : phase shift

The above equation describes the temporal evolution of the charge in an R-C series branch. Calling T the sinusoid period, the "remanent polarization" is positive when the time is an odd multiple of the half period and negative when it is an even multiple. This gives eq 3.6

$$\begin{aligned} Q_{RC+}(n) &= Q_1 \sin(\delta) (1 - e^{-\frac{(2n+1)T}{2\tau}}) \\ Q_{RC-}(n) &= Q_1 \sin(\delta) (-1 - e^{-\frac{nT}{\tau}}) \end{aligned} \quad (3.6)$$

$Q_{RC\pm}$: remanent polarization
n: positive integer, n-th cycle
T: period of the sinusoid

Equation 3.6 is the expression of the positive and negative "remanent polarization" as a function of the number of cycles. If n is high enough we are in the permanent regime and the two values are opposite. At the frequencies we deal with, the transient regime is over by the end of the first cycle (n=2). Therefore, the leakage current is the only possible explanation to the polarization offset and the difference between the positive and negative "remanent polarization" we observe. Now we can remove the leakage currents directly and calculate the mean conductance in the process (equation 3.7).

$$G = \frac{2\omega \Delta Q_{remn}}{U_0} \quad (3.7)$$

G: Device conductance
 ω : sinusoid pulsation
 U_0 : sinusoid amplitude
 ΔQ_{remn} : difference between remanent polarizations (\pm)

Once leakage contribution is removed, the ellipse opening is only due to the phase offset δ_{elec} giving the first equation to identify the R_2C_2 components. The other equation is obtained with the difference between first and second cycle, ascribed to the transient regime in the R_2C_2 branch. The remaining polarization is a linear slope, due to the parallel capacitance response. With these four equations, we get an analytical system to identify the different components. The system is not linear and a numerical solution is more easily obtained. Applying it to the breadboard circuit of fig 3.7 gives the values in table 3.1.

	R_p ($k\Omega$)	C_p (nF)	R ($k\Omega$)	C (nF)
Manufacturer	100	10	47	10
Extracted	98.7	10.1	46.8	9.84

Table 3.1: Manufacturer and extracted values

With a single polarization cycle we successfully identified each component and especially the pure losses present in the dummy circuit. The following question was whether this could be applied to P(VDF-TrFE) and P(VDF-TrFE-CTFE). Figure 3.8 is an example of a terpolymer sample polarization cycle at 0.4Hz and 6.3Hz with a maximum electrical field inferior to $2V.\mu m^{-1}$.

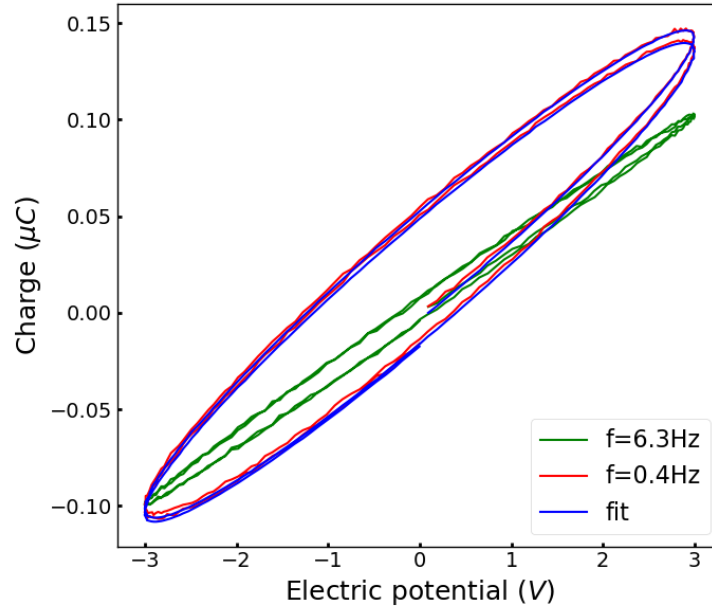


Figure 3.8: Polarization of a terpolymer at 6.3Hz and at 0.4Hz with the result of the fit

The red cycle in figure 3.8 is measured at 0.4 Hz and the blue cycle is the fit calculated with the equivalent electrical circuit in figure 3.6. This is very similar to the test circuit studied above and at low electrical fields co and ter-polymers behave as lossy dielectric materials. Physically this can be interpreted as one capacitive contribution with a long time response (RC serieis) while the others capacitive mechanisms are all much faster and represented by the same parallel capacitance. In figure 3.8 the green cycle is the terpolymer polarization acquired at 6.3 Hz. The cycle is almost symmetrical and the transient regime is over quickly. The polarization mechanism modelled by the R-C series branch only occurs at low frequencies. We can quantify the frequency dependence by monitoring the equivalent circuits components values, as displayed in figure 3.9.

The $R_2 - C_2$ branch decays rapidly which is consistent with a phenomenon such as ions displacement [4], interfacial polarization [5] or, relaxations in the amorphous phase [2]. Our electromechanical measurements are conducted at 1 or 2 Hz (our maximum actuation frequency) and the dielectric losses are limited. The leakage currents have an important impact on the measurement but can be easily removed as discussed above. The "low electrical fields" denomination includes electrical fields up to $20V.\mu m^{-1}$. Above that value, the aforementioned description cannot properly describe the polarization cycle.

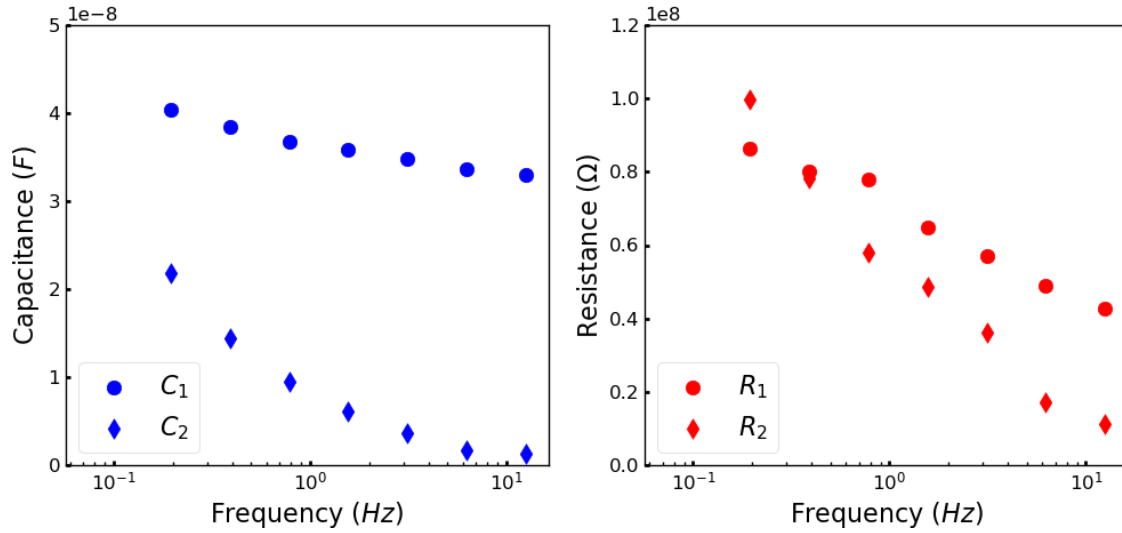


Figure 3.9: Evolution of the extracted electrical components as a function of frequency. On the left series and parallel capacitance and on the right series and parallel resistance

Conclusion 10: Making use of the raw data

Complete polarization data contain more information on the dielectric material than an impedance measurement. Using the transient response of the material we can model the polarization cycle of our polymers with an electrical circuit. The principal interest of this approach is that it constitutes a simple way to remove the contributions of leakage current directly from the remanent polarization asymmetry.

3.2 Transition to high electrical fields

At low electrical fields, both copolymer and terpolymers behave as lossy dielectric materials. Moving on to higher electrical fields the non-linear behaviour due to their ferroelectric and relaxor nature are expected to come into play.

3.2.1 Copolymer

Aside from the losses, we observed that the slope of the polarization curve matched the capacitance value below $20 \text{ V} \cdot \mu\text{m}^{-1}$. We check if this holds as the electrical field is increased from 20 to $80 \text{ V} \cdot \mu\text{m}^{-1}$. The measurements are done with unipolar cycles in order to avoid the switching of ferroelectric domains and the results are displayed in fig 3.10.

Fig 3.10 displays the unipolar polarization cycle of a copolymer at different electrical fields. We also added the theoretical response of an ideal dielectric material with a permittivity of $\epsilon_r = 10$ corresponding to the polymer value. At $80 \text{ V} \cdot \mu\text{m}^{-1}$ the polarization reaches $1 \mu\text{C} \cdot \text{cm}^{-2}$ instead

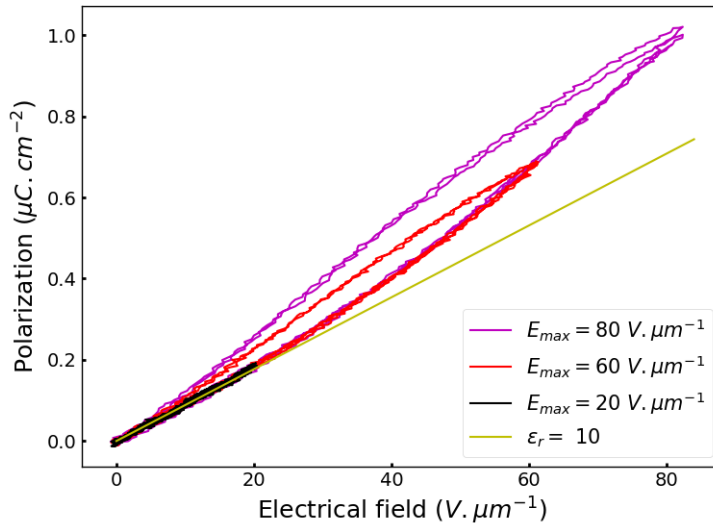


Figure 3.10: Unipolar polarization cycles of a copolymer with different electrical fields amplitudes.

of the expected $0.8 \mu C.cm^{-2}$ and shows significant hysteresis following the Rayleigh law [6]. So the polarization exhibits a deviation of $\approx 25\%$ from the capacitive behaviour due to an additional hysteretic contribution. From a physical point of view this kind of behaviour could be attributed to orientation of ferroelectric domains not fully aligned with the other crystallites or could stem from field induced crystallization of the amorphous/crystalline interface.

The second deviation from the lossy dielectric behaviour is due to the ferroelectric nature of the copolymer. The ferroelectric domains can be switched if the electrical field is strong enough to overcome their cooperation. If we submit the copolymer to a unipolar signal, the domains may or may not be switched depending on their initial orientation. Using that feature we can get the signature of the ferroelectric domain switching as the difference between the response to the same solicitation but with different starting polarization states (up or down). That is the principle behind the established PUND method available in the Radiant tester software. Figure 3.11 shows the measured cycles and the resulting ferroelectric cycle.

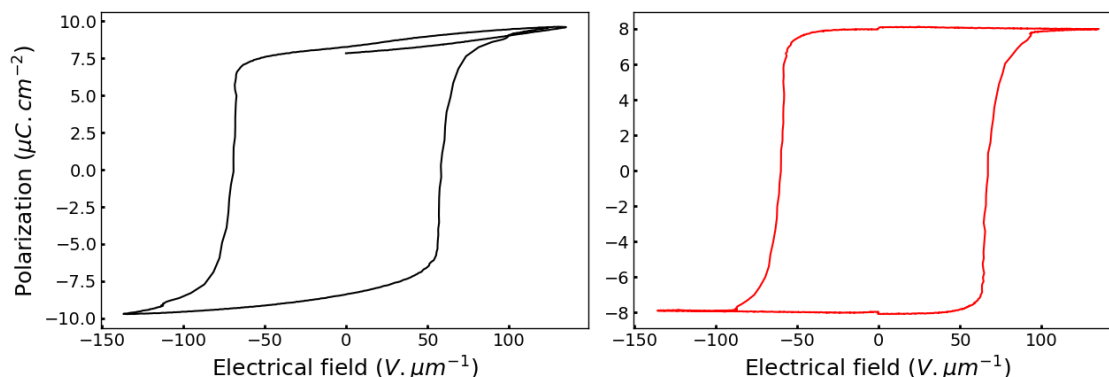


Figure 3.11: Left: polarization cycle of a copolymer with its ferroelectric domains oriented positively. Right: polarization signature of the ferroelectric switching obtained from the left figure

The left panel in figure 3.11 shows the polarization response of a copolymer biased positively before the measurement. The small loop is similar to the unipolar cycle in fig 3.10 because we do not switch any ferroelectric domain. Subtracting this loop to the full cycle gives the ferroelectric cycle displayed in the right panel. The ferroelectric contribution to the polarization is easily accessible through measurement. This will be of use when we attempt to explain how this ferroelectric domain switching impacts the copolymer strain response.

Conclusion 11: Copolymer at high fields

The capacitance measurements cannot describe the unipolar polarization cycles in their entirety. An hysteretic phenomena also contributes to the polarization response, it accounts for 20% of the total value at $80 V.\mu m^{-1}$. In bipolar regime, that contribution is superimposed to the polarization variation induced by ferroelectric domains switching. The ferroelectric cycle can easily be isolated with the adapted method.

3.2.2 Terpolymer

As we mentioned before, the leakage current in terpolymers cannot be neglected. We apply the principle discussed previously to remove the contribution of said current. This approach supposes that no ferroelectric contribution is present in the material. The leakage correction applied to a terpolymer cycle is shown fig 3.12

The left panel of fig 3.12 displays the polarization cycle at 1 and 20Hz of a terpolymer. The right panel shows the corrected 1 Hz cycle assuming an ohmic leakage current, and the 20Hz cycle as an element of comparison. The difference between the two cycles is due to the frequency dependence of other contributions.

Once the leakage correction is applied we have polarization data only depending on the bound

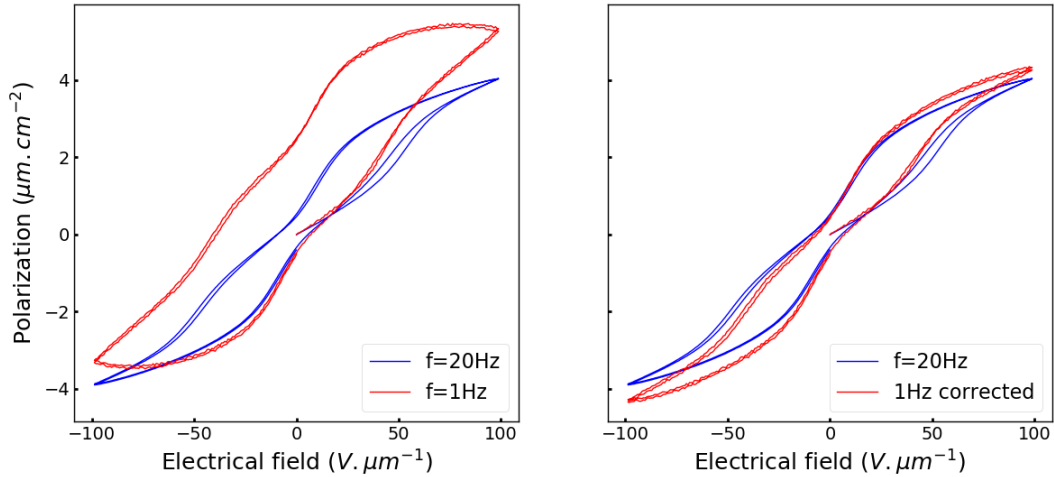


Figure 3.12: Left: polarization cycle of a terpolymer at 1Hz and 20 Hz. Right: 1Hz cycle after correction, the 20Hz cycle is left as an element of comparison

charges of the system. We want to break down this response as much as possible for the analyze of strain-polarization dependence in terpolymers. That way we can correlate any mechanical oddities to a particular contribution. We start by looking at how the polarization cycle relates to the capacitance measurements. The capacitance of three types of polymers as a function of the electrical field are measured with an impedance-meter and displayed in fig 3.13. We also added the PVDF-TrFE-CFE measurement for the following section.

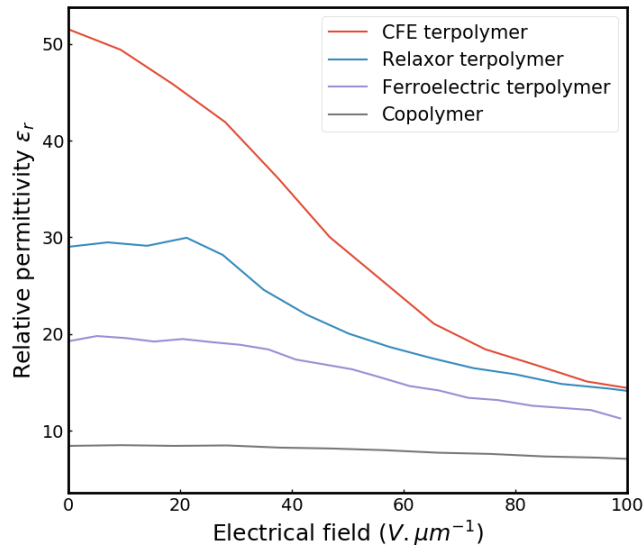


Figure 3.13: Capacitance as a function of the electrical field of the different types of polymers

We saw in the previous chapter how the addition of CTFE in the copolymer transforms it and, among other changes, increases its permittivity. Fig 3.13 shows that the new capacitive

mechanism introduced depends on the electrical field. Without bias the relaxor terpolymer has an ϵ_r of 29, 3.5 times that of the copolymer while at $100 \text{ V}\mu\text{m}^{-1}$ it is only twice as high. Understanding the origin of this electrical field dependence would require to know the origin of the increased permittivity, which is still debated to this day [7], [8]. Regardless of the origin, what we want to estimate here is how this impacts our polarization measurements, using equation 3.8.

$$P_{capa} = \int_0^{E_{max}} \epsilon_0 \epsilon_r(E) dE \quad (3.8)$$

P_{capa} = reversible polarization when the material is submitted to small electrical variations.

Applying equation 3.8 to data in fig 3.13 gives us what we refer to hereafter as capacitive or dielectric polarization. The associated mechanisms are reversible and the typical mechanisms are shown in figure 3.3. Although there are associated losses we dismiss them as small enough not to interfere with our study. The dielectric polarization of each polymer is represented in figure 3.14.

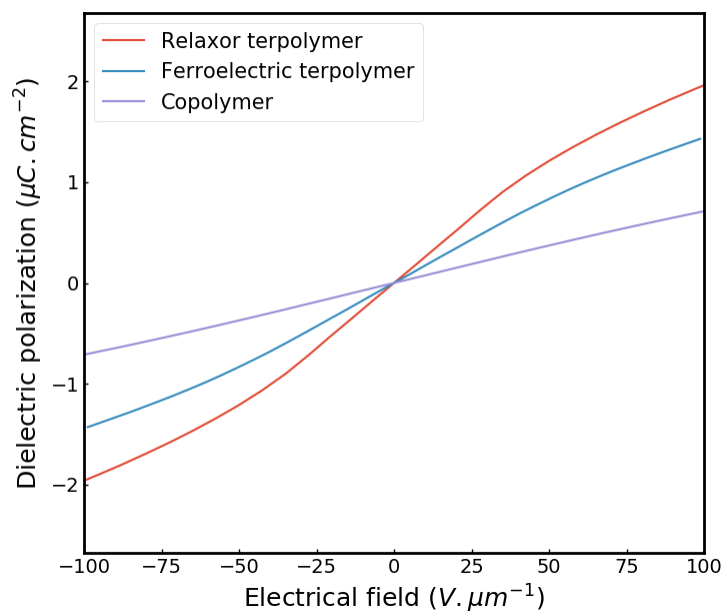


Figure 3.14: Calculated polarization response of a dielectric with the measured capacitance values

The copolymer small signal (or dielectric) polarization is almost linear but not that of terpolymers which are better described by a Langevin function [9]. Having isolated the dielectric polarization we compare it to the total cycle in figure 3.15.

On the left panel we have the polarization cycle of a terpolymer with leakage correction alongside the dielectric polarization. The right panel is the difference between the two cycles. This cycle does not show Rayleigh nonlinearities at high electrical fields unlike what we observed in

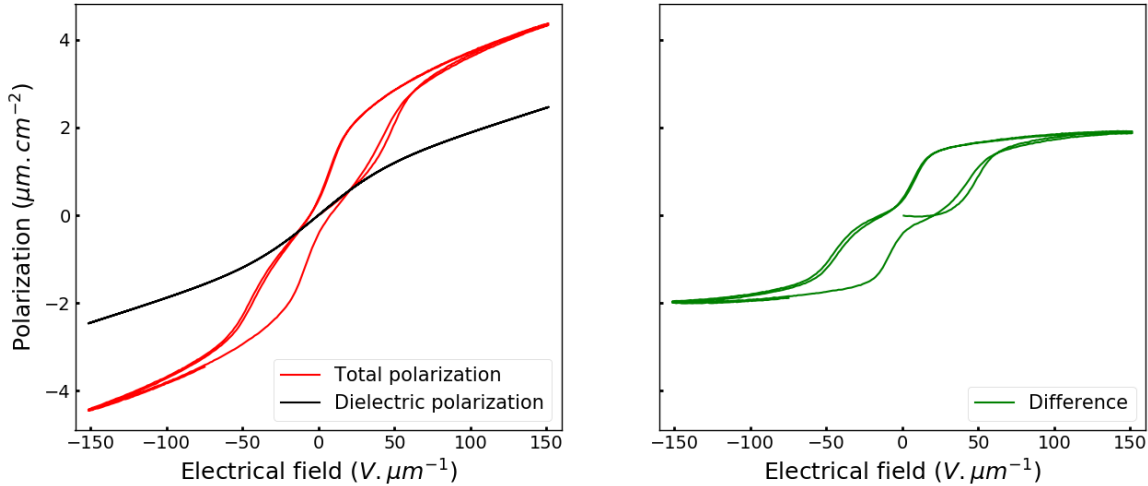


Figure 3.15: Left: Polarization cycle of a terpolymer alongside with the polarization calculated from capacitance measurements. Right: difference between the two left cycle, this hysteretic behavior is ascribed to a field-induced phase transition

copolymer (fig 3.10). As we can see, the dielectric polarization only account for half of the total polarization value reached at $100 \text{ V}\mu\text{m}^{-1}$. Another contribution is present, whose shape (green cycle) reminds of an anti-ferroelectric cycle. The green (and red) cycles are identical regardless of the previous polarization state in the material thus there is no ferroelectric contribution. We propose that save from some dielectric losses and leakage correction error, the green cycle in the right panel is due to a phase transition of the crystal phase toward a more polar phase. This hypothesis is based on reports in the literature of such phenomenon happening in another PVDF derivative, the PVDF-TrFE-CFE.

Conclusion 12: Terpolymers at high fields

At high electrical fields the capacitance becomes field dependent leading to a diminution of the corresponding polarization. Besides capacitive and resistive response, a third component must be added to fully describe the polarization cycle. This contribution is hysteretic and resembles that of an anti-ferroelectric material.

Phase transition in the litterature

There is no direct evidence of an electrically induced transition toward a ferroelectric phase in terpolymers but the existence of such a transition was inferred soon after the discovery of their important strain response [10]. The current understanding of the micro-structural arrangement of terpolymer chains is for a good part based on the work of Yang & al. Yang worked toward a description linking the terpolymers polarization response and their chains conformation [7] [4] [11]. The following picture is a summary of the impact of CFE and CTFE in the copolymer chain.

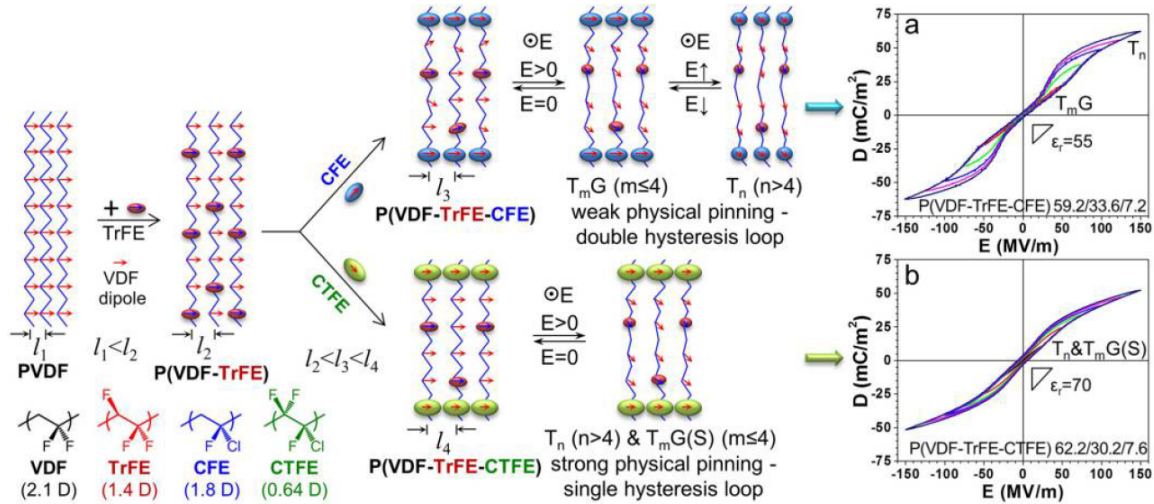


Figure 3.16: Impact of the introduction of CFE/CTFE monomers in the copolymer chain and resulting polarization cycle. Taken from [7]

On the left side a PVDF domain is represented, with a distance l_1 between chains. The introduction of TrFE in the chain increases the interchain distance, allowing for the addition of bigger third monomer like CTFE or CFE. The case of CFE is represented in the upper row and CTFE in the lower row. The CFE monomers, containing a large chlorine atom, pin the ferroelectric domains every few VDF-TrFE repetitions. When an electrical field is applied the dipoles in-between two CFE monomers can freely rotate with little regard to the rest of the chain. At higher electrical fields the CFE monomers also rotate and the global cooperation induces an opening of the polarization cycle. This CFE "unpinning" was described as a field-induced phase transition toward a ferroelectric phase. The P(VDF-TrFE-CFE) polarization cycle is referred to as double hysteresis loop (DHL).

In figure 3.16 the case of CTFE is represented in the lower row and differs from that of CFE. The idea is similar except that a stronger pinning renders the orientation of the CTFE monomers impossible which results in a single hysteresis loop (SHL) with no phase transition. Zhu & al proposed a classification of the different dielectric materials based on the degree of cooperation between dipoles (fig 3.17).

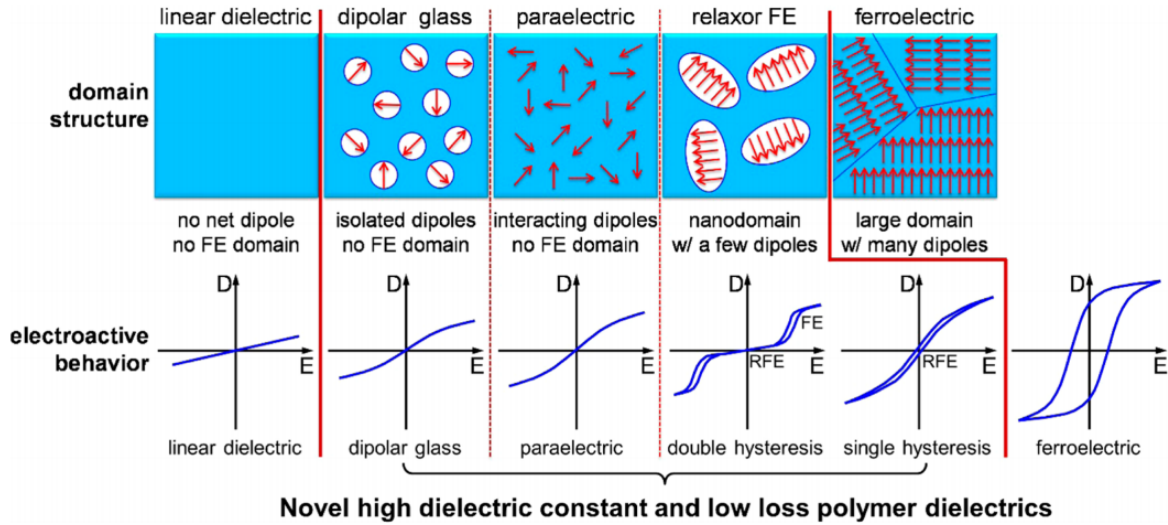


Figure 3.17: Classification of the categories of dielectrics with different levels of cooperation. Taken from [12]

In figure 3.17 lower row, the CFE terpolymers would be the 4th electroactive behaviour starting from the left, and CTFE the 5th. However, the residual polarization cycle we isolated in $P(VDF-TrFE-CTFE)$ reminds of the DHL i.e the 4th schematic representation. Therefore, we propose that the green polarization cycle in figure 3.15 is also the signature of a field-induced phase transition toward a ferroelectric FE phase. Although Yang & al suggested that such transition does not occur in CTFE, it could simply be less discernible. This DHL behaviour is actually visible in our polarization cycles and has also been reported in another study [11].

It should be noted that the polymers in figure 3.16 were uni-axially stretched, maybe making it more difficult to observe the DHL in $P(VDF-TrFE-CTFE)$. Still, the DHL does not need to be visible to infer the presence of the so-called phase transition. This can be observed with the discrepancy between permittivity values calculated from the polarization cycle slope and those measured with an impedance-meter.

If extracted from the polarization cycle in fig 3.16, $P(VDF-TrFE-CTFE)$ permittivity reaches 70 while with impedance measurements we measure it at 30. Therefore the polarization cycle must be enhanced by an additional hysteretic contribution.

We can note that in the case of CFE terpolymers, the two methods give an identical permittivity value, around 50 (fig 3.13). As the "field induced phase transition" is only present at higher electrical fields, it does not impact the polarization value near $0 \text{ V } \mu\text{m}^{-1}$ and the explanation on RFE behaviour is consistent with both polarization and impedance measurements.

There are no direct evidence of a field-induced phase transition in terpolymers and the mechanisms behind the relaxor ferroelectric nature are still debated [8]. Still, this hypothesis describes

quite well the polarization cycles of PVDF derivatives and explains the anti-ferroelectric like cycle in figure 3.15. In the following section we will try to see if this explanation is consistent with the strain response of terpolymers.

Conclusion 13: Phase transition in the literature

The DHL (double hysteresis loop) has been observed in P(DVF-TrFE-CFE) and ascribed to a field-induced phase transition. It is very likely that the same thing occurs in P(DVF-TrFE-CTFE). Having removed leakage and capacitive contributions from the polarization cycle we even isolated the electrical signature of this supposed transition.

Polarization at higher temperatures

We break down the polarization cycle of our terpolymer as the sum of leakage currents, (lossy) capacitance and phase transition cycle. To strengthen this approach we look at how polarization evolves with temperature and check whether this evolution is consistent with our description. Fig 3.18 displays the permittivity measured without electrical bias between 12 and 75°C.

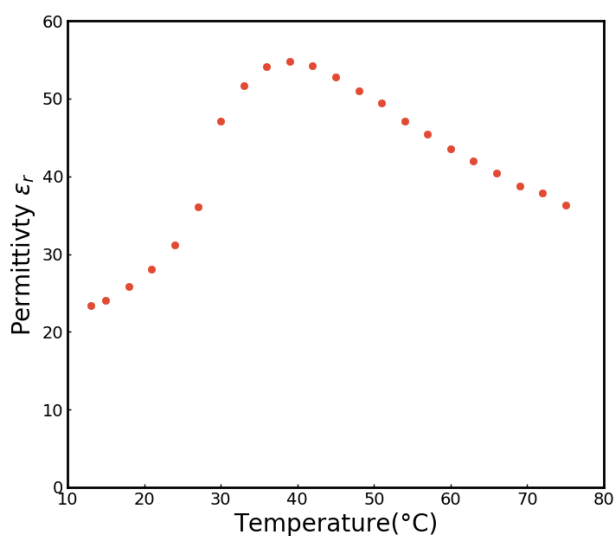


Figure 3.18: Evolution of the permittivity at 0V with temperature of a relaxor terpolymer. The peak position is the Curie temperature

In figure 3.18 the Curie temperature is the peak maximum position, located around 40°C in this 8.3% CTFE terpolymer. We assume that past the curie temperature the field induced phase transition is at least partially inhibited. We will verify this assumption with X-Ray analysis in the following chapter. The idea is to compare the polarization cycles below and above the Curie temperature. Permittivity, dielectric losses and leakage are all function of the temperature

but we hope these variations are small enough not to hinder the interpretation. The measured polarization cycles are showed in 3.19.

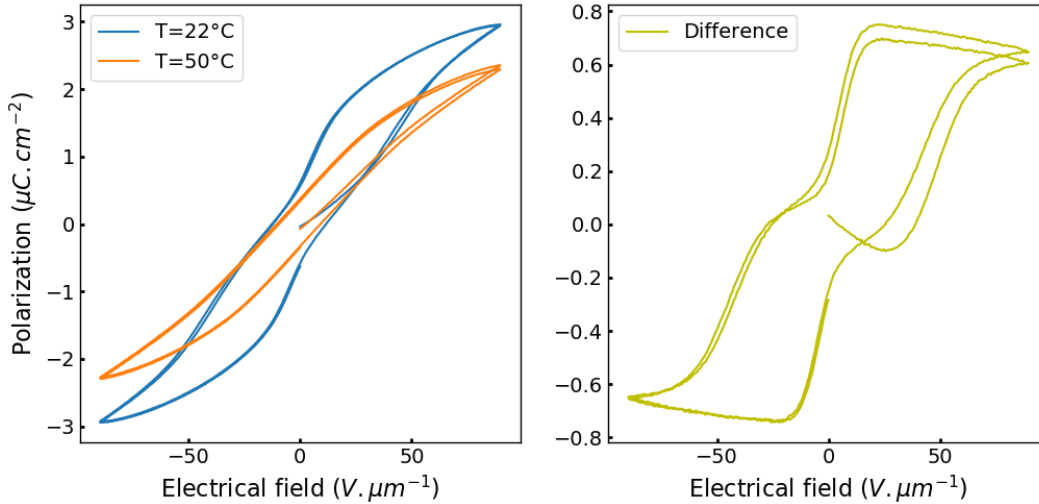


Figure 3.19: Left: polarization cycles measured at 22°C and 50°C at 20Hz (raw data). Right: difference between the two cycles.

On the left panel of fig 3.19 we measured the polarization cycle of a device at 22°C and 50°C. We chose this temperature and not a higher one because the dielectric losses increase dramatically with the temperature and interfere with our measurements. The measurements are made at 20Hz on this particular dataset thus we do not apply a leakage correction and these are raw data. As it turns out, the difference between the two polarization cycles results in a clean signature, much like the anti-ferroelectric cycle in figure 3.15. This result supports the aforementioned hypothesis: polarization cycles of PVDF-TrFE-CTFE at ambient temperature are the sum of a capacitive response and an hysteretic cycle attributable to field induced phase transition. Above the Curie transition, this transition is not present any longer.

Conclusion 14: Polarization at higher temperatures

By comparing the polarization cycle below and above the Curie temperature we isolate once again the polarization signature of phase transition.

3.3 Strain

We now have a good understanding of the meaning of a polarization cycle and will try to correlate it with the strain response of the polymers.

3.3.1 In terpolymers

State of the art of strain in terpolymers

We start with a quick overview of the current understanding of the strain origin in terpolymers. In this state of the art, the term "terpolymers" refers indistinguishably to our polymers (PVDF-TrFE-CTFE) or to PVDF-TrFE-CFE. This is because the literature is rather scarce on the subject and these polymers are likely to share similar strain mechanisms.

Terpolymers are said to be electrostrictive materials [5], [13] but saying of a material that it is electrostrictive does not explain the underlying physical mechanisms. It is merely a statement that follows the phenomenological law:

$$S = QP^2 \quad (3.9)$$

S: strain

Q: electrostrictive coefficient

P: Polarization

The squared term in equation 3.9 implies that an electrostrictive material can only be strained in one direction. Ceramics typically have a positive Q_{33} coefficient while PVDF and its derivatives have a negative Q_{33} (the subscript has been introduced in chapter 2). There are several physical effects that can induce strain in a material submitted to an electrical field. For an overview of electrostrictive mechanisms, one can look at the work of Li & al [14]. In terpolymers there are three likely candidates contributing to electrostriction.

- 1- Electrically induced phase transition
- 2- Intrinsic electrostriction
- 3- Maxwell stress

The phase transition would induce a strain in the material because of the lattice difference between the two conformations. After the discovery of the relaxor properties of terpolymers, it was proposed that such a phase transition existed and explained the large strain in terpolymers [15] [16]. Following studies showed that this contribution could not explain the majority of the observed strain [17] although this idea can still be found in a recent work [18]. The intrinsic electrostriction relates to how the displacement of atoms in the lattice can translate into a macroscopic strain [14]. Maxwell strain is due to the coulombian attraction between two surfaces with opposite charges. The attraction between the electrodes meets the mechanical resistance of the material and the induced strain is then obtained as eq 3.10 [19].

This effect is completely disregarded in copolymers but terpolymers are less rigid and have a higher permittivity. Sometimes Maxwell strain is discarded entirely, sometimes it supposedly accounts for part of the response [20] and in [9] it is regarded as the sole mechanism behind the

$$S_3 = \frac{\epsilon}{2Y}(1 + 2\nu)E^2 \quad (3.10)$$

S_3 : Strain in the thickness direction

ϵ : permittivity

Y : Young's modulus

ν : Poisson ratio

strain. If we estimate the physical parameters to be $\nu = 0.35$, $Y=160$ MPa and $\epsilon = 30\epsilon_0$ we get a value for the electrostrictive coefficient: $Q_3 \approx 18 \text{ m}^4\text{C}^{-2}$. This value is to be compared with the electrostrictive coefficient we measure in the following section at $Q_1 \approx 23 \text{ m}^4\text{C}^{-2}$. Q_1 characterizes the longitudinal strain and in both co- and terpolymers the thickness strain is larger than the longitudinal one: $Q_3 > Q_1$. Although we cannot conclude precisely because of this difference as well as uncertainties on Y and ν , the Maxwell strain is likely to contribute significantly to the total strain.

Conclusion 15: State of the art in terpolymers

The knowledge on the origin of strain in terpolymers is limited. Three phenomena are likely to contribute: Field induced phase transition in the crystalline phase, Maxwell strain and intrinsic strain.

Impact of phase transition on the strain in PVDF-TrFE-CTFE

First, we need to evaluate the strain-polarization relationship of terpolymers in the electrical field range where they were behaving as linear dielectric materials. Fig 3.20 shows the normalized deflection of a terpolymer based cantilever at electrical fields below $20 \text{ V}\mu\text{m}^{-1}$.

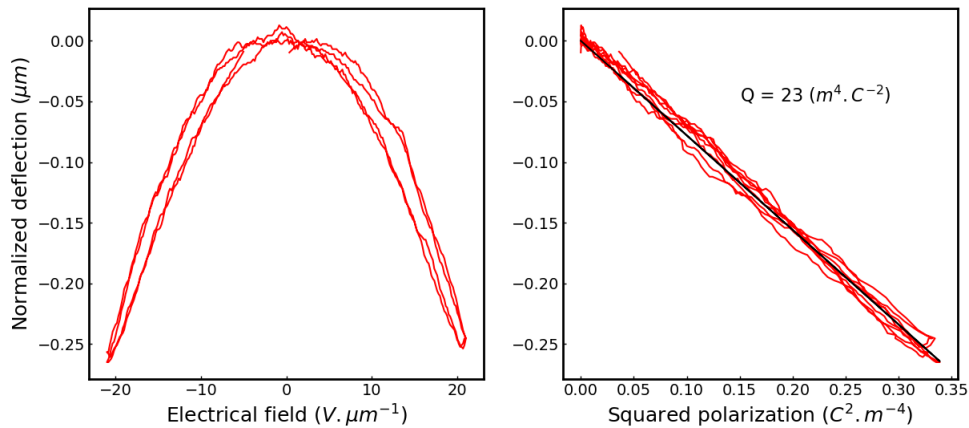


Figure 3.20: Normalized deflection of a cantilever as a function of electrical field (left) and of the squared polarization (right)

Both panels display the cantilever deflection but the left panel x-axis is the electrical field while the right panel x-axis is the squared polarization. As we can see, the deflection and therefore the strain are perfectly described by an electrostrictive law. We can extract a value for the coefficient $Q = 23 \text{ m}^4 \text{ C}^{-2}$ using the formalism detailed in the previous chapter 2.10. We reiterate this measurement but under a higher electrical field. The results are displayed in fig 3.21

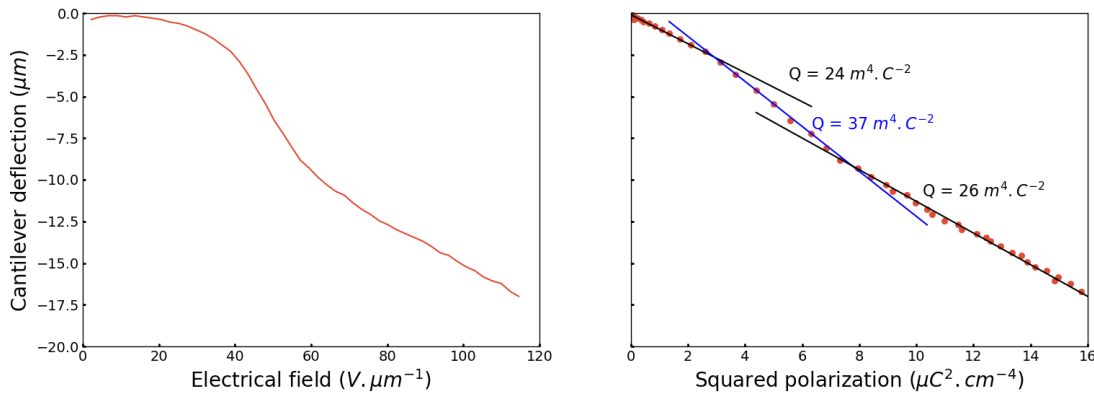


Figure 3.21: Left: cantilever displacement as a function of the electrical field. Right: cantilever displacement as a function of the squared polarization

In fig 3.21 only the forward direction is shown in order to make the figure easier to read. When the strain is plotted not as a function of electrical field (panel (a)) but as a function of squared polarization (panel (b)) we can see a discrepancy with the electrostrictive law. The strain evolves quadratically with the polarization but the coefficient Q increases by 50% from 24 to $37 \text{ m}^4 \text{ C}^{-2}$ on a limited range between 2 and 7 μC.cm^{-2} . In the previous section we proposed that the phase transition impacted the electrical response of terpolymers. We singled out its contribution to polarization and located it on an electrical field range between 40 and 60 V.μm^{-1} . This seems to coincide with the rupture in the $Q - P^2$ evolution of figure 3.21. We take a closer look at this correlation by putting in front of one another fig 3.21 and fig 3.15 in figure 3.22.

Figure 3.22 displays data from the same measurement: electrical field, polarization (raw and phase transition contribution), and displacement. Each letter (A,B,C) is given as a visual aid and corresponds to a unique state of the material in time. This way we can highlight the following result: the increase in electrostrictive coefficient (A_1-B_1) happens precisely where we placed phase transition with the anti-ferroelectric like polarization cycle (A_2-B_2). As a consequence we can ascribe the increase in strain between 40 and 60 V.μm^{-1} to the difference in lattice parameters between two phases involved in the transition.

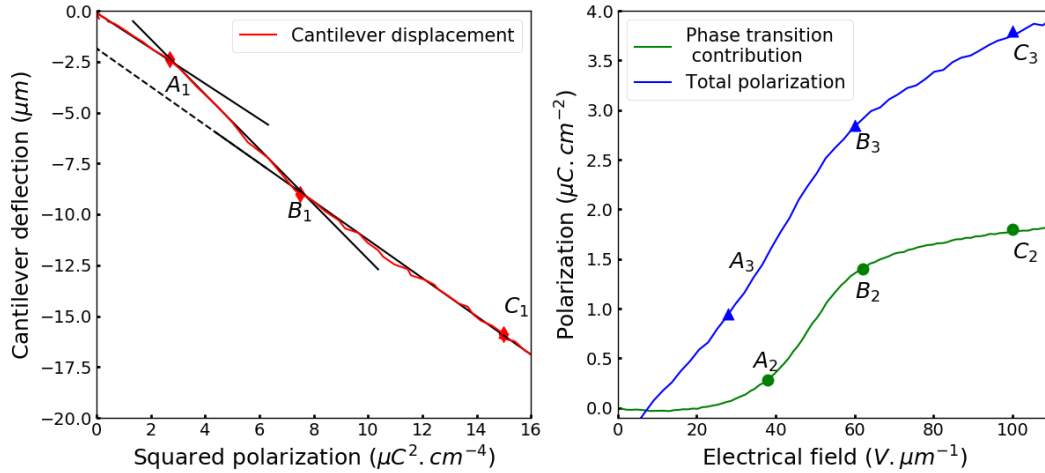


Figure 3.22: Left: cantilever displacement as a function of the squared polarization in fig 3.12. Right: simultaneously measured polarization cycle and the extracted phase transition signature

We can quantify the impact of the additional strain as it corresponds to the difference between the two black lines in fig 3.21 and amounts to $2 \mu m$. At $60 V.\mu m^{-1}$ these $2 \mu m$ represent 20% of the total strain and only 12% at $100 V.\mu m^{-1}$. To summarize what has been said so far on terpolymers we propose an explanation of the role of phase transition in strain, summed up in fig 3.23 and 3.24.

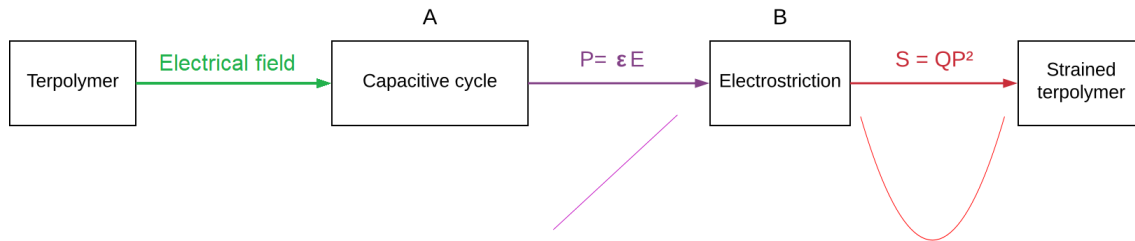


Figure 3.23: Strain in PVDF-TrFE-CTFE terpolymers at low electrical fields

Figure 3.23 is a schematic representation of electrostriction at low electrical fields. When submitted to an electrical field the terpolymers have a linear capacitive response corresponding to mechanisms reversible under a small excitation (A). Through mechanisms such as Maxwell stress or intrinsic electrostriction, the electric response strains the terpolymer (B).

When the electrical field is higher and reaches values beyond $20 V.\mu m^{-1}$ a field induced phase transition occurs and the strain mechanisms are better represented by fig 3.24.

(A) and (B) are the same mechanisms as in figure 3.23. The difference is that dielectric polarization (A) is described by a Langevin function rather than a linear relationship with the electrical field. The other change is the apparition of a field-induced phase transition (C). The two phases involved have different lattice parameters, and the transition induces a strain of the

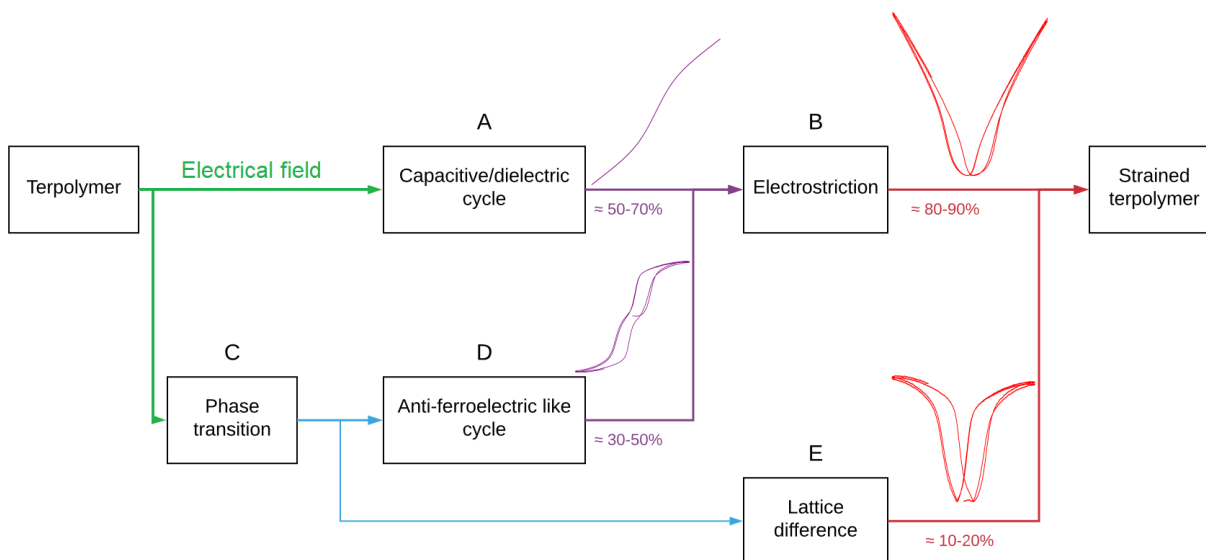


Figure 3.24: Proposed model of strain in PVDF-TrFE-CTFE terpolymers at high electrical fields

crystalline phase (E). This step (E) is the reason behind the increase in coefficient Q between 20 and $60 \text{ V} \cdot \mu\text{m}^{-1}$. The field-induced phase has a higher polarization and its contribution to the overall cycle resembles that of an anti-ferroelectric material (D). The total polarization (A+D) undergoes the same mechanisms (B) as in fig 3.23. The mechanisms in (B), Maxwell stress and intrinsic electrostriction, are responsible for the larger part of the terpolymers strain. Both strains (B) and (E) add up to give the total strain in the terpolymer.

It should be noted that with this phenomenological description we quantify the relative contribution of each mechanism in average (macroscopic measurements). The lattice difference due to phase transition (E) happens only in the crystalline phase. We do not now how much of it, if any at all, is transmitted to the amorphous phase. On the contrary, mechanisms such as Maxwell stress are likely to strain mostly the amorphous phase, because of its lower rigidity compared to the crystalline phase.

Conclusion 16: Impact of the phase transition on the strain in PVDF-TrFE-CTFE

With strain measurements, we observed an increase of the electrostrictive coefficient on an intermediate range of electrical fields. This mechanical change matches precisely the polarization increase in the phase transition cycle. Based on these observations we propose a phenomenological description to explain the role of the field-induced transition in terpolymers.

Strain at high temperatures

Just like we did with the polarization response (fig 3.18 and 3.19), we can check if the phenomenological description presented above is consistent with the behaviour at higher temperatures. We put the cantilevers above a hotplate and measured the deflection as a function of the electrical field. The temperature in figure 3.25 is that of the hotplate and not of the sample itself.

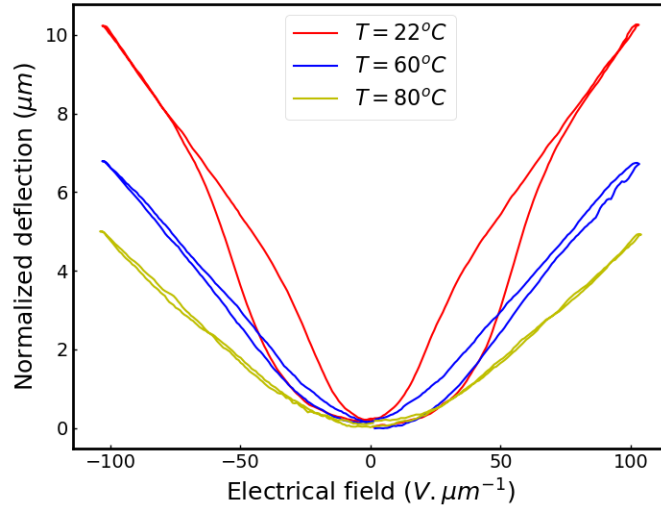


Figure 3.25: Deflection of a cantilever with 8.5% CTFE at 0.8Hz for three different temperatures. The temperature is that of the hotplate below, the cantilever is located a few millimetres above

At high temperatures the cantilever still moves significantly but the hysteresis disappears. This is consistent with the idea of a field induced transition, hindered by temperature and responsible for the hysteresis. To further check the sturdiness of our description, we measure the polarization and take a look at the polarization-strain relationship. In figure 3.26 we show the polarization alongside the cantilever deflection at 80°C and 0.8Hz.

In figure 3.26 the left panel shows the polarization cycle of the terpolymer at 80°C. At that temperatures the dielectric losses are much more important and conduction mechanisms are exacerbated and potentially non-linear [21], hence the yellow cycle. Instead of trying to fit the polarization with complex laws we assume that the lossless cycle is the one represented in green. This cycle is the dielectric polarization calculated from $C(V, T=80^\circ)$ measurements (annex) and using equation 3.14. Without phase transition that would be the only contribution left as per the decomposition shown in figure 3.15. We apply equation 3.9 to the green cycle and compare it to the cantilever deflection. The results are displayed on the right panel and are consistent with the description presented so far. Above the Curie temperature, there is no phase transition and we are able to fit the strain with dielectric measurements alone.

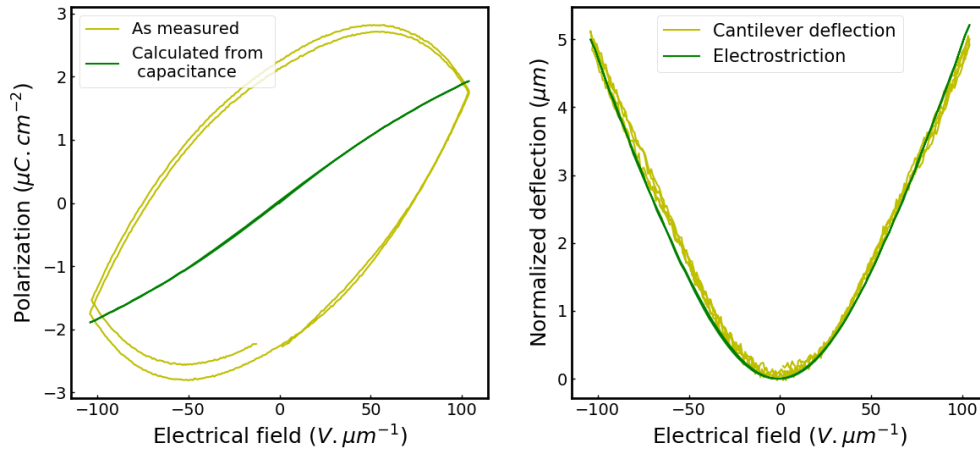


Figure 3.26: Measurements at $T=80^\circ\text{C}$. Left: polarization cycle, measurement in yellow and calculated from capacitance measurements in green. Right: Cantilever deflection, measurement in yellow and the green curve is the green polarization from left panel squared.

Conclusion 17: Strain at high temperatures

The strain measurements at high temperature are consistent with our phenomenological description of strain mechanisms in terpolymers. The field-induced phase transition is most likely hindered by the increasing temperature.

3.3.2 Copolymer and ferroelectric terpolymers

We proposed an explanation for the impact of field-induced phase transition in terpolymers but the majority of the electrostrictive mechanisms are still not explained (box B in fig 3.24). Beside a few considerations on Maxwell strain, there are very few attempts to fill this void in the literature. Given that copolymers have been studied more extensively, it seems appropriate to start from the strain mechanism in copolymers and see how they evolve with the addition of CTFE in the chain.

State of the art of strain in copolymers

The origin of piezoelectricity in PVDF and PVDF-TrFE is supposed to be electrostriction biased by the remanent polarization [22]. Using equation of electrostriction 3.9 in presence of remanent polarization gives equation 3.11.

$$\begin{aligned}
S &= QP^2 \\
S &= Q(P_{diel} + P_r)^2 \\
S &= QP_r^2 + 2QP_rP_{diel} + QP_{diel}^2
\end{aligned} \tag{3.11}$$

P: total polarization

P_{diel} : Polarization in unipolar regime (fig 3.10)

P_r : remanent polarization

Away from the coercive field, polarization is formulated as the sum of a constant term due to the alignment of the ferroelectric domains (P_r , fig 3.11) and of the electrical field induced polarization (P_{diel} , fig 3.10). This expression is injected into the strain equation and its development gives equation 3.11. The first term (QP_r^2) is a constant and the quadratic term (QP_{diel}^2) is negligible at first order before the linear one ($2QP_rP_{diel}$). Therefore, the polymer response is piezoelectric but only as a consequence of electrostriction.

Regarding the physical origin of electrostriction, until 2015 there were two main hypothesis to explain it. The first one is the so called dimensional model [23], [24] and the other one is an intrinsic effect in the crystalline phase. In 2015, Katsouras & al [25] observed through synchrotron measurements that the lattice parameter change in crystallites corresponds to the macroscopic strain. With this experiment they discarded at once the dimensional model and showed that strain came from the displacement of atoms inside the crystalline lattice. Thanks to these recent observations the understanding of strain in PVDF and PVDF-TrFE is pretty much complete.

- 1- Piezoelectricity is only a consequence of an electrostrictive behaviour.
- 2- The electrostriction itself comes from the displacement of atoms inside the crystalline phase.

However there is a problem with statement 1 above: It fails to describe the strain cycle in bipolar regime. This was first evidenced first by Yuki & al [26] and recently addressed by Katsouras & al [25] in an attempt to round off the discussion. They proposed that this discrepancy is due to an additional piezoelectric mechanism adding to the PVDF strain, giving equation 3.12.

$$S = Q.P^2 + d_{coupling}p.E \tag{3.12}$$

$d_{coupling}$: piezoelectric coefficient

p: parity function as explicited in fig 3.27

This hypothesis was based on the observation that adding a linear term in equation 3.11 allowed for a complete description of the bipolar strain cycle, as shown in 3.27. As a physical explanation of its origin, Katsouras & al proposed that it comes from the amorphous phase stressing the crystalline phase under the application of an electrical field.

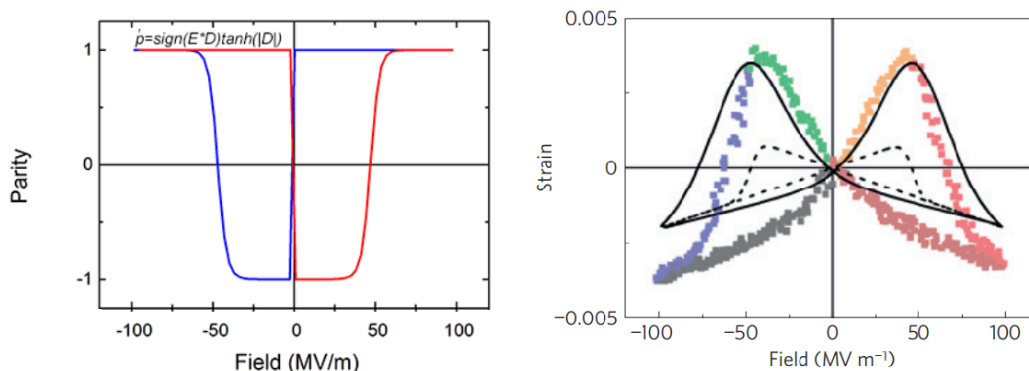


Figure 3.27: Proposed model of strain in PVDF-TrFE-CTFE terpolymers

The left panel is what they defined as the parity function p , used in equation 3.27. It is to account for the fact that the piezoelectric coefficient depends on the orientation of the ferroelectric domains (the sign of P_r). The right panel shows the two components of equation 3.12 applied to the measured strain. The plain line is the QP^2 term and the dotted line stands for the piezoelectric contribution. Although it does not appear in fig 3.27 the sum matches properly the experimental strain.

Conclusion 18: State of the art of strain in copolymer

Most of the strain in PVDF and its copolymer PVDF-TrFE would come from electrostriction in the crystalline phase. Away from the coercive field, the induced polarization is biased by a constant ferroelectric polarization and this results in an apparent piezoelectric behaviour. Electrostriction fails to account for the whole copolymer strain and an additional piezoelectric effect is needed to fully describe the bipolar strain cycle.

Copolymer strain measurements

The aim of the following study is to propose a different interpretation of the strain in copolymer, in particular of the missing 'piezoelectric' effect.

As we did with terpolymers we start at low electrical fields and confront our measurements to the theoretical framework. At low electrical field we can approximate P_{diel} with ϵE (fig 3.10). This yields an analytical expression for the piezoelectric coefficient d introduced in chapter 1.

$$d = 2QP_r\epsilon_0\epsilon_r \quad (3.13)$$

d : piezoelectric coefficient

If the ferroelectric domains have been oriented by a positive bias, the coefficient d is negative as $Q < 0$ in PVDF. And if the copolymer has been negatively polarized d should be positive. We

measured the deflection of a copolymer and a 4% CTFE ferroelectric terpolymer with the two polarization states. The results are shown in fig 3.28.

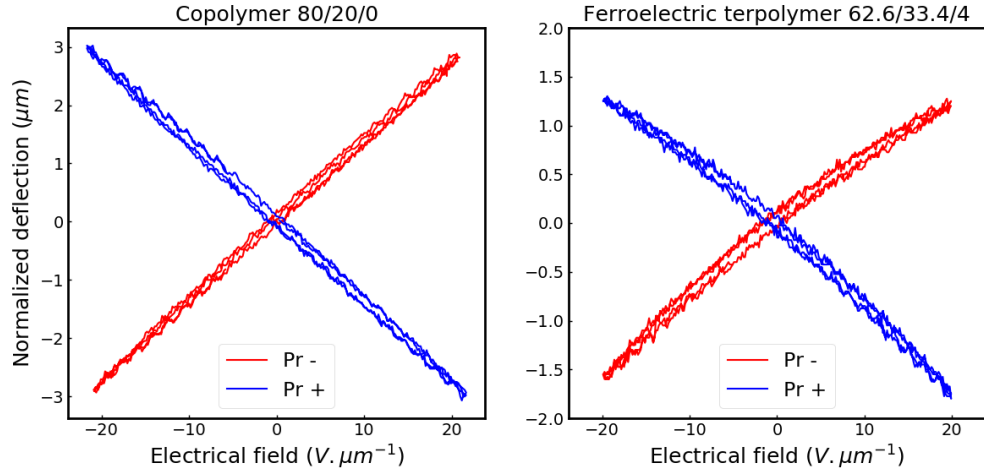


Figure 3.28: Normalized displacement of two cantilevers: copolymer and 4% CTFE terpolymers. Each one with the two possible orientations of ferroelectric domains

The left panel shows the normalized deflection of a copolymer based cantilever and the right panel of a ferroelectric terpolymer with 4% CTFE. The copolymer has the expected strain response (eq 3.13), with a linear dependence to the electrical field whose sign depends on the remanent polarization. The FT deflection shows both a quadratic and a linear dependence to the electrical field. The linear dependence has a sign following the ferroelectric polarization while the quadratic part remains negative. This is consistent with equation 3.11 and the mixed behavior of FT further confirms the sturdiness of the electrostrictive development. Interestingly, our ferroelectric terpolymers (FT) are mostly dominated by the piezoelectric component. This is not unexpected based on the high field cycles in chapter 2 but in contradiction with the only report (to the best of our knowledge) of similar measurements [5] in the literature.

With the copolymer polarized in the positive state we increased the electrical field while keeping it positive. That way we can observe possible non-linearities without the influence of ferroelectric switching. We extract the piezoelectric coefficients d and g following eq 3.14 and normalize them with respect to the first measurement. The results are displayed in fig 3.29.

$$\begin{aligned} S_{max} &= d_{31}E_{max} \\ S_{max} &= g_{31}P_{max} \end{aligned} \quad (3.14)$$

d_{31} and g_{31} : piezoelectric coefficients

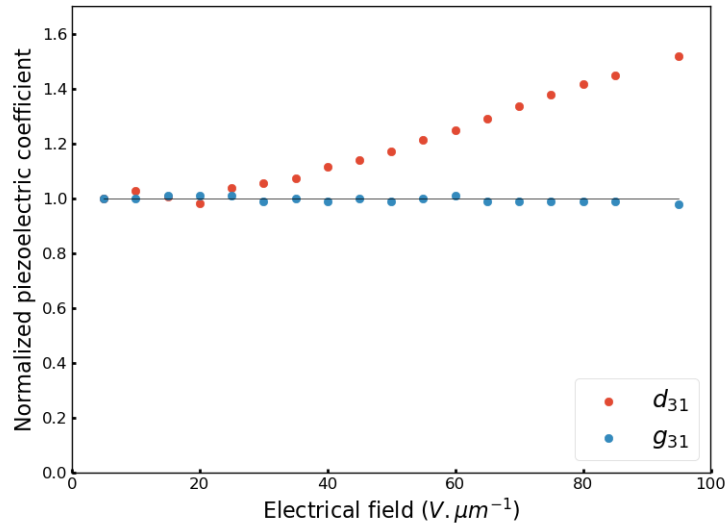


Figure 3.29: Piezoelectric d_{31} and g_{31} coefficients as a function of the electrical field extracted from the same set of measurements

d_{31} is not constant, corresponding to the polarization changes observed in fig 3.10. The fact that g_{31} is constant shows that no change in the electrostrictive mechanisms occurs when reaching higher electrical fields (without ferroelectric switching). The polarization becomes non-linear with regard to the electrical fields but the electrostriction equations still apply.

Conclusion 19: Copolymer strain measurements

The hypothesis of electrostriction biased by the ferroelectric polarization describes perfectly the behavior of the copolymer and ferroelectric terpolymers even at high electrical field.

3.3.3 Origin of butterfly shape in copolymer

The electrostrictive formalism describes correctly the strain response of copolymers. That description does not function when the electrical sollicitation is bipolar. In that regime, the switching of ferroelectric domains is at the origin of a butterfly shaped strain cycle, as displayed in figure 3.30.

The blue curve is the deflection of a copolymer based cantilever measured at 1 Hz. At the same time we acquired the copolymer polarization and used it to calculate the strain according to equation 3.9. We normalized the data so that the model fit the measurement away from the coercive field. Normalizing is just a matter of fixing a value for the coefficient Q and figure 3.30 highlights how electrostriction fails to describes the copolymer strain around the coercive field. The polarization used in the electrostriction equation is the charge surface density measured at the electrode (provided that $D \approx P$). Away from the coercive field, all the ferroelectric domains

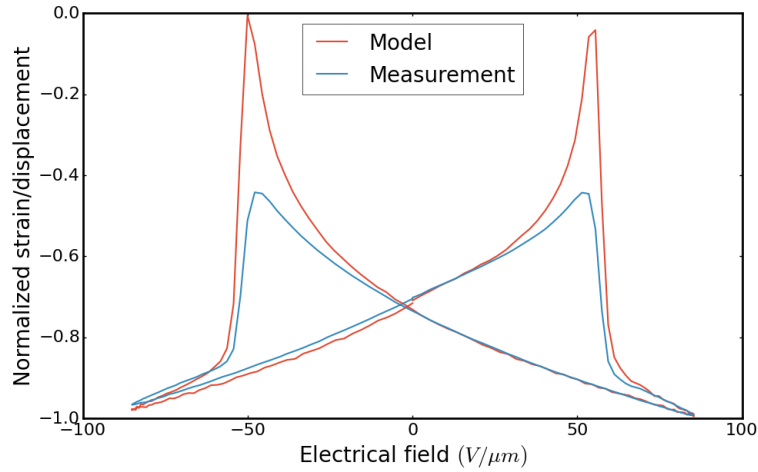


Figure 3.30: Strain cycle in a copolymer and comparison with the electrostrictive law $S = QP^2$

are oriented in the same direction, so this average polarization is equal to the local value at any point inside the material. However, around the coercive field the average polarization might not account for the inhomogeneities in the copolymer. To illustrate that we represented in figure 3.31 two different microscopic states resulting in the same polarization measured at the electrodes.

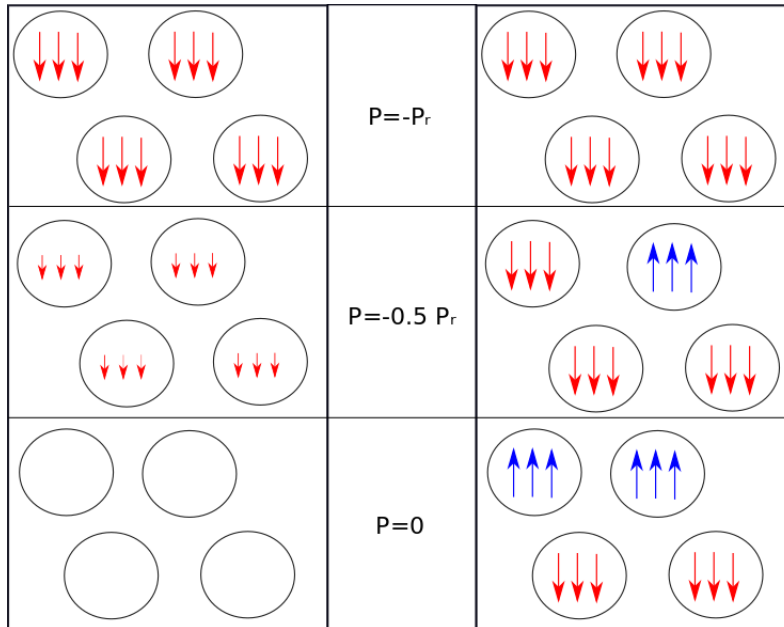


Figure 3.31: Simplified representation of two different switching mechanisms leading to an identical polarization. The circles are ferroelectric domains in the amorphous matrix

The circles drawn in figure 3.31 represent ferroelectric domains. The arrows inside a circle account for the orientation and amplitude of the dipoles within the domain. A smaller (or null)

amplitude does not imply that the dipoles disappeared but that they are not aligned with the electrical field. That is to say an empty circle can be interpreted as an in-plane polarization vector, orthogonal to the electrical field.

In figure 3.31 the left and right columns correspond to two different types of domain switching, although they both result in the same polarization measured experimentally. Applying the electrostriction equation ($S = QP^2$) directly to the measured polarization is valid if the material follows an evolution such as the one represented in the left column. When all the domains are in an identical state, the average polarization describe correctly the polarization inside any ferroelectric domain. Applied to copolymer this approach gives the modelled strain in fig 3.30 hinting that this description is not adapted to copolymer. The calculated polarization value is plummeting around the coercive field, as $P^2 = 0$ implies no strain of the ferroelectric domains.

The right column is another possible mechanism where ferroelectric domains switch one after the other. This representation is a simplification but it has recently been observed to be much closer to the actual evolution of PVDF-TrFE [27]. At the coercive field ($P=0$) the dipoles are oriented with or against the electrical field and therefore the overall strain is not necessarily null. The strain-polarization relationship around the coercive field cannot be calculated with an an average polarization value that do not reflect the internal inhomogenities in the material.

3.3.4 Isolated domain hypothesis

We want to see how the coexistence of opposite orientations can impact the strain response. As a start we will consider that the ferroelectric domains inside the copolymer are not influenced by the rest of the material. A crystalline domain only 'sees' the external electrical field we apply, and not the field generated by dipoles in other domains or in the amorphous matrix. The polarization of such isolated ferroelectric domains depends on their orientation and we write it as equation 3.15

$$\begin{aligned} P_+ &= P_r + \epsilon_{\text{apparent}}E \\ P_- &= -P_r + \epsilon_{\text{apparent}}E \end{aligned} \quad (3.15)$$

P_+ : Polarization of an up domain

P_- : Polarization of a down domain

P_r : remanent polarization of a ferroelectric domain

$\epsilon_{\text{apparent}}$: apparent permittivity

In equation 3.15, the P_r term is the remanent polarization, a positive constant. This value is the one we would measure in a copolymer monocrystal and we take it as $16 \mu\text{C.cm}^{-2}$. This is mostly a guess [28] based on the macroscopic value of P_r and the copolymer 50% crystallinity but an error on P_r is not troublesome as it merely impacts the extracted value of electrostrictive coefficient Q . It does not change the qualitative considerations hereafter provided that $2Pr \gg \epsilon_{\text{apparent}}E$ is still respected.

For a given orientation, up or down, the influence of electrical field is the term $\epsilon_{apparent}$. We saw previously (figure 3.10) that at high electrical field the permittivity does not account totally for the unipolar polarization and an hysteretic contribution is also present. We neglect the hysteresis and approximate the unipolar polarization field by a linear law. Therefore $\epsilon_{apparent}$ has no physical meaning and is just a way of simplifying the equations hereafter.

With the isolated domains polarization in hand we use an electrostrictive law to obtain their strain, (equation 3.16).

$$\begin{aligned} s_+ &= Q(P_r + \epsilon_{apparent}E)^2 \\ s_- &= Q(P_r - \epsilon_{apparent}E)^2 \end{aligned} \quad (3.16)$$

s_+ : strain of an up domain
 s_- : strain of a down domain

To estimate the total strain as the sum of the local strains, we also need the relative amount of each orientations inside the material. This information can be obtained from the ferroelectric cycle similar to the one in fig 3.11. We call f_+ the ratio of ferroelectric domains in the up state and f_- the ratio of domains in the down state. In this simplified approach, the sum of both orientation accounts for all the ferroelectric domains inside the copolymer which is equivalent to equation 3.17.

$$f_+ + f_- = 1 \quad (3.17)$$

f_+ : ratio of positively oriented domains
 f_- : ratio of negatively oriented domains

In figure 3.31, at $P = -0.5P_r$ we have $f_+ = \frac{1}{4}$ and $f_- = \frac{3}{4}$. More generally, functions f_+ and f_- relate to the ferroelectric cycle through equation 3.18.

$$P_{ferro} = f_+P_{r,macro} - f_-P_{r,macro} \quad (3.18)$$

P_{ferro} : polarization due to domain switching (fig 3.11)
 $P_{r,macro}$: copolymer remanent polarization

The value $P_{r,macro}$ is the remanent polarization obtained from standard P(E) cycle around $8 \mu C.cm^{-2}$, as measured in the previous chapter. We do not call it P_r not to confuse with the remanent polarization of a monocrystal in equation 3.15. Combining equations 3.17 and 3.18 we can calculate f_+ and f_- .

f_+ and f_- can be obtained from the ferroelectric polarization cycle. The last step to get the total strain lies in taking the strain of each orientation and weighting it by the amount of domain in the corresponding state. This gives equation 3.20.

$$f_{-(E)} = \frac{1}{2} \left(1 - \frac{P_{ferro(E)}}{P_{r,macro}} \right) \quad (3.19)$$

$$f_{+(E)} = \frac{1}{2} \left(1 + \frac{P_{ferro(E)}}{P_{r,macro}} \right)$$

$$\boxed{S = f_+ s_+ + f_- s_-} \quad (3.20)$$

In equation 3.20, s and f are obtained from data in a polarization cycle and Q is the only degree of freedom to link strain to polarization.

We confront the model to experiment in figure 3.32.

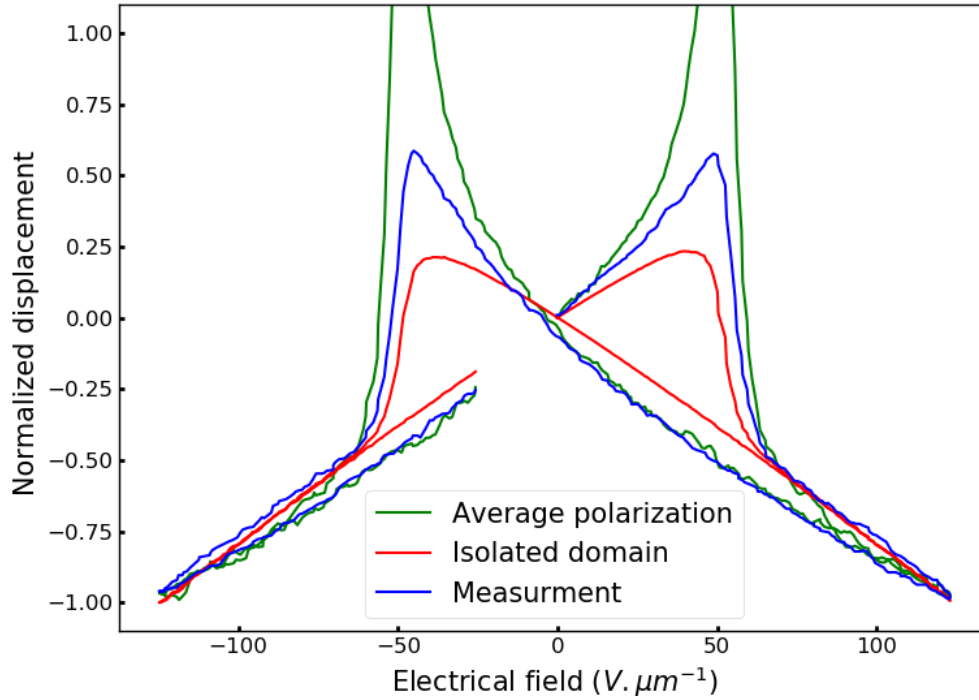


Figure 3.32: Normalized strain cycle of a copolymer. Blue is the measured cycle, green is the calculated strain with the average polarization and the red cycle is the strain calculated with isolated domains hypothesis

In figure 3.32 we represented the measurements of a cantilever displacement and the strain calculated with the two approaches: average polarization ($S = QP^2$ in green) and isolated domains (in red). The strain calculated with the new approach does not show the dramatic drop around the coercive field like the standard description, but the butterfly is squeezed and is hardly a proper fit of the measurement. The hypothesis we made of ferroelectric domains free of any influence from the rest of the material is likely to be the issue and building on the formalism presented so far we try a more realistic description.

3.3.5 Combined descriptions

We considered the ferroelectric domains in copolymer PVDF-TrFE to be isolated because it is embedded in an amorphous matrix. However, the other domains might not be far enough to be disregarded as they make up for 50% of the volume. In addition the amorphous phase is a dielectric and as such can be polarized. The base hypothesis we make now is that the influence from the rest of the copolymer (outside the ferroelectric domain) is proportional to the average polarization. Thus, the polarization inside a ferroelectric domain is somewhere between that of an isolated domain and the average polarization of the material, value that we measure at the electrodes. Mathematically we write it as equation 3.21.

$$\begin{aligned} P_{+(E)} &= \alpha(P_r + \epsilon_{\text{apparent}}E) + (1 - \alpha)P_{(E)} \\ P_{-(E)} &= \alpha(-P_r + \epsilon_{\text{apparent}}E) + (1 - \alpha)P_{(E)} \end{aligned} \quad (3.21)$$

P_{\pm} : Polarization of a ferroelectric domain

$\epsilon_{\text{apparent}}$: apparent permittivity

P_r : remanent polarization

$P_{(E)}$: average polarization, measured at the electrodes

α : quantifies the deviation from the isolated domain hypothesis

In equation 3.21, $\alpha=1$ is the isolated domain hypothesis as described previously. $\alpha=0$ corresponds to an homogeneous polarization inside the copolymer, i.e the standard approach with equation 3.9. Therefore α is an unknown parameter quantifying how much a ferroelectric domain 'sees' the rest of the material. The expression of polarization is the only difference with the rest of the previous development (eq 3.16 - 3.20). With the electrostrictive coefficient Q, α brings to two the number of fitting parameters to explain the copolymer strain. This is the same number of parameters as in [25] with the additional piezoelectric effect. We have yet to see if this description can explain the strain cycle in copolymer. The strain calculated with equation 3.21 is displayed in fig 3.33 alongside the actual measurements.

The red cycle in figure 3.33 was found for $\alpha = 0.9$ that is to say a relatively modest contribution from the surrounding polymer onto the ferroelectric domain (10%). This is enough to change significantly the cycle in fig 3.32 and the model matches well the measurement. The main difference is the strain away from the coercive field. That is most likely due to the linear approximation of polarization we made when we neglected the hysteresis in figure 3.10 and used $\epsilon_{\text{apparent}}$ instead.

This approach:

- Has only two physical unknown parameters, similar to the only other explanation proposed so far
- Has a different interpretation of the bipolar strain that takes into account the actual microstruc-

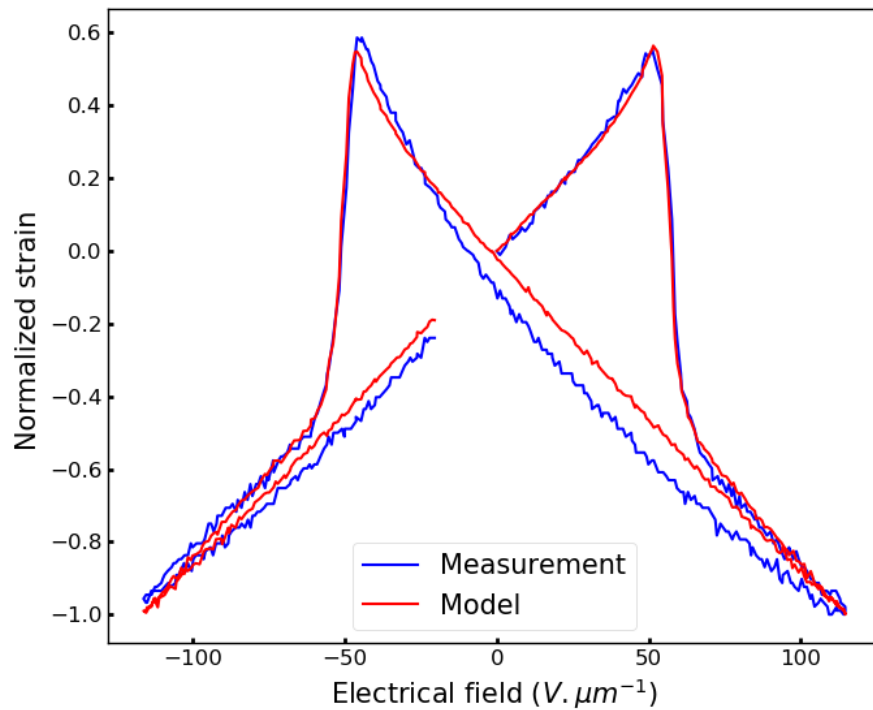


Figure 3.33: Normalized copolymer strain and comparison with the model

tural organisation of the copolymer around the coercive field

The main implication of this phenomenological description is that electrostriction alone can account for every nonlinear response with regard to the electrical field, whether it is the evolution of d_{31} in unipolar regime or the butterfly strain cycle in bipolar regime.

3.4 Conclusion

In this chapter we studied the polarization response of polymers. At low electrical fields, below $20 \text{ V} \cdot \mu\text{m}^{-1}$ both co- and ter-polymers behave like dielectric materials with losses and leakage currents. Even then, polarization measurements give more information than measurements performed with an impedance meter as they also display the electrical temporary regime. This allows for the identification and removal of the leakage current contribution.

The electrostrictive formalism functions perfectly on the low electrical field range. The ter-polymers are electrostrictive with a quadratic dependence to the electrical field. The copolymer is also electrostrictive but due to the large remanent polarization it has a linear dependence to the electrical field. This behaviour is described as piezoelectric and we can impose a sign to the piezoelectric coefficients d by choosing the remanent polarization orientation. Owing to their

mixed nature, the ferroelectric terpolymers have a strain behaviour in between that of relaxor ferroelectric and copolymers. Their strain is dominated by the piezoelectric coefficient.

Deviations from the dielectric and electrostrictive formalism appear at higher electrical fields. In copolymers we started by studying the unipolar regime: the d coefficient is field-dependent while g remains constant. This indicates that the electrostrictive mechanisms do not change but the nonlinear behaviour comes from the polarization response.

In bipolar regime the electrostriction equation fails to describe properly the butterfly shape of the strain response. We proposed that the issue lies with an incorrect use of the electrostrictive formalism and not an additional contribution to strain. Near the electrical field, the ferroelectric domains have different orientations and the inhomogeneous state of the material cannot be properly described by the average value measured at the electrodes.

In terpolymers, we used capacitance versus electrical field measurements to remove the reversible contribution to polarization. The remaining cycle, once corrected of the leakage currents, looks like that of an anti-ferroelectric material. After that, the electrostrictive description was tested out by studying the strain versus squared polarization curve. This allowed for the extraction of an electrostrictive coefficient Q . It appears that Q is not constant on the entire polarization range and during a short period between 30 and 60 $V.\mu m^{-1}$, it is 50% higher. The 30-60 $V.\mu m^{-1}$ electrical field range corresponds precisely to the polarization increase in the anti-ferroelectric like cycle.

As both nonlinearities in polarization and electrostriction coefficient happen on the same electrical field range, they are likely to have the same origin. Based on these observation as well as the state of the art, we propose a phenomenological description of the strain mechanism in terpolymers.

While the existence of a field induced phase transition seems likely, there is no evidence of its existence. Furthermore, the contribution to strain was ascribed to the lattice parameters difference between phases, which is nothing more than a guess. It would require confirmation by measurements of said lattice parameters. The next chapter is focused on XRD measurements of polymers electrically stressed to determine the validity of those assumptions.

Bibliography

- [1] A. N. Hanna, U. S. Bhansali, M. A. Khan, and H. N. Alshareef, "Characterization of current transport in ferroelectric polymer devices," *Organic Electronics*, vol. 15, pp. 22–28, Jan. 2014.
- [2] D. Guyomar, R. Belouadah, B. Ducharne, B. Guiffard, M.-Q. Le, and K. Yuse, "Strain in ferroelectric polymers under low-frequency electric fields: Experiments and modeling," *Journal of Intelligent Material Systems & Structures*, vol. 25, p. 1323, July 2014.

- [3] T. Prodromakis and C. Papavassiliou, "Engineering the Maxwell–Wagner polarization effect," *Applied Surface Science*, vol. 255, pp. 6989–6994, May 2009.
- [4] L. Yang, B. A. Tyburski, F. D. Dos Santos, M. K. Endoh, T. Koga, D. Huang, Y. Wang, and L. Zhu, "Relaxor Ferroelectric Behavior from Strong Physical Pinning in a Poly(vinylidene fluoride-co-trifluoroethylene-co-chlorotrifluoroethylene) Random Terpolymer," *Macromolecules*, vol. 47, pp. 8119–8125, Nov. 2014.
- [5] J.-F. Capsal, J. Galineau, M.-Q. Le, F. Domingues Dos Santos, and P.-J. Cottinet, "Enhanced electrostriction based on plasticized relaxor ferroelectric P(VDF-TrFE-CFE/CTFE) blends," *Journal of Polymer Science Part B: Polymer Physics*, vol. 53, pp. 1368–1379, Oct. 2015.
- [6] O. Boser, "Statistical theory of hysteresis in ferroelectric materials," *Journal of Applied Physics*, vol. 62, no. 4, pp. 1344–1348, 1987.
- [7] L. Yang, X. Li, E. Allahyarov, P. L. Taylor, Q. M. Zhang, and L. Zhu, "Novel polymer ferroelectric behavior via crystal isomorphism and the nanoconfinement effect," *Polymer*, vol. 54, pp. 1709–1728, Mar. 2013.
- [8] A. Pramanick, N. C. Osti, N. Jalarvo, S. T. Mixture, S. O. Diallo, E. Mamontov, Y. Luo, J.-K. Keum, and K. Littrell, "Origin of dielectric relaxor behavior in pvdf-based copolymer and terpolymer films," *AIP Advances*, vol. 8, no. 4, p. 045204, 2018.
- [9] J.-F. Capsal, M. Lallart, J. Galineau, P.-J. Cottinet, G. Sebald, and D. Guyomar, "Evaluation of macroscopic polarization and actuation abilities of electrostrictive dipolar polymers using the microscopic Debye/Langevin formalism," *Journal of Physics D: Applied Physics*, vol. 45, no. 20, p. 205401, 2012.
- [10] Q. M. Zhang, V. Bharti, and X. Zhao, "Giant Electrostriction and Relaxor Ferroelectric Behavior in Electron-Irradiated Poly(vinylidene fluoride-trifluoroethylene) Copolymer," *Science*, vol. 280, pp. 2101–2104, June 1998.
- [11] M. R. Gadinski, Q. Li, G. Zhang, X. Zhang, and Q. Wang, "Understanding of Relaxor Ferroelectric Behavior of Poly(vinylidene fluoride–trifluoroethylene–chlorotrifluoroethylene) Terpolymers," *Macromolecules*, vol. 48, pp. 2731–2739, Apr. 2015.
- [12] L. Zhu, "Exploring Strategies for High Dielectric Constant and Low Loss Polymer Dielectrics," *The Journal of Physical Chemistry Letters*, vol. 5, pp. 3677–3687, Nov. 2014.
- [13] F. Bauer, E. Fousson, and Q. Zhang, "Recent advances in highly electrostrictive P(VDF-TrFE-CFE) terpolymers," *IEEE Transactions on Dielectrics and Electrical Insulation*, vol. 13, pp. 1149–1154, Oct. 2006.
- [14] F. Li, L. Jin, Z. Xu, and S. Zhang, "Electrostrictive effect in ferroelectrics: An alternative approach to improve piezoelectricity," *Applied Physics Reviews*, vol. 1, p. 011103, Mar. 2014.

- [15] X. F., C. Z.-Y., X. H.S., L. H.F., Z. Q.M., K. G.J., T. R.Y., A.-S. G., and B. K.D., “High electromechanical responses in a poly(vinylidene fluoride–trifluoroethylene–chlorofluoroethylene) terpolymer,” *Advanced Materials*, vol. 14, no. 21, pp. 1574–1577, 2002.
- [16] Q. M. Zhang, Z.-Y. Cheng, and V. Bharti, “Relaxor ferroelectric behavior in high-energy electron-irradiated poly(vinylidene fluoride-trifluoroethylene) copolymers,” *Applied Physics A*, vol. 70, pp. 307–312, Mar. 2000.
- [17] Roland, C and Garrett, J, “Mechanical and Electromechanical Properties of Vinylidene Fluoride Terpolymers,” *Chemistry of materials*, 2004.
- [18] N.Sigamani, “Effect of carbon nanofillers on the microstructure and electromechanical properties of electroactive polymers,” *Thesis manuscript*, 2015.
- [19] I. Krakovský, T. Romijn, and A. P. d. Boer, “A few remarks on the electrostriction of elastomers,” *Journal of Applied Physics*, vol. 85, pp. 628–629, Jan. 1999.
- [20] S. G. Lu, X. Chen, T. Levard, P. J. Diglio, L. J. Gorny, C. D. Rahn, and Q. M. Zhang, “Large Displacement in Relaxor Ferroelectric Terpolymer Blend Derived Actuators Using Al Electrode for Braille Displays,” *Scientific Reports*, vol. 5, p. srep11361, June 2015.
- [21] A. N. Hanna, U. S. Bhansali, M. Khan, and H. Alshareef, “Characterization of current transport in ferroelectric polymer devices,” *Organic Electronics*, vol. 15, no. 1, pp. 22 – 28, 2014.
- [22] T. Furukawa and N. Seo, “Electrostriction as the origin of piezoelectricity in ferroelectric polymers,” *Japanese Journal of Applied Physics*, vol. 29, no. 4R, p. 675, 1990.
- [23] Y. Wada and R. Hayakawa, “A model theory of piezo- and pyroelectricity of poly(vinylidene fluoride) electret,” *Ferroelectrics*, vol. 32, no. 1, pp. 115–118, 1981.
- [24] G. Zhu, Z. Zeng, L. Zhang, and X. Yan, “Piezoelectricity in beta-phase PVDF crystals: A molecular simulation study,” *Computational Materials Science*, vol. 44, pp. 224–229, Dec. 2008.
- [25] I. Katsouras, K. Asadi, M. Li, T. B. van Driel, K. S. Kjær, D. Zhao, T. Lenz, Y. Gu, P. W. M. Blom, D. Damjanovic, M. M. Nielsen, and D. M. de Leeuw, “The negative piezoelectric effect of the ferroelectric polymer poly(vinylidene fluoride),” *Nature Materials*, vol. 15, pp. 78–84, Jan. 2016.
- [26] T. Yuki, E. Yamaguchi, T. Koda, and S. Ikeda, “Electrostrictive phenomena associated with polarization reversal in ferroelectric polymers,” *Japanese Journal of Applied Physics*, vol. 38, no. 3R, p. 1448, 1999.

- [27] D. Zhao, T. Lenz, I. Katsouras, P. W. M. Blom, and D. M. de Leeuw, “Global excitation and local probing of ferroelectric domains,” *Organic Electronics*, vol. 47, pp. 189–193, Aug. 2017.
- [28] N. J. Ramer and K. A. Stiso, “Structure and born effective charge determination for planar-zigzag beta-poly(vinylidene fluoride) using density-functional theory,” *Polymer*, vol. 46, no. 23, pp. 10431 – 10436, 2005.

Chapter 4

In-situ structural study

4.1 Experiments

We focused this study on a 61.4/30.3/8.3 VDF/TrFE/CTFE terpolymer which is a composition representative of the relaxor polymers family. In chapter 2 we saw that the electrical and mechanical properties are nearly identical between 7.8 and 9.7% CTFE. Therefore, we assume the results from this study can be applied to other compositions as well. Regarding the ferroelectric terpolymers with a CTFE content below 7.8%, their properties are a mix between those of copolymers and of relaxor terpolymers. Understanding their behaviour first requires a proper comprehension of the relaxor terpolymers.

The XRD study was performed on an EMPYREAN diffractometer, as shown in picture 4.1, and a PANALYTICAL diffractometer for temperature measurements.

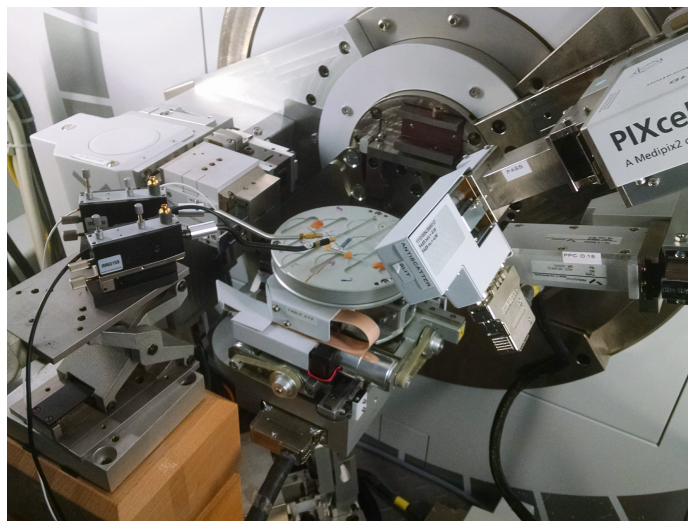


Figure 4.1: Picture of a 8.3% CTFE terpolymer sample during an in-situ study

The electrical bias is applied through contact needles or soldered cables and driven by a Keithley 2600. The diffractometer is used in Bragg-Brentano configuration (illustration in annex). The relevant information for the following study is that the diffracting planes of a crystalline domain need to be parallel to the surface in order to contribute to the XRD signal.

With Bragg-Brentano optical configuration, if the sample is not thick enough a part of the acquired signal comes from the substrate. To facilitate the data interpretation we need a substrate whose background is as transparent as possible to X-ray diffraction.

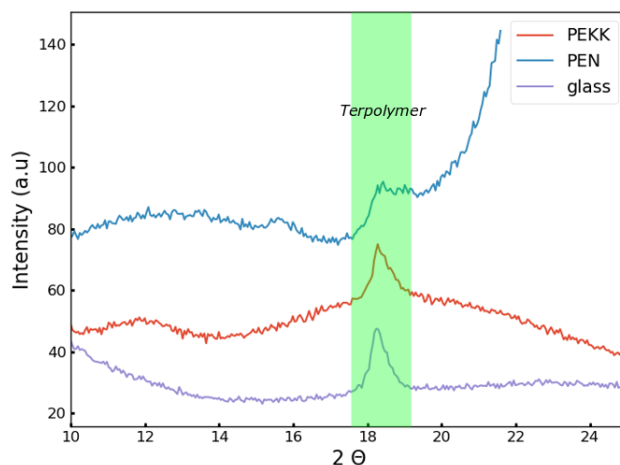


Figure 4.2: XRD spectra of an unbiased sample on different substrates

The samples studied in the previous chapter were deposited onto PEN substrate. However as displayed in figure 4.2 the polymer diffraction peak is drowned into the PEN background. It is possible to fit and remove undesired PEN contributions but that requires measurements performed on a wide angle range. It is an unnecessary step that lengthens measurements duration. The samples studied hereafter are printed onto a glass substrate that does not generate any problematic background.

The need to shorten the measurements duration is due to the high probability of failure of our devices during the in-situ study. The first limitation we encountered was the degradation of polymers due to irradiation, as illustrated in figure 4.3.

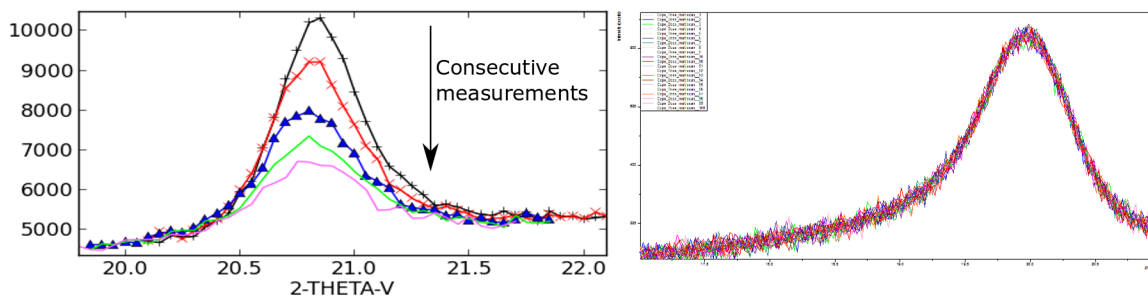


Figure 4.3: Left: consecutive acquisitions of an unbiased terpolymer spectrum on the synchrotron beamline. Right: Consecutive measurement on a diffractometer

Taking advantage of an opportunity and thanks to Nicolas Vaxelaire of CEA LETI, the first attempt at observing polymers under an electrical bias was conducted on beamline B028 at the European Synchrotron Radiation Facility. The results of five successive scans are displayed in figure 4.3 left panel, before any electrical field is applied. The black peak corresponds to the first acquisition and the smaller peaks are the subsequent measurements at a few minutes of interval.

The changes are irreversible and correspond to a reduction of crystallinity due to irradiation. In a standard diffractometer the radiation energy is much lower but the exposure is also longer so we needed to assess whether polymers could withstand it. In figure 4.3 right panel a hundred 5 minutes long consecutive scans are displayed. They were performed on a copolymer sample using the standard diffractometer. The spectrum shows no evolution during measurements as the sample is not affected by the X-rays.

Throughout the study all samples broke down at some point, especially during the bias measurement at high temperatures. We ruled out the irradiation as the reason behind the sample degradation so this difficulty comes from electrical breakdown. The chosen study parameters are a trade off between spectrum resolution and sample life expectancy.

Conclusion 20: Experiments

The terpolymer chosen for this study contains of 8.3% of CTFE. Most scans are performed on a glass substrate and on a small 3 degrees angular range with a Bragg-Brentano setup. This allows for scans as short as 2 minutes, which increases our chances of acquiring a full electrical cycle before the sample breaks down.

4.2 In-situ study of P(VDF-TrFE)

4.2.1 State of the art: structure and XRD characterization

The three phases α , β and γ have been introduced in chapter 1, figure 1.2. These terms are quite ambiguous because they can designate either the organization of monomers inside a polymer chain or the arrangement of those chains with respect to one another. The chain organization is identified by the nature of successive conformations (trans or gauche) between VDF monomers. Combined with the chain packing, it is responsible for the polymer crystalline structure.

This dual designation is legitimate in PVDF because each chain conformation is associated to a crystalline symmetry [1]. However it can become confusing when this terminology is applied to PVDF derivatives. As an example, it is not uncommon to see the P(VDF-TrFE-CTFE) paraelectric (PE) phase referred to as α -phase [2] [3]. Yet, the α phase of PVDF is monoclinic and the terpolymer PE phase is orthorhombic.

To visualize the impact of the conformations nature (T or G) on the chain organization, one should refer to figure 1.2. The α phase corresponds to a succession of trans (T) and gauche (G) conformations ($TGT\bar{G}$). The PVDF β phase is a succession of trans conformations ($TTTT$) and the γ phase is a succession of trans conformations regularly interrupted by a gauche one ($T_3GT_3\bar{G}$).

The ferroelectric properties of a given phase arise from both the molecular conformation (trans or gauche) and the chains packing (crystal structure). The monomers arrangement inside the polymer chains is best investigated with FTIR measurements while the crystalline lattice is observable with XRD. Therefore XRD and FTIR are complementary and the most common techniques for the structural analysis of PVDF. Figure 4.4 displays the XRD and FTIR signatures of the α , γ and β PVDF phases.

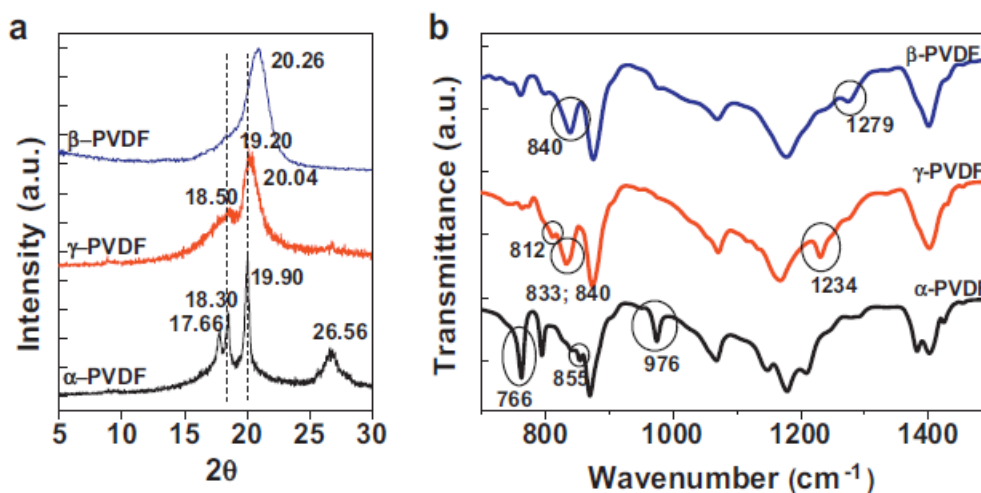


Figure 4.4: a: XRD pattern of the three main phases of PVDF. b: FTIR spectra of the phases. Reproduced from [4]

As for the P(VDF-TrFE) copolymer, it depends on the composition but a 75/25 VDF/TrFE copolymer can have either one of two phases: paraelectric (PE) above the Curie temperature or ferroelectric (FE) below that temperature. The FE phase is very similar to PVDF β -phase but the PE phase has no PVDF equivalent. Table 4.1 sums up the organization of the different phases, the data are taken from [1] [5] and [6].

	Molecular conformation	Crystal class
α	$TGT\bar{G}$	Monoclinic
β	$TTTT$	Orthorhombic
γ	$T_3GT_3\bar{G}$	Monoclinic
Copolymer (PE)	$TGT\bar{G}$	Orthorhombic
Copolymer (FE)	$TTTT$	Orthorhombic

Table 4.1: Molecular conformation and crystalline class of PVDF and P(VDF-TrFE phases)

The information we will obtain from XRD measurements are related the crystalline organi-

zation. Figure 4.5 is a schematic representation to visualize what this means in terms of polymer structure.

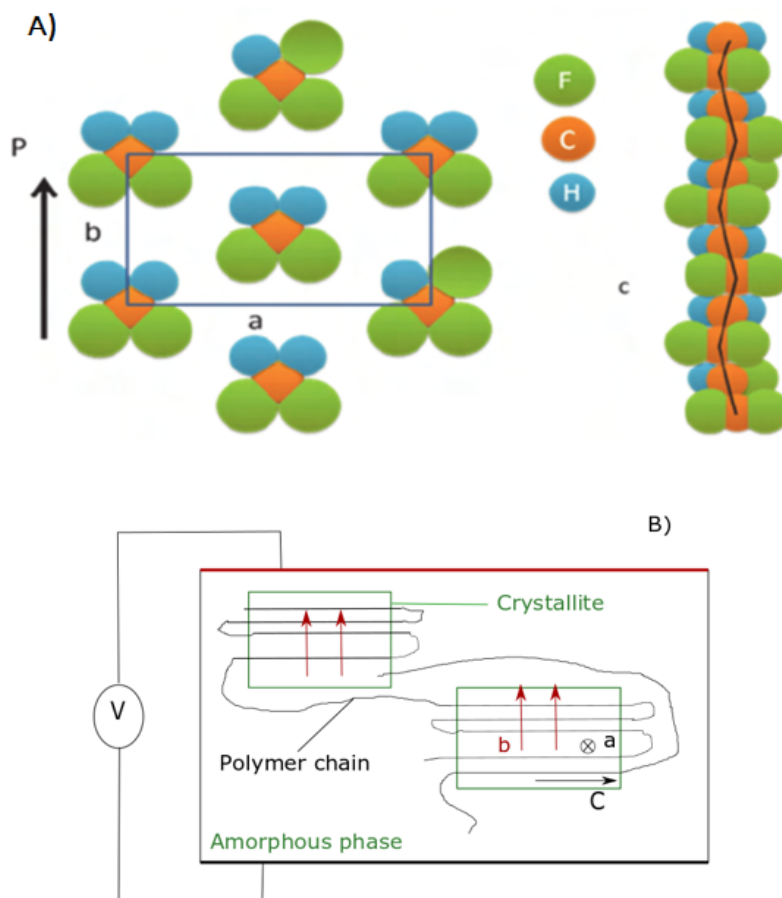


Figure 4.5: A: Representation of the lattice parameters a , b , c and how they relate to the polymer chain orientation, taken from [7]. B: zoom out from A, a representation of the chain arrangement in the amorphous and crystalline phase. The domains are ferroelectric so the lattice parameter b is in the electrical field direction. Lattice parameter a and c are orthogonal to the electrical field direction

Panel A is taken from [7] and represents the three lattice directions of the copolymer crystal. The lattice is orthorhombic with a quasi-hexagonal symmetry [8]. The dipolar moments of the CF_2 atoms are aligned with the b lattice parameter and the c parameter is directed along the chain axis.

Panel B is a schematic representation to visualize how the chains are positioned with respect to the crystalline domains and the rest of the sample. The squares are crystallites; the polymer chain inside them are parallel to one another and to the surface. The ferroelectric polarization is represented by red arrows and is aligned with the electrical field direction. This means that the

b-axis of the crystal lattice is normal to the sample surface and consequently the directions a and c are parallel to the surface. In this illustration, the direction a is perpendicular to the drawing sheet plane but it could actually be in any direction perpendicular to b . One should keep in mind that it is a simplified representation. In an actual material all physical quantities such as the polarization orientation are statistically distributed around a mean value.

This crystalline organisation gives the XRD spectrum displayed in figure 4.6 [9].

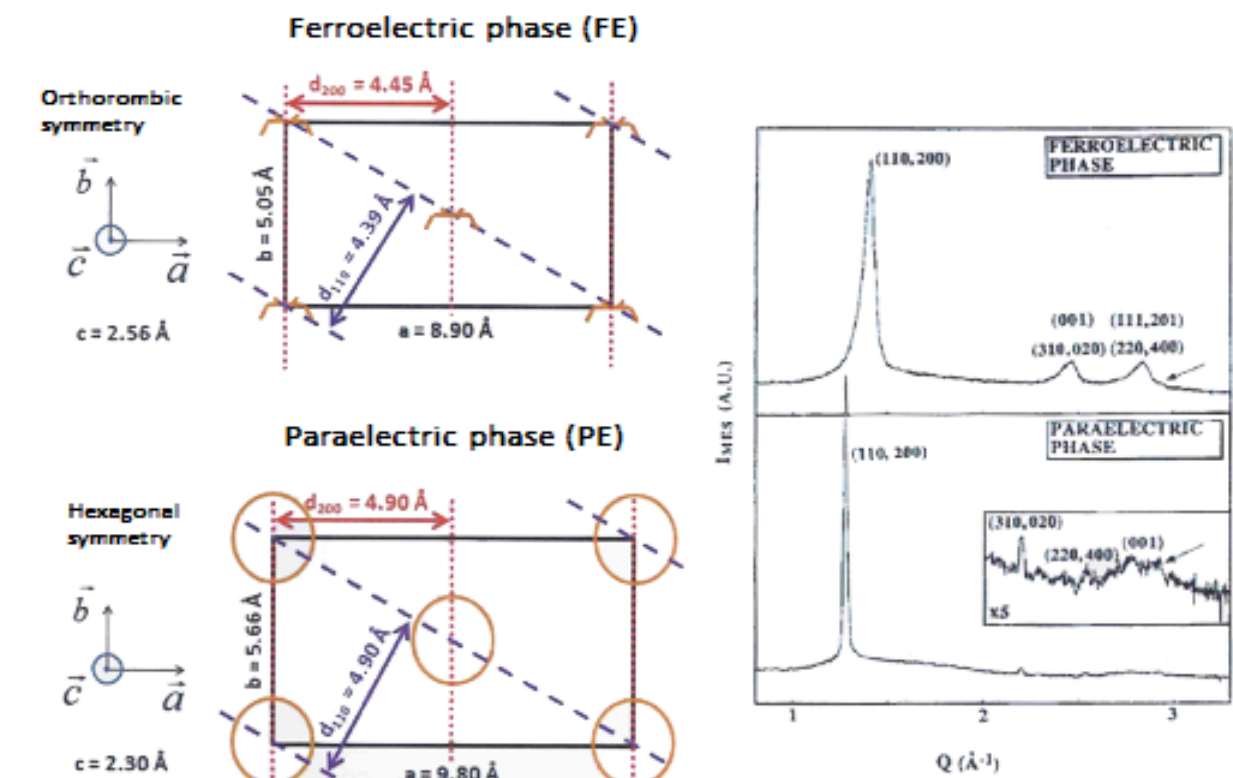


Figure 4.6: Copolymer PE and FE phases. Left: lattice representation, right: XRD pattern. Taken from [9]

The left part of fig 4.6 is a schematic representation of the copolymer crystalline lattice. The right part displays the corresponding XRD spectra. It highlights the point that will be a recurring issue throughout this study: the most intense diffraction peak is the superposition of two different peaks, (110) and (200).

In its PE phase, the copolymer lattice has an hexagonal symmetry. The (200) and (110) peaks are superimposed which results in a thin diffraction peak measured experimentally. When in FE phase, the lattice has a quasi-hexagonal symmetry. The two distances d_{200} and d_{110} are slightly different and as a result the diffraction peak is a bit wider. The two copolymer phases are

easily distinguishable from one another, owing to their significantly different unit cell parameters.

The dipolar moments along the b-axis are at the origin of the ferroelectric properties of P(VDF-TrFE). During polarization switching, i.e the remanent polarization changing sign, the dipolar moments make a 180° rotation. This motion is achieved with the dipoles rotating around the chain (c-axis) but the chains nor the crystallites do not move in the process.

During poling or polarization reversal, the dipoles rotation associated with ferroelectricity occurs by 60° steps to align at best with the electrical field. Figure 4.7, taken from [10] displays a key evidence of this mechanism. This study is of particular interest here because it involves an XRD analyse of the influence of electrical field on the PVDF structure.

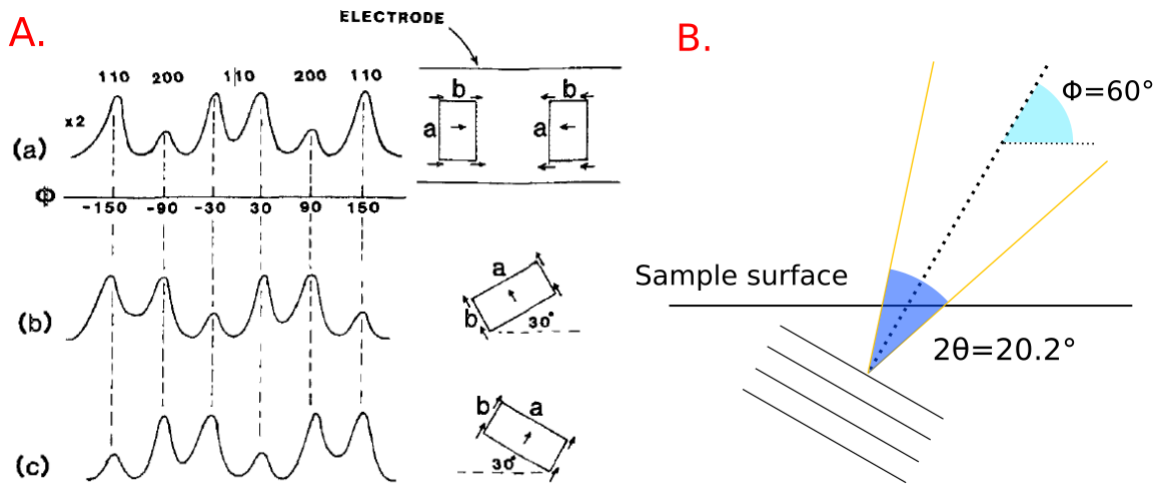


Figure 4.7: Left: Schematic representation of the crystallites orientation in the tailored β -PVDF sample and the corresponding Φ -scans. A.(a): unpoled, A.(b)+(c): poled [10]. B: principle of a Φ -scan.

In [10], the PVDF sample was in β phase. Using a dedicated mechanical process, Bur & al were able to align all crystallites identically. The b-direction bearing the dipolar moment is parallel to the sample surface, as represented in panel A:(a). The XRD setup is so that 2θ angle corresponds precisely to the Bragg's condition of the (110/200) diffraction planes ($2\theta \approx 20.2^\circ$). The scan is performed for different values of Φ , as defined in panel B. For an isotropic sample, a Φ scan would result in a constant line because of the crystallites random orientation. However, having all the crystallites aligned identically change that into XRD pattern (a). In the resulting Φ -scan, each peak corresponds to either (110) or (200) direction of the only two positions available to crystallites. The (200) peaks have a different structure factor from (110) and thus a lower amplitude.

The state (a) corresponds to an unpoled sample. If the domains were to rotate of 60° due to poling,

case (a) would transform into (b)+(c). This is precisely what Bur & al observed experimentally, confirming that ferroelectric domains orientation occurred through 60° stepwise rotations.

Conclusion 21: Copolymer

The ferroelectric properties of PVDF and P(VDF-TrFE) originate from the dipole conformation inside the chain as well as the organization of chains with respect to one another. Due to their pseudo-hexagonal symmetry the (200) and (110) peaks are very close in copolymer diffraction patterns.

4.3 Copolymer

4.3.1 Results

The sample used for this study was a 75/25 VDF/TrFE copolymer and was in a poled state before measurement. We ramped up the temperature rapidly to 100°C then heated up the sample more slowly with 5°C increments. At each step, an XRD measurement was performed after temperature stabilization. Once at 135°C we kept the temperature constant and applied an electrical field of 25 $V.\mu m^{-1}$. We acquired the XRD spectrum and repeated the measurement 4 times with 25 $V.\mu m^{-1}$ increments, up to 125 $V.\mu m^{-1}$. The dataset with all electrical fields and temperatures can be found in annex but for sake of readability we only plotted some of them in figure 4.8.

In figure 4.8-A, the spectra at four different temperatures are represented. The peak at $2\theta = 19.8^\circ$ is the FE phase and the one at $2\theta = 18^\circ$ corresponds to the PE phase. As expected from a first order transition, there are no intermediate states and a crystalline domain is either in FE or PE conformation. At 125°C both phases coexist in the sample. The PE diffraction peak at 130°C is slightly more intense than the FE peak at 100°C but also thinner due to the (200)/(110) superposition. In order to verify if the width and intensity variations compensate each other we extracted the peaks area at each temperature.

To calculate the diffraction peaks total area we fitted the experimental data using pseudo-Voigt functions, the resulting values are displayed in figure 4.8-B. The orange curve is the FE peak area and the blue curve is the PE peak area. The green curve is the sum of the two others and is proportional to the total amount of diffracting matter. At 135°C, the total diffraction pattern area is down to 75% of its original value. We will discuss this in the following section.

In figure 4.8-C, the copolymer is heated at 135°C and the spectra are acquired at four different electrical field values. At 0 $V.\mu m^{-1}$ the copolymer is in its PE phase and the diffraction peak is located near $2\theta = 18^\circ$. Between 0 and 100 $V.\mu m^{-1}$ there are no signs of a FE phase but the diffraction peak changes significantly. The width increases, the intensity decreases and the

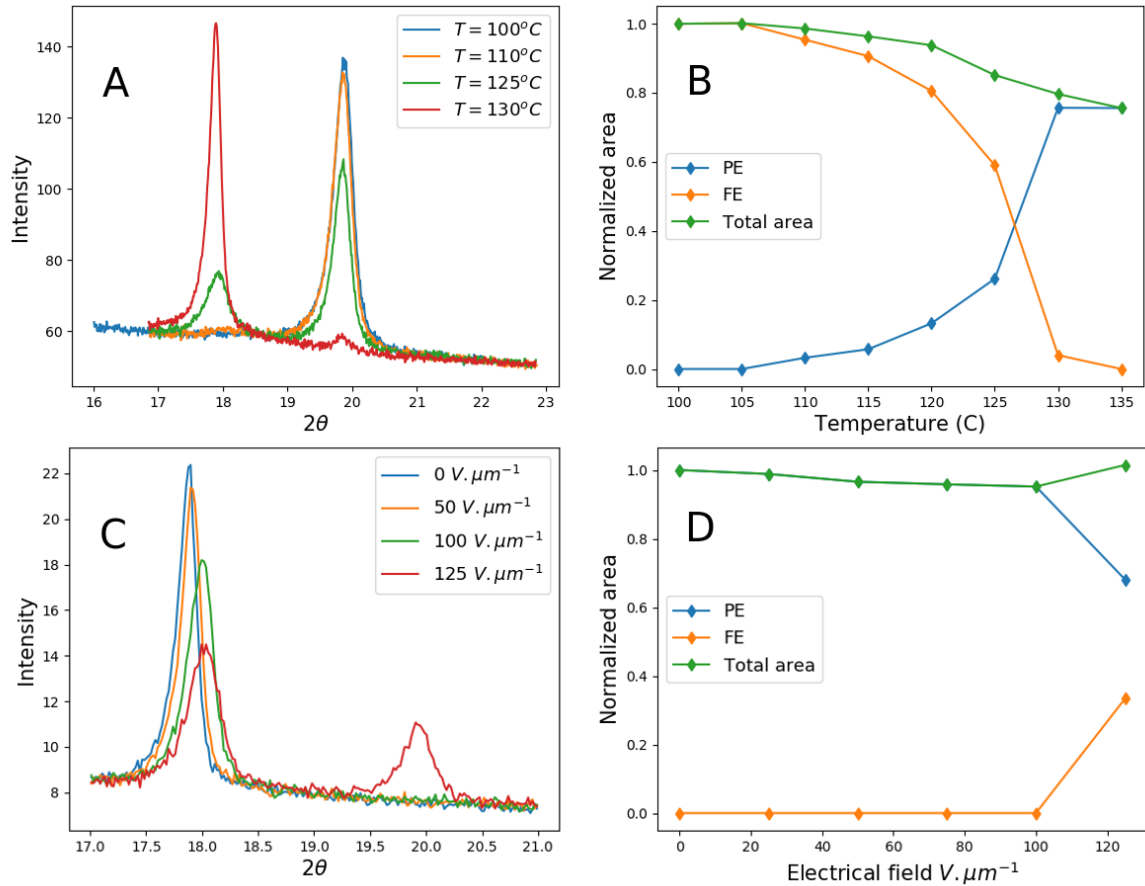


Figure 4.8: A: XRD spectra of the copolymer at 0V and four different temperatures. B: Surface versus temperature of the two peaks at $2\theta = 19.8$ and $2\theta = 18$ in panel A. C: XRD spectrum of the copolymer sample at 135°C and four different biases. D: Area versus electrical fields of the two peaks from C.

position goes toward higher 2θ . At $125 \text{ V.}\mu\text{m}^{-1}$ a peak at $2\theta = 19.90^\circ$ appears, indicating the presence of the FE phase.

Figure 4.8-D displays the peak area at each bias value of panel C. Between 0 and $100 \text{ V.}\mu\text{m}^{-1}$ the surface has decreased of 5%. With the FE phase apparition, the total area increases slightly above the initial value in the unbiased sample.

4.3.2 Discussion

Field-induced phase transition

The first result we get out of XRD measurements is the presence of a field induced phase transition. In panel C, the two peaks at $125 \text{ V.}\mu\text{m}^{-1}$ indicate the coexistence of two phases. Given the position of the newly formed phase it must be the FE phase reappearing. The presence of

such a transition was already evidenced with conformational changes in FTIR measurements [11]. However, this is the first report of this transition using XRD, i.e a direct observation of changes in the crystalline structure. If these spectra were that of a terpolymer instead of a copolymer we would have had all the evidence we needed to support the phenomenological description of strain presented in chapter 3. In **figure 3.24**, box E would be the difference in d-spacing between FE and PE peak and the polar nature of FE phase would explain box D. These are copolymer spectra but this example illustrates what we will be looking for in terpolymers.

Electrostriction

Besides phase transition, a noteworthy change induced by the electrical field is the diffraction peak shift in position. In figure **4.8-A** between 125 and 130°, the PE peak moves toward lower angles. According to Bragg's Law ($2d.\sin(\theta) = \lambda$) it corresponds to an increase of the interplanar distances i.e a lattice strain. This strain is nothing more than thermal expansion, noticeable in PE phase but barely present in the FE phase of copolymers [12].

In fig **4.8-C**, the PE peak shifts in the opposite direction compared to thermal expansion. This negative strain of the lattice corresponds to electrostriction and is consistent with the sign of P(VDF-TrFE) electrostrictive coefficient ($Q_{33} < 0$).

There is another consequence of the electrostrictive effect on the XRD spectra. Between 50 and 100 $V.\mu m^{-1}$ the diffraction peak amplitude goes from 21.5 to 18 (arbitrary units), a 16% drop. This variation is compensated by a larger width and the total peak area remains somewhat constant. The PE peak shape variations could be due electrostriction, with the (110) and (200) peaks drifting apart from one another.

When the material is strained, whether it is thermal expansion or electrostriction, both the (200) and (110) diffraction peaks are affected. However, the only way for the diffraction peak to keep an identical shape throughout the strain modifications would be for the two interplanar distances d_{110} and d_{200} evolve identically. This might be the case with thermal expansion because the lattice expands in all directions. The electrostrictive effect on the other hand contracts the lattice in one direction and expands it in the two others: all directions are not equivalent. This results in a separation of the (200) and (110) diffraction peaks and most likely explains the change in intensity and width observed in figure **4.8-C**. We drew figure **4.9** to illustrate this idea.

In figure **4.9** we have different system axis: that of the sample and that of crystallites. The electrical field is applied in the direction 3 of the sample system axis. The optical setup is so that we observe the diffraction planes parallel to the surface ($\Phi = 90^\circ$ in fig **4.7**); this is also direction 3 of the sample system axis. Aligning the electrical field and the measurement direction

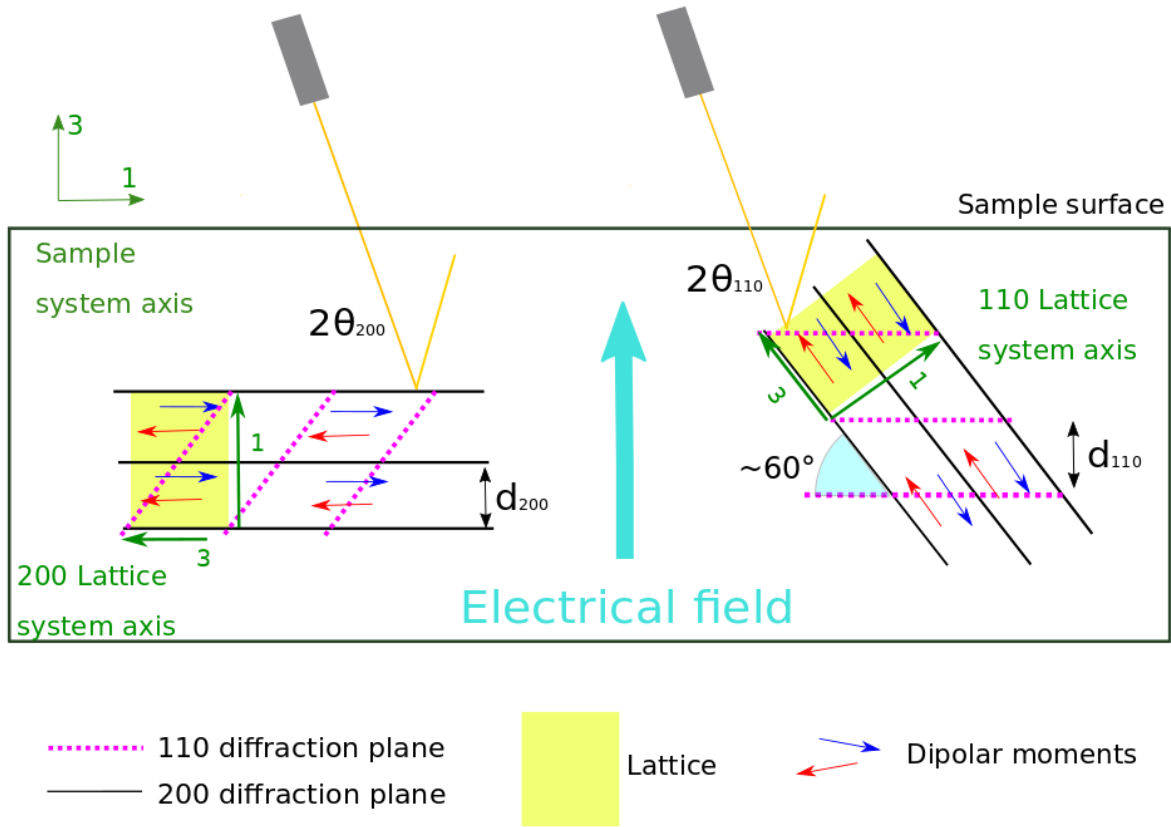


Figure 4.9: Representation of two crystalline domains oriented differently and contributing to the XRD signal. Left: the (200) plane is in Bragg condition. Right: the (110) plane is in Bragg condition

is practical for macroscopical calculations but the electrostrictive response of a crystalline domain does not depend on our choice of a particular system. The electromechanical response of a given crystallite depends on its orientation and the electromechanical equations must be applied in the lattice system axis.

To keep a consistent description between macroscopic and microscopic formalism, the b-direction of a lattice will be referred to as 3. The direction along a and c will be respectively 1 and 2. The two crystallites families we observe with XRD measurements at $\Phi = 90^\circ$ are displayed in figure 4.9. The strain of the left crystallite is expressed with equation 4.1.

$$S_{200} = S_1 = M_{11} \cdot E^2 \quad (4.1)$$

S_{200} = strain of the (200) diffraction plane

S_a = strain of the lattice parameter a

M_{11} = electrostrictive coefficient

E = electrical field amplitude

This case is pretty straightforward because the electrical field and the measured strain are in the lattice principal direction a . Moving on to the crystallite on the right in figure 4.9, the strain has a more complex expression because the measurement direction does not coincide with a lattice principal axis.

$$S_{110}^{\vec{}} = \vec{S}_1 + \vec{S}_3 \quad (4.2)$$

$$\begin{aligned} S_1 &= \frac{E}{2}(M_{11} + \sqrt{3}M_{31}) \\ S_2 &= \frac{E}{2}(\sqrt{3}M_{33} + M_{13}) \end{aligned} \quad (4.3)$$

There is little use in identifying the different elements of the copolymer electrostrictive tensor because we are not working with a monocrystal. However, this point was discussed in order to highlight two issues. First, comparing equation 4.1 and 4.3 we can see that these two values might very well be different. This is possibly the explanation behind the change in PE diffraction peak with the electrical field: the (110) and (200) peaks are drifting apart.

The second issue is the difficulty to compare, at least quantitatively, the macroscopic strain and the crystalline strain. The crystalline strain is a function of several electromechanical coefficients and even knowing them would not be enough. We only observe two particular sets of crystallites while the total crystalline phase response is the sum of all the different orientations, each one strained differently.

Domains rotation

The last unexplained variations in the XRD measurements fig 4.8 are the changes in total peak area, panel B and D. There is a 25% decrease in the total diffraction area throughout the heating process of the unbiased sample (B). There are no obvious reasons why the domains size would be affected by the Curie transition. This variation is more likely explained by the changes in crystallites orientation following the loss of ferroelectric order.

This can be understood with the work of Bur & al [10] (4.7-A). The first poling of a PVDF sample aligns the ferroelectric domains with rotation of either 60°, 120° or 180° toward the electrical field direction. With the apparition of a preferential direction, the amount of crystallites in Bragg's condition is affected. In figure 4.7-A, this would correspond to the transition from (a) toward (b)+(c). We can see that this results in an increase of the diffraction peak intensity at $\Phi = 90$ (our setup). Now, this is an ideal case with only a few possible orientations but it helps understanding how a similar evolution can be expected during a change in the anisotropic distribution of crystallites. In figure 4.8-B, as temperature increases the ferroelectric order is

lost and so is the preferential orientation of domains. With the progressive return to an isotropic distribution of crystallites, the peak area decreases. This explanation is consistent with the small increase in fig 4.8-D once the FE phase has appeared.

There is a difference between a study comparing the structure before and after poling such as [10] and direct in-situ measurements. In addition to the effect of ferroelectric orientation, the in-situ measurements are also impacted by the dielectric response of the material. In the previous chapter, we separated these two notions of ferroelectric and dielectric (or capacitive) response. As the polarization is intrinsically linked to the structural changes inside the polymer, the same dichotomy is in order here. Assuming that the dielectric response is also due to orientation mechanisms, one could wonder if it also impacts the XRD spectra. We can infer the crystallites rotation angle due to capacitive response by correlating dipole orientation and polarization cycle.

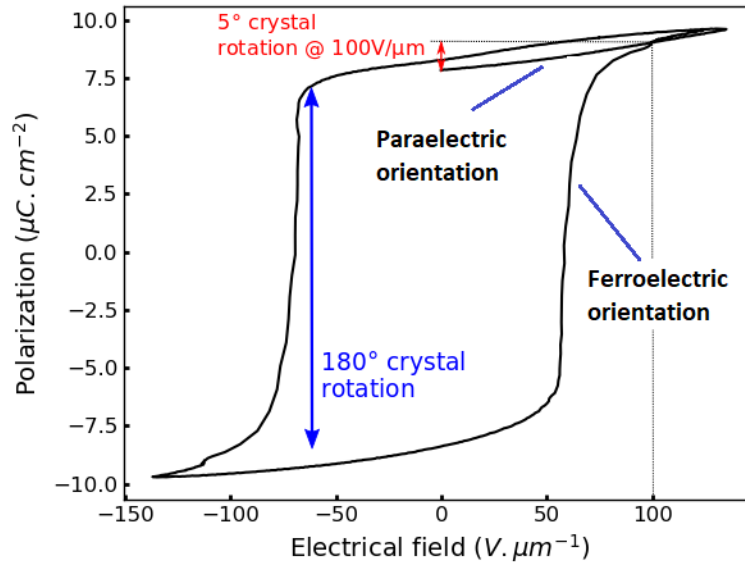


Figure 4.10: Polarization measurement of a copolymer sample poled positively beforehand.

The ferroelectric domain switching induces a polarization variation of $16 \mu C.cm^{-2}$ and corresponds to the 180° rotation of dipoles inside the crystal domains. At $100 V.\mu m^{-1}$, the dielectric response reaches $1 \mu C.cm^{-2}$. Assuming half of that contribution comes from the orientation of dipoles inside the crystal, it yields a 5° rotation in average of the crystallites. This is an overestimation because the crystal permittivity is lower than that of the amorphous phase [13] and we disregarded other physical mechanisms. Therefore, that value of 5° is more of an upper limit for the average dielectric rotation. Even so, it is more than 10 times smaller compared to the 60° stepwise rotations of ferroelectric domains. We assume dielectric orientation does not disrupt the statistical distribution much, especially compared to ferroelectric orientation.

There are numerous other physical phenomena capable of influencing a diffraction pattern. This includes the number of defects present in the crystal, the crystalline domains size or the sample crystallinity. Any dependence of said quantities on the electrical field could complicate the data interpretation. As this experiment is a first attempt at the in-situ study of polymers we will disregard these other contributions to begin with.

Conclusion 22: Copolymer

We reported direct evidence of the field-induced PE-FE transition in copolymers near the Curie temperature. The effect of electrostriction was observed in the PE crystalline phase of a copolymer and the variations are consistent with the negative sign of its electrostrictive coefficient.

Two other effects of electrical fields on the XRD spectra were also discussed. Firstly, the electrostriction distorts the diffraction peak because it affect differently the (200) and (110) peaks. Secondly, the annealing of copolymer un-poles it and as a consequence the preferential orientation is lost. The changes in anisotropy affects the peaks intensity and total area.

With a general idea of how electrical field can impact the polymers spectra, we move on to the terpolymer study.

4.4 P(VDF-TrFE-CTFE) in-situ study

4.4.1 State of the art

The introduction of CTFE monomers in the copolymer chain hinders the crystallization which drops from 50% to 30 % in average. Because of the larger chlorine atom, the inter-chain distance increases and the diffraction peak is located at lower 2θ values than for copolymer, as displayed in fig 4.11. This crystalline phase is referred to as relaxor ferroelectric (RFE) phase.

To describe the impact of CFE and CTFE introduction on the polymer structure, Yang & al introduced the notion of pinning in the polymer chain (fig 3.16) [15] [16] [17]. The CTFE or CFE units are distributed every few VDF-TrFE repetitions and pin the chain preventing a global cooperation of dipoles. Instead of dipoles cooperating to form ferroelectric domains, the VDF-TrFE sequences would contribute to the permittivity through dipolar orientation. Under the action of an electrical field, the CFE dipoles would also orient in the electrical field direction, resulting in a transition toward a ferroelectric phase which would explain the polarization cycles hereafter.

These polarization cycles are that of a CFE terpolymer but we already discussed previously that these considerations were most likely applicable to our polymers as well. Figure 4.12-B dis-

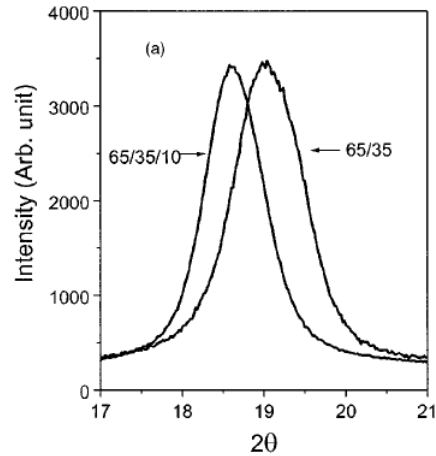


Figure 4.11: XDR pattern of a copolymer and a 59.1/31.8/9.1 terpolymer. Taken from [14]

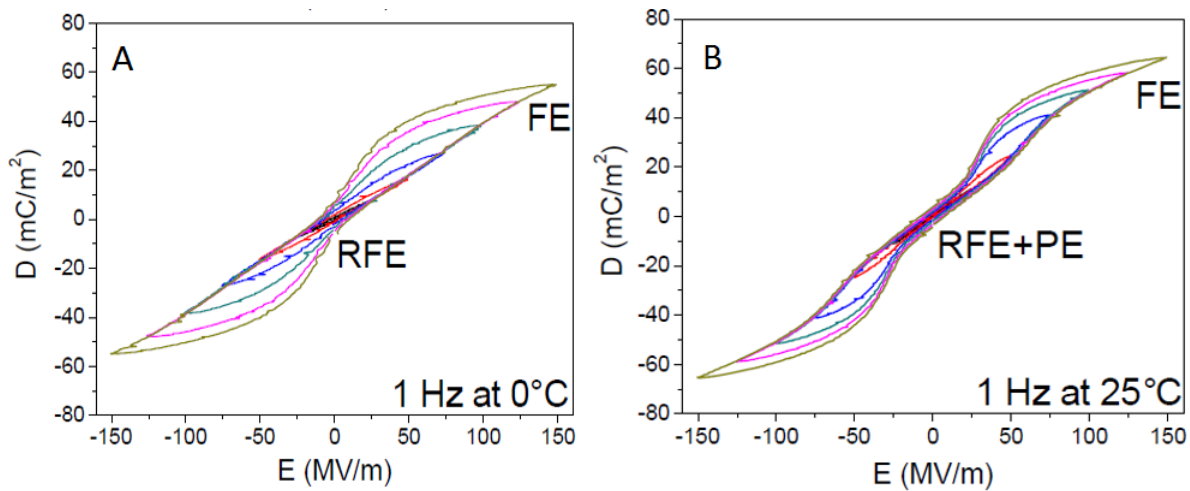


Figure 4.12: Polarization cycles of P(VDF-TrFE-CFE) terpolymer at two different temperatures and the hypothesized crystal order [16]

plays RFE+PE to signify the presence of both PE and RFE phase in the terpolymer at ambient temperature .

The exact nature of those phases is still unclear and this notion of RFE+PE phase was recently refined by Bargain & al [9]. They proposed that the terpolymer phase at ambient temperature is in the middle of a continuous transitions from RFE to PE, as illustrated in figure 4.13.

Figure 4.13 is taken from [9] and sums up the phenomenological description Bargain & al proposed to explain the phase transition with temperature. On the left, the chains are below 0° C, in RFE phase. The red dots are the CTFE pinning units making gauche conformation in an otherwise all-trans (TTTT) chain. As temperature increases, gauche conformations progressively appear in-between the CTFE units in the VDF-TrFE sequence. These conformations are called

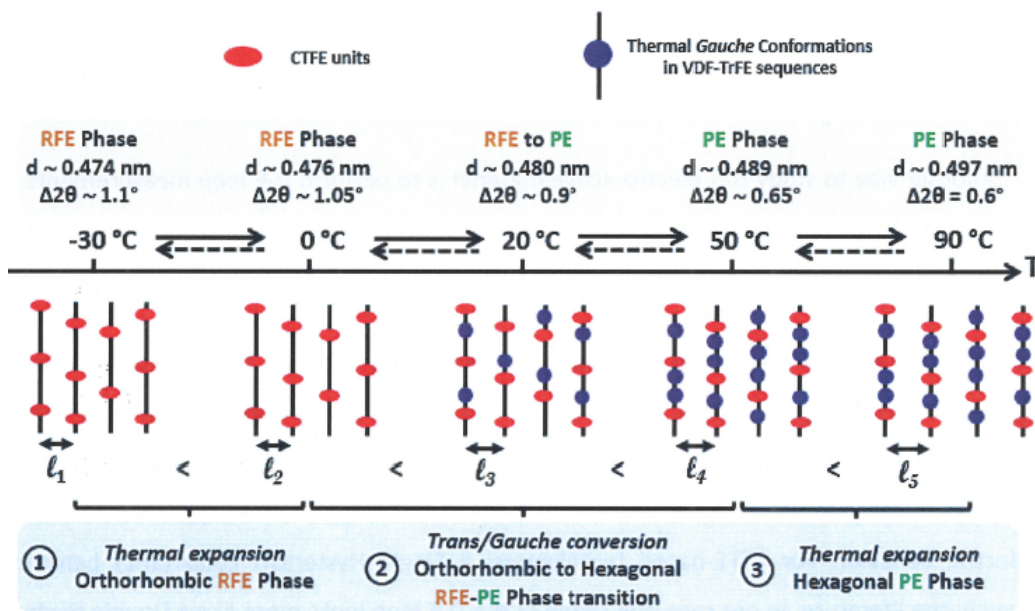


Figure 4.13: Model for the continuous phase transition with temperature in relaxor P(VDF-TrFE-CTFE) [9]

thermal gauche to distinguish them from the CTFE induced gauche conformations. At ambient temperature the phase is in an intermediary state we will refer to as RFE/PE. Above the Curie temperature, that is here 50°C, the VDF-TrFE units do not have all-trans sequence any longer and the phase is referred to as PE.

From a crystallographic point of view, the RFE phase presents a broad diffraction peak that becomes significantly thinner as the temperature increases. This was interpreted as a change in the crystal symmetry, from pseudo-hexagonal to hexagonal. The PE phase has an hexagonal symmetry and therefore a superposition of the (110) and (200) diffraction peaks. The RFE phase has a pseudo-hexagonal symmetry where the (110) and (200) peaks are slightly shifted, hence the larger width. This broader peak at low temperatures was one of the experimental observations that helped Bargain & al to build the model in figure 4.13.

Based on the current state understanding of the terpolymers structure, three main results can be expected from XRD in-situ measurements.

First, an experimental confirmation that an electrical field induces structural changes in terpolymers crystalline phase. Although polarization measurements strongly point in that direction, there is no evidence as of yet. Second, a link between structural changes and electromechanical observations from the previous chapter. The idea is to provide a physical explanation for the variation of electrostrictive coefficient (fig 3.22) and the overall description of strain mechanisms in terpolymers (fig 3.24). The last objective is to shed some light on the nature of this (FE)

phase and how it relates to the RFE-PE order. While XRD measurements alone are unlikely to characterize the whole structure it can be a starting point for following studies.

4.5 Terpolymers

4.5.1 Ambient temperature

Measurements

We acquired the XRD spectra of a terpolymer sample under electrical fields up to $165V.\mu m^{-1}$ at ambient temperature. The raw data are presented in fig 4.14 and separated into 3 categories based on the XRD pattern evolution.

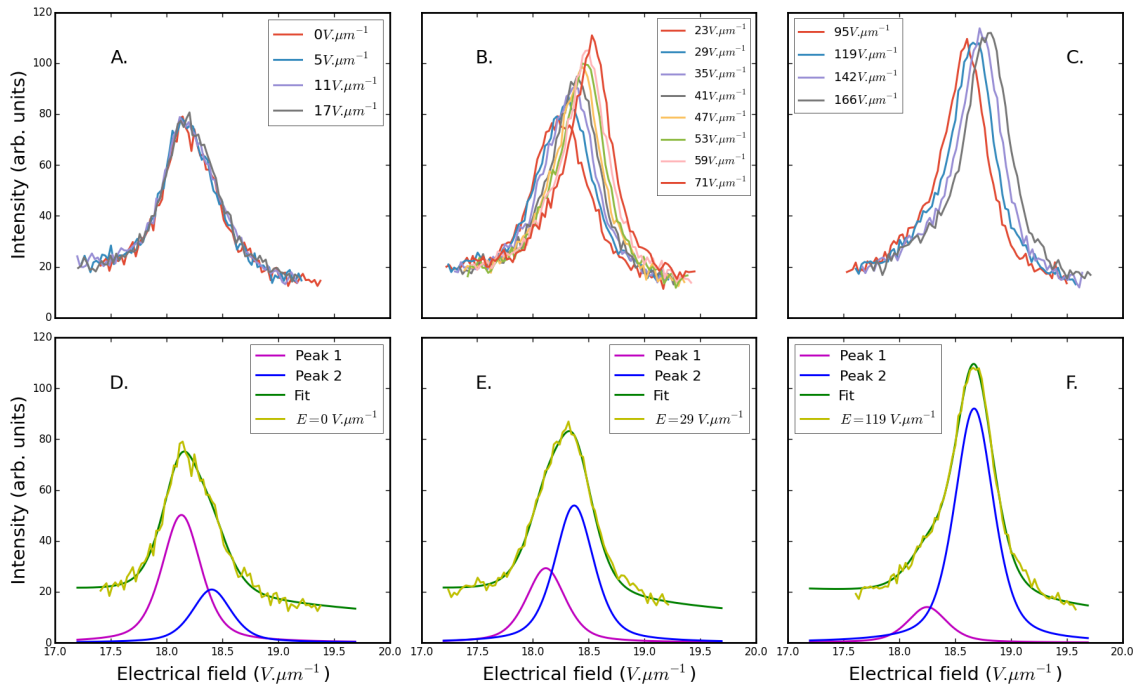


Figure 4.14: Raw spectra of a terpolymer under electrical field. The data are separated into three panels based on their behaviour. Left: $0-17V.\mu m^{-1}$, middle $23-71V.\mu m^{-1}$ and right $95-166V.\mu m^{-1}$. The lower row displays examples of the fit used to extract the peak parameters.

Figure 4.14-A displays the diffraction peak of a terpolymer from 0 to $16V.\mu m^{-1}$ with is no visible dependence to the electrical field. In figure 4.14-B the electrical field ranges from 22 to $66V.\mu m^{-1}$. The peak becomes more intense and thinner while the asymmetry switches from left to right. Figure 4.14-C displays XRD patterns for electrical fields up to $166V.\mu m^{-1}$, the peak transitions towards high 2θ while maintaining an almost identical shape.

On the whole electrical field range, the diffraction peak can be fitted with two pseudo-Voigt functions. Three fit examples are displayed in figure 4.14 **D-F** with the two fitting functions called peak 1 and peak 2. The fit of all spectra are performed in a single run: the boundary conditions and initial parameters are identical throughout the operation. Below $20 \text{ V}\cdot\mu\text{m}^{-1}$ two peaks at least are required to fit the asymmetry (D). Between 24 and $72 \text{ V}\cdot\mu\text{m}^{-1}$ (E), the change in shape is matched with one peak increasing at the expense of the other. At higher electrical fields (F), only one peak with a small tail is needed to fit the diffraction peak. This peak keeps an identical shape while shifting toward high angles.

To go further than discussing the experimental diffraction peak alone, we also monitor the evolution of the fitting functions. In copolymers, there were countless possibilities to fit the spectra and we did not care for the chosen functions. In terpolymers, because of the much more limited number of solutions, we estimate that these fitting functions draw a realistic picture of the structural changes. There are several hypothesis to explain their evolution, visible in figure 4.14 **D-F**.

First, each fitting peak could correspond to a different phase and the XRD spectra evolution would then be the direct image of a field-induced phase transition: one phase grows as the other disappears. This is a possibility but it leaves some important questions unanswered and among them the unexpected width of the high electrical-fields diffraction peak. In the state of the art section, we saw that the low temperature phase of terpolymers (RFE) and the FE phase of copolymers both exhibit a broader diffraction peak due to their pseudo-hexagonal symmetry. Yet, we observe the opposite evolution as the electrical field increases.

The second possibility is that each peak corresponds to the (110) and (200) diffraction planes of the same crystalline phase. In that case, the asymmetry switching side observed in figure 4.14 **B** would correspond to the orientation of crystallites in the electrical field direction. A (110) plane in Bragg's condition makes a 30° angle with the electrical field while a (200) diffracting plane makes a 90° angle with the field. An orientation in the electrical field direction would, among other changes invisible to our optical setup, increase the (110) diffracting population and reduce the (200) one.

The third hypothesis is that we have a more complex situation with any number of phases, each one with possibly several peaks which may or may not rotate with the electrical field. While this is a distinct possibility, short of leaving the interpretation to imagination there is not much to do with this hypothesis and XRD measurements alone.

Conclusion 23: Terpolymer

We observed with XRD measurements that the terpolymer displays significant structural changes with the electrical field. The data interpretation is not as simple as it was in copolymer and several mechanisms could explain the spectra variation. The idea of crystallites rotation with the electrical field allows for an easier interpretation of the data and we choose to continue the study in light of this hypothesis.

Discussion

The first parameter we extracted from figure 4.14 is the d-spacing evolution versus electrical field.

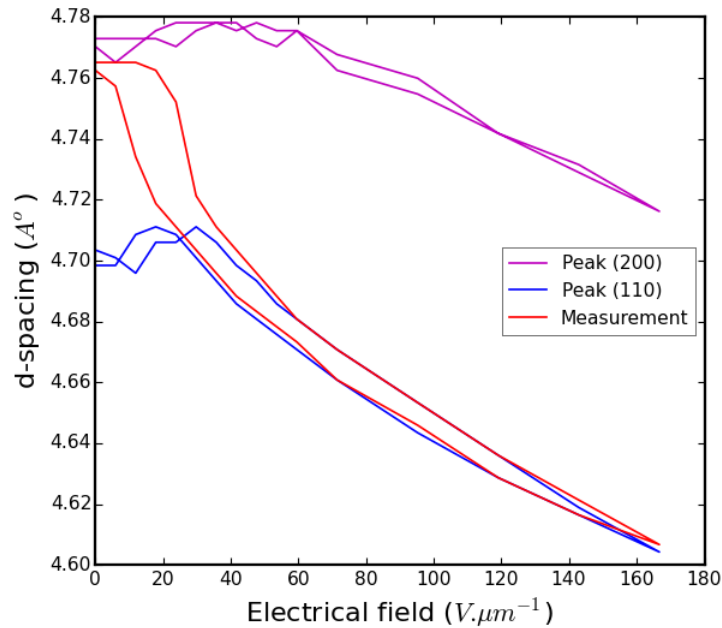


Figure 4.15: d-spacing calculated from the diffraction peaks position.

The red curve in figure 4.15 is the interplanar distance calculated from the diffraction peak position. The reduction of d-spacing is consistent with the negative electrostrictive coefficient of terpolymers. The purple and blue curves are the (200) and (110) interplanar distances.

On the 20-50 $V.\mu m^{-1}$ range, we observe a large variation of d-spacing while the (110) and (200) peaks remain at the same position. This variation corresponds to the shift from one peak to another. The two peaks have different lattice parameters (4.775 Å and 4.70 Å), hence the measured change in d-spacing. Past the 50 $V.\mu m^{-1}$ mark, the transition is over and the diffraction peak consists only of the (110) peak with a small tail. On the 50-160 $V.\mu m^{-1}$ range, the d-spacing variation is ascribed to electrostriction straining the crystal.

This behaviour is consistent with the variations of electrostrictive coefficient Q we observed in the previous chapter. On an intermediate electrical field-range, the coefficient Q had a 50% increased value. This corresponds most likely to the jump in d-spacing from 4.775 \AA and 4.70 \AA we can see in figure 4.15.

To correlate the structural changes to macroscopic measurements we regrouped in table 4.2 the strain values calculated from XRD measurements and those from chapter 3.

	Macroscopic	XRD
"Phase transition"	0.3%	-1.4%
Total strain	2.8%	-3.5%

Table 4.2: Strain values of the terpolymer at $160 \text{ V}\cdot\mu\text{m}^{-1}$ and contribution ascribed to phase transition in chapter 3.

The notion of phase transition is debated here but it was the terminology previously used in the previous chapter, hence the notation "phase transition" in table 4.2.

The first interest of table 4.2 is that it shows the strains order of magnitude. As it turns out the crystalline phase strain reaches values similar to that of the entire sample. This was not a given because the terpolymers have a crystallinity ratio between 30 and 40 %. As the amorphous phase is much softer than the crystalline part, it could have born most of the deformation.

The second noteworthy comparison in table 4.2 is the relative contribution of "phase transition" to the total strain. This value is much higher in the XRD measurements than in the macroscopic acquisitions. This observation tends to show that the nonlinear electrostrictive behavior originates from the crystalline phase, as proposed in chapter 3. However in light of the orientation hypothesis, the strain model from chapter 3 should be slightly modified, as illustrated with 4.16.

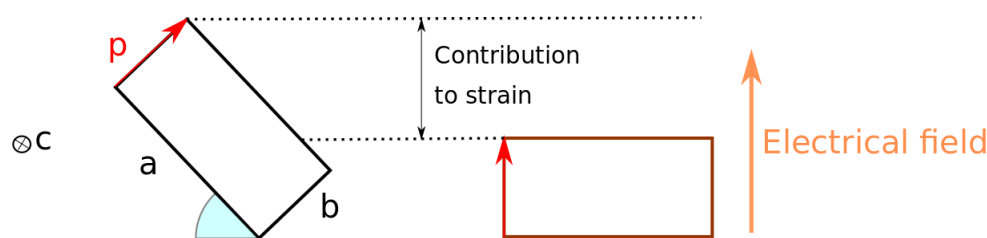


Figure 4.16: Illustration of the impact of a cell unit orientation on the strain and polarization.
Left: before electrical field, right: after electrical field

The dipolar moment is along the b-axis of the lattice and the parameter b is about half that of parameter a . So, the additional strain we associated to a difference in lattice parameter between two phases is most likely a rotation of the crystallites in the electrical field direction.

Beside the diffraction peak position we also extracted their width, intensity and area, displayed in figure 4.17.

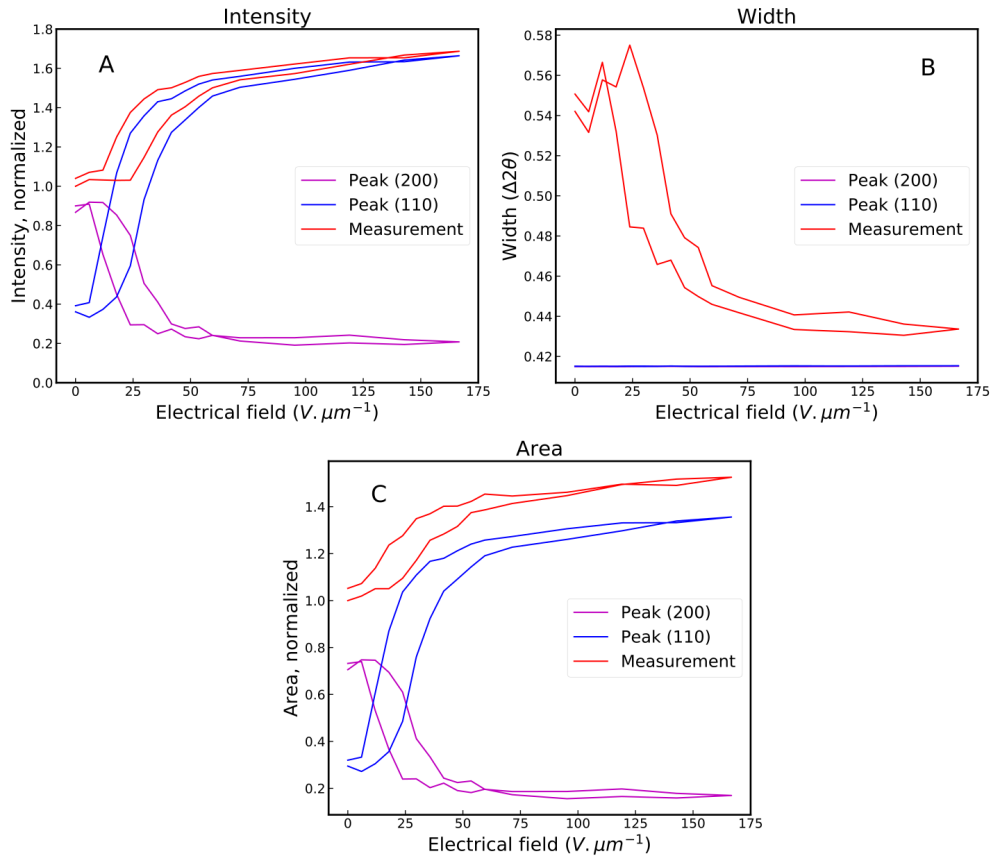


Figure 4.17: Diffraction peak parameters versus electrical field. A:Width, B: Intensity, C: Area

Figure 4.17 A displays the diffraction peaks intensity as a function of the electrical field. The experimental value (red) increases then saturates, which is perfectly described by the (110) peak growing while the (200) is shrinking. Figure 4.17 B displays the diffraction peak width, following an evolution opposite to that of intensity. It gets thinner between 20 and 60 $V.\mu m^{-1}$ then saturates past that point. The width was an unnecessary degree of freedom for the (110) and (200) peaks as it remains constant throughout the fit. Fig 4.17 C displays the total area of each peak versus the electrical field. With the intensity increasing and the width decreasing, the total area value could have gone either way but it actually increases by 40% on the 20-60 $V.\mu m^{-1}$ range.

The intensity and width variations confirm the results from the d-spacing extraction: what

we observe with XRD measurements is the structural counterpart of the electromechanical nonlinearities measured macroscopically. The area variations are also consistent with the rotation hypothesis. As discussed with copolymer, the apparition of a preferential orientation can increase the number of crystallites in Bragg's conditions.

However, there is one important discrepancy between XRD and electromechanical measurements: the hysteresis width. In figure 4.17 the cycle width is about $20 \text{ V} \cdot \mu\text{m}^{-1}$ wide, about half that of the macroscopic hysteresis (fig 3.15). We ascribe this difference to the frequency dependence of the domains rotation. To validate this hypothesis, the strain response of a terpolymer was measured at different frequencies. The results are displayed in fig 4.18.

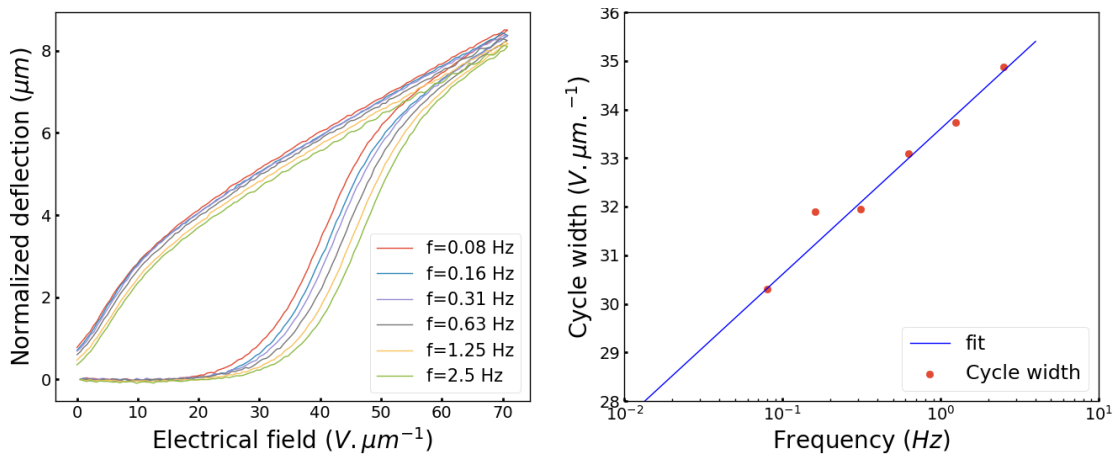


Figure 4.18: Left: normalized cantilever deflection at different frequencies. Right: width of the mechanical cycle versus frequency

Figure 4.18 left panel contains the normalized deflection of a cantilever measured at different frequencies, ranging from 0.08 to 2.5Hz. We measured the cantilever deflection cycle width and reported the values in the right panel. There is a significant dependence of the hysteresis width on the frequency. If we extrapolate the trend in fig 4.18 right panel to the XRD measurement frequency ($2 \cdot 10^{-4} \text{ Hz}$), we find a value of $20 \text{ V} \cdot \mu\text{m}^{-1}$. This value is identical to that of our XRD measurements in fig 4.17 and explains the difference between macroscopic and XRD hysteresis.

To transition or not to transition ?

So far, we have seen that the XRD spectra and the strain nonlinearities could be explained by the orientation of crystalline domains. As discussed in the previous section, the rotation associated to the dielectric nature of the material is mild and can be disregarded. So what could be at the origin of this dramatic orientation ?

The notion of field-induced transition toward a ferroelectric phase becomes once again in order and could explain the sudden rotation. If such a transition happens, the terpolymer would be in a state much like that of an unpoled β -PVDF or copolymer. As the transition takes place, the newly formed ferroelectric domains are oriented in the electrical field direction and this subsequent rotation is actually what we observe. Unfortunately this means that we have no information on the structural changes associated to this hypothetical transition, as they are drowned in texturation effects.

Conclusion 24: Terpolymer at ambient temperature

The XRD measurements of electrically biased samples provide evidence that the macroscopic nonlinearities in the polarization and strain behaviour of terpolymers originate from their crystalline phase. The increase in electrostrictive coefficient is most likely due to the rotation of crystalline domains. The sudden orientation of crystallites could be due to a phase transition but we cannot distinguish an eventual structural change from rotation effects.

4.5.2 At higher temperatures

We reproduced the XRD study at higher temperatures in an attempt to obtain some information on the nature of phase transition. The terpolymer sample was first heated without any bias, the results are displayed fig 4.19-A. As a visual element of comparison, we also added the electrical measurements conducted at 40°C.

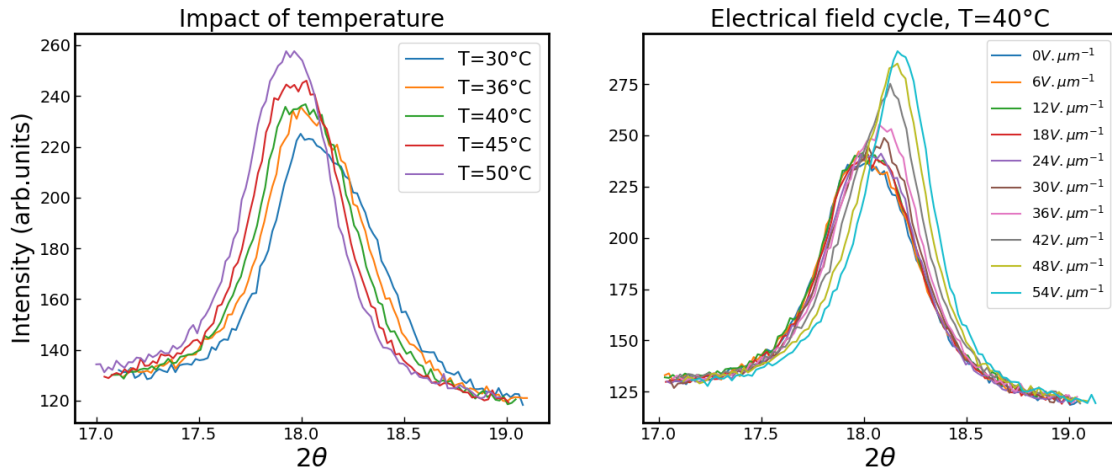


Figure 4.19: Left: Diffraction peak of an unbiased terpolymer sample at increasing temperatures. Right: electrical cycle at 40°C

The temperature spectra in figure 4.19 left panel are consistent with similar reports from the literature (c.f state of the art section). The diffraction peak becomes thinner as the symmetry becomes hexagonal and the (200) and (110) diffraction planes merge into one another.

At each of these temperatures we performed a complete electrical cycle, the 40°C cycle is given as an example in fig 4.19 right panel. The other spectra can be found in annex and the extracted width and intensity are displayed in figure 4.20. To limit the risks of failure, the maximum field is only $60\text{V}\cdot\mu\text{m}^{-1}$, still the terpolymer broke down during the 60°C acquisition.

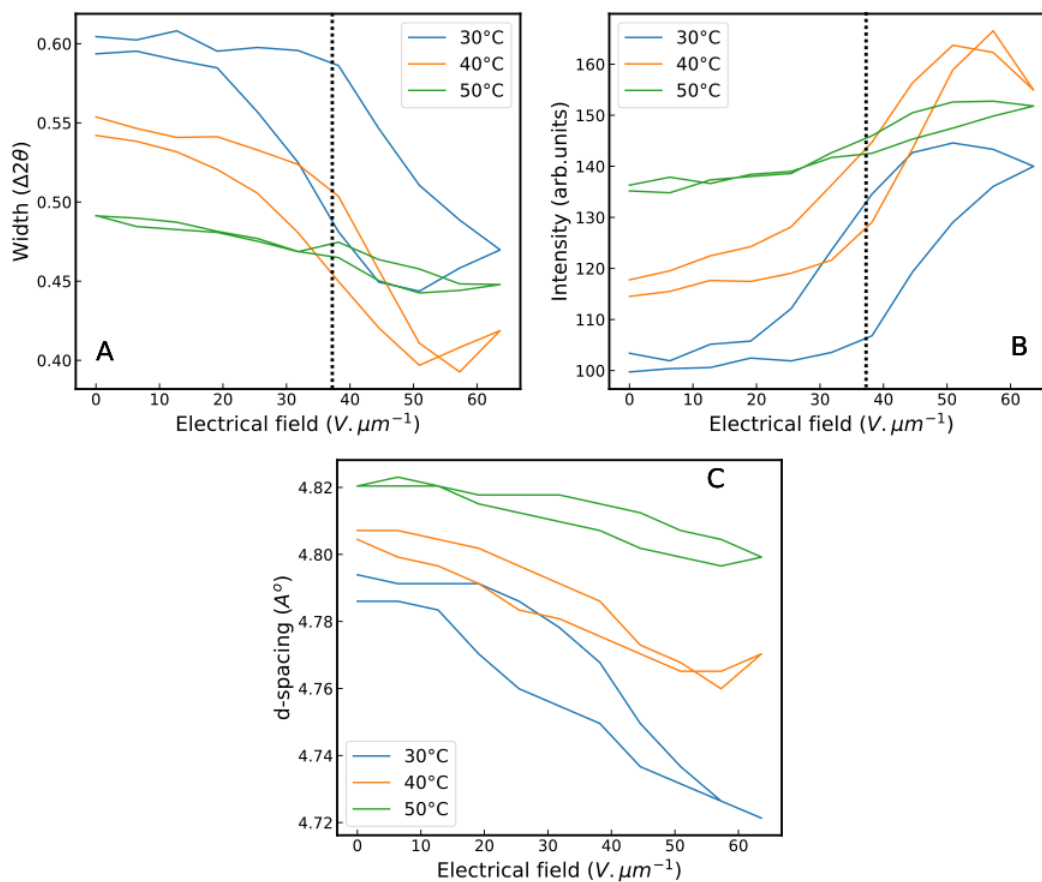


Figure 4.20: Electrical study performed at different temperatures. A: d-spacing versus electrical field B: diffraction peak width. C: diffraction peak intensity

Fig 4.20 A displays the peak width versus electrical field at 30°C, 40°C, and 50°C. The abrupt thinning of the peak we associated to the crystallites rotation is still present at 30°C and 40°C although in the latter case the hysteresis appears to be smaller. At 50°C, above the Curie temperature, there is no sign of a similar phenomenon.

Fig 4.20 B displays the diffraction peak intensity. Width and intensity are correlated and the same observations as above can be made here. The crystals rotation occurs at 30°C and also at 40°C, albeit less hysteretic this time.

Panel 4.20 C displays the d-spacing values calculated from the diffraction peak positions.

This time we observe that at 40°C the strain is different from the 30°C response and is closer to the 50°C measurement. A possible explanation is that the (110) and (200) peaks are closer to one another and the jump from (110) to (200) does not affect the d-spacing much.

Two more pieces of information will help us draw a picture of the structural changes. Firstly, the phase transition seems to appear around the same electrical field value regardless of the temperature, as highlighted by the dotted line in figure 4.20. This means the RFE/PE polar ordering does not influence much the occurrence of this transition. Secondly, the hysteresis is reduced as the temperature increases which means the newly formed phase is less stable. The RFE/PE order might play a role in the FE phase stability.

Even completed with temperature measurements, this study does not allow us to conclude on the nature of the structural changes inside terpolymers. However, building on the current state of the art we can propose a phenomenological description that is consistent with the XRD data acquired so far. Figure 4.21 is based on the models of Yang & al and Bargain & al, presented in the state of the art section.

First we need a clear description of the symbols used in the terpolymers representation. The red and blue arrows are VDF-TrFE units, red arrows in the same direction represent trans conformations, resulting in a net dipolar moment. A blue and red arrow represent a gauche conformation induced by temperature. We drew the dipolar moments in an anti-ferroelectric 2D fashion for sake of simplicity. The actual form of gauche conformations is of little importance here and the relevant information is that the resulting dipolar moment is null. The green dots are pinning domains due to CTFE units. They also form gauche conformations with the neighbouring units and are different from the blue arrows because they are not due to temperature but to the presence of a chlorine atom. A succession of VDF-TrFE dipoles between two pinning units will be referred to as a sequence. The PE, RFE/PE and RFE phases were described with figure 4.13 and are represented in fig 4.21 upper right corner.

Now the question is how does the electrical field affect this dipole arrangement? In copolymers we saw that applying an electrical field was equivalent to cooling the material. Applied to terpolymers this would mean pushing the RFE/PE equilibrium toward a RFE phase. However, the notion of CTFE 'unpinning' is necessary because the RFE phase is not ferroelectric and the PE->RFE phase transition cannot explain alone a ferroelectric-like behaviour.

The description starts near ambient temperature, in an unbiased terpolymer sample: this is the representation **A-1**. To make the link with XRD data this temperature will be considered to be 30°C. The polymer is in RFE/PE phase and each sequence has a net dipolar moment. Still the RFE phase is not ferroelectric and thus the sequences are not oriented in the same direction. This is due to the pinning units which allow the sequences to rotate freely. In terms of XRD

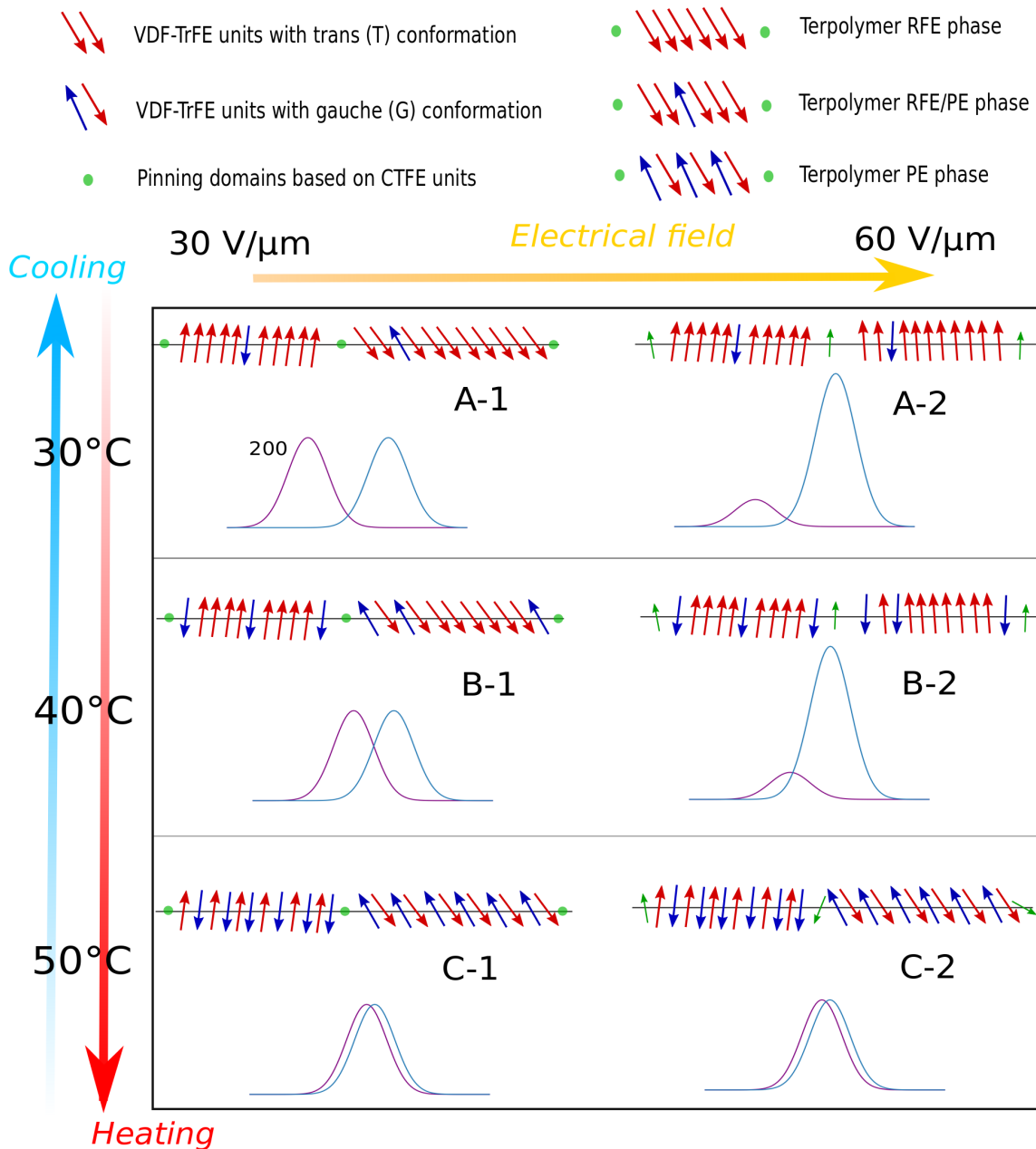


Figure 4.21: Description of structural changes in terpolymers with temperature and electrical field

patterns, the two diffraction peaks are slightly separated owing to the pseudo-hexagonal packing of RFE phase. We exaggerated the distance between the peaks to facilitate the reading.

Applying an electrical field above $30 \text{ V} \cdot \mu\text{m}^{-1}$ makes the terpolymer go to state **A-2**. Past that value, the electrical field starts to weaken the pinning applied by CTFE units. This allows the VDF-TrFE sequences to cooperate with one another, forming the terpolymer FE phase. This

conformation holds as long as the pinning domain are weak enough. Once the ferroelectric phase is formed, the local field seen by the pinning domains is not only the external field but also the contribution of neighboring, oriented, RFE/PE sequences. So even when the electrical field is decreased past the $30V.\mu m^{-1}$ mark, the pinning unit are kept in a weakened state by the ordered RFE/PE sequence (FE phase). This is at the origin of the hysteresis observed in terpolymers. Regarding the XRD spectra, we do not distinguish the phase transition but observe mostly the subsequent rotation of FE domains: the (110) peak increases while the (200) peak shrinks.

Removing the electrical field and increasing the temperature brings us to a state represented in **B-1**. The terpolymer is still in an RFE/PE phase but closer to the PE side. The average moment of each sequence is lower than in A-1. In terms of XRD pattern the proximity to PE phase means the (110) and (200) diffraction peaks are closer to one another.

The electrical field is increased once again past the $30 V.\mu m^{-1}$ mark and we get to the state **B-2**. The same thing happens as in A-2: the pinning effect weakens, the PE/RFE sequences cooperate and a ferroelectric order is achieved in the polymer chain. Once again, this order is lost as the electrical field returns to 0 and the pinning units regain their strength. However, the average contribution of FE order to the pinning units local field is lower this time. This is due to the smaller average moment of RFE/PE sequences and results in a less stable FE phase. This would explain why phase transition is still present but almost hysteresis free right below the Curie temperature. In terms of XRD patterns, the diffraction peak variations are similar to A-2 albeit less hysteretic, due to this less stable phase.

At $50^{\circ}C$, the terpolymer is in its PE state with no average dipolar moment in a VDF-TrFE sequence, as illustrated in **C-1**. At $30 V.\mu m^{-1}$ (**C-2**) the "unpinning" still occurs but as the terpolymer has achieved a PE order, there is no average moment that could force an alignment with the electrical field. The absence of ferroelectric domains means there are no rotations nor variation in the XRD pattern.

In this description we completely disregarded the reversal of thermal gauche conformations (blue arrows to red arrows) i.e the PE->RFE transition. If we make the parallel with copolymer it is likely to happen, at least to some extent. A good way to study that question would be completing the experiment with in-situ FTIR acquisitions. FTIR cannot detect changes in the crystal symmetry but it informs about conformation changes inside the polymer chain. That is pretty much the opposite of XRD and the two techniques are complementary. Conformation changes outside the phase transition range ($20-60 V\mu m^{-1}$) would be ascribed to thermal conformations i.e PE->RFE transition.

While the changes induced by an electrical field can be called a phase transition from an

electrostatic standpoint, they do not imply much of a structural evolution. We saw in the state of the art section how the transition from RFE to PE was a subtle change in terms of structure. Yet it was about half the terpolymer conformations changing from gauche to trans. Here it is only one conformation every dozen or so that requires transforming to change the phase from RFE/PE to FE. In terms of structural change this should be barely noticeable.

4.6 Conclusion

In the previous chapter we observed non linearities in the electromechanical behaviour of PVDF-TrFE-CTFE, namely polarization hysteresis and increase in electrostrictive coefficient Q . Based on the literature, these oddities were ascribed to a field induced phase transition. The aim of this chapter was to ascertain the link between macroscopic and structural evolutions and to validate the terpolymer strain phenomenological description proposed previously. Then if possible, shed some light on the nature of this transition.

To better understand the impact of electrical field on XRD patterns we started our study with PVDF-TrFE copolymer, a well known material with a first order PE-FE transition. We reported direct evidence of the field-induced phase transition above the Curie temperature. Besides phase transition, two significant effects of electrical field were observed: electrostriction and orientation of crystalline domains. The main difficulty in interpret XRD data comes from the nature of the diffraction peak, a superposition of the (200) and (110) peaks. Unlike temperature variations and the thermal expansion it induces, the electrical field affects the (200) and (110) peaks differently, which can make the data interpretation delicate.

Moving on to the terpolymer, we observed a significant evolution of the diffraction patterns with the electrical field. From the diffraction peak position we calculated the strain in the crystalline phase and it turned out to be of the same order of magnitude as in the amorphous phase. The crystalline phase also appeared to be more affected by the nonlinearities in electrostriction than what we observed macroscopically. At last, we extracted from XRD data the variations in shape and intensity of the diffraction peak. Aside from a width discrepancy we ascribed to frequency effects, the XRD cycles matched the polarization and strain measurements. With these results we successfully tied the macroscopic nonlinearities to structural changes happening in the crystalline phase.

Going further required an interpretation of the functions used to fit the diffraction peaks. The first possibility is that each fitting peak corresponds to a crystalline phase and the XRD changes are direct evidence of a field induced phase transition. Another possibility is that the two peaks used for the fit correspond to the (110) and (200) diffraction planes of a single phase. In that case,

the XRD changes are due to the rotation of domains in the electrical field direction. The rotation hypothesis seems more plausible at this time as it explain some experimental oddities such as the thin diffraction peak of the FE phase. Either way, there must be a field-induced transition toward a ferroelectric phase happening at some point in terpolymers to explain the abrupt changes.

The terpolymer strain mechanism proposed in the previous chapter is validated by the in-situ experiments. It requires one minor correction: the variation of electrostrictive coefficient we ascribed to a difference in lattice parameter is more likely due to an orientation of crystallites, with the smaller b-lattice parameter in the thickness direction.

The electrical study was reproduced at higher temperatures, past the Curie point and we proposed a description of the field-induced phase transition to account at best for the XRD changes. The pinning effect introduced by Yang & al [16] can explain on its own the experimental observations. Ferroelectric phase appears when pinning domains lose their strength, due to the application of an electrical field. The RFE/PE order seems to govern the stability of the newly formed FE phase. It is possible a PE->RFE phase transition is also present but it would be a mild and second order effect. The notion of field-induced phase transition in terpolymers is relevant from an electrostatic standpoint but this is mostly due to domains rotation and the structural changes are likely to be very small.

Bibliography

- [1] Zhaoliang Cui, Naser Tavajohi Hassankiadeh, Yongbing Zhuang, Enrico Drioli, and Young Moo Lee. Crystalline polymorphism in poly(vinylidene fluoride) membranes. *Progress in Polymer Science*, 51:94 – 126, 2015. Environmentally Relevant and Hybrid Polymer Materials.
- [2] Yingying Lu, Jason Claude, Luis Enrique Norena-Franco, and Qing Wang. Structural Dependence of Phase Transition and Dielectric Relaxation in Ferroelectric Poly(vinylidene fluoride chlorotrifluoroethylene trifluoroethylene)s. *The Journal of Physical Chemistry B*, 112(34):10411–10416, August 2008.
- [3] Inseok Chae, Saad Ahmed, Hassene Ben Atitallah, Jiawei Luo, Qing Wang, Zoubeida Ounaies, and Seong H. Kim. Vibrational Sum Frequency Generation (SFG) Analysis of Ferroelectric Response of PVDF-Based Copolymer and Terpolymer. *Macromolecules*, 50(7):2838–2844, April 2017.
- [4] P. Martins, A. C. Lopes, and S. Lanceros-Mendez. Electroactive phases of poly(vinylidene fluoride): Determination, processing and applications. *Progress in Polymer Science*, 39(4):683–706, April 2014.

- [5] Ilias Katsouras, Kamal Asadi, Mengyuan Li, Tim B. van Driel, Kasper S. Kjaer, Dong Zhao, Thomas Lenz, Yun Gu, Paul W. M. Blom, Dragan Damjanovic, Martin M. Nielsen, and Dago M. de Leeuw. Supplementary informations: The negative piezoelectric effect of the ferroelectric polymer poly(vinylidene fluoride). *nature materials*, 2015.
- [6] Bellet-Amalric, E. and Legrand, J. F. Crystalline structures and phase transition of the ferroelectric p(vdf-trfe) copolymers, a neutron diffraction study. *Eur. Phys. J. B*, 3(2):225–236, 1998.
- [7] Duo Mao, Bruce E. Gnade, and Manuel A. Quevedo-Lopez. Ferroelectric properties and polarization switching kinetic of poly (vinylidene fluoride-trifluoroethylene) copolymer. In Mickaël Lallart, editor, *Ferroelectrics*, chapter 4. IntechOpen, Rijeka, 2011.
- [8] E. Bellet-Amalric and J.F. Legrand. Crystalline structures and phase transition of the ferroelectric p(vdf-trfe) copolymers, a neutron diffraction study. *The European Physical Journal B - Condensed Matter and Complex Systems*, 3(2):225–236, May 1998.
- [9] F.Bargain. Structure semi-cristalline et propriétés d’usage de films de copolymères fluoeres electroactifs: influence de la composition et de la mise en forme. *Thesis manuscript*, 2017.
- [10] A. J. Bur, J. D. Barnes, and K. J. Wahlstrand. A study of thermal depolarization of polyvinylidene fluoride using x-ray pole-figure observations. *Journal of Applied Physics*, 59(7):2345–2354, 1986.
- [11] Jin Kim Kap, Reynolds Nicholas M., and Ling Hsu Shaw. Spectroscopic studies on the effect of field strength upon the curie transition of a vdf/trfe copolymer. *Journal of Polymer Science Part B: Polymer Physics*, 31(11):1555–1566, 1993.
- [12] François Bargain, Pierre Panine, Fabrice Domingues Dos Santos, and Sylvie Tencé-Girault. From solvent-cast to annealed and poled poly(vdf-co-trfe) films: New insights on the defective ferroelectric phase. *Polymer*, 105:144 – 156, 2016. Structure and Dynamics of Polymers studied by X-ray, Neutron and Muon Scattering.
- [13] Weimin Xia, Zhuo Xu, Qiuping Zhang, Zhicheng Zhang, and Yuanqing Chen. Dependence of dielectric, ferroelectric, and piezoelectric properties on crystalline properties of p(VDF-co-TrFE) copolymers. *Journal of Polymer Science Part B: Polymer Physics*, 50(18):1271–1276, September 2012.
- [14] Haisheng Xu, Z.-Y. Cheng, Dana Olson, T. Mai, Q. M. Zhang, and G. Kavarnos. Ferroelectric and electromechanical properties of poly(vinylidene-fluoride–trifluoroethylene–chlorotrifluoroethylene) terpolymer. *Applied Physics Letters*, 78(16):2360–2362, April 2001.

- [15] Lianyun Yang, Brady A. Tyburski, Fabrice Domingues Dos Santos, Maya K. Endoh, Tadanori Koga, Daniel Huang, Yijun Wang, and Lei Zhu. Relaxor Ferroelectric Behavior from Strong Physical Pinning in a Poly(vinylidene fluoride-co-trifluoroethylene-co-chlorotrifluoroethylene) Random Terpolymer. *Macromolecules*, 47(22):8119–8125, November 2014.
- [16] Lianyun Yang, Xinyu Li, Elshad Allahyarov, Philip L. Taylor, Q. M. Zhang, and Lei Zhu. Novel polymer ferroelectric behavior via crystal isomorphism and the nanoconfinement effect. *Polymer*, 54(7):1709–1728, March 2013.
- [17] L.Yang. Novel ferroelectric behavior in poly(vinylidene fluoride-co trifluoroethylene) based random copolymers. *Thesis manuscript*, 2015.

Chapter 5

Discussion

The work presented so far can be divided into two main contributions. First, a comparative study on different P(VDF-TrFE-CTFE) terpolymers, to assess the impact of CTFE content on actuation performances. Building on this work, the comparison could be extended to other PVDF derivatives. We will present here a first series of measurements on a closely related polymer: P(VDF-TrFE-CFE).

The second part of our study was focused on understanding the origin of strain in terpolymers. There is still many work to be done on the subject and in this chapter some ideas and preliminary results for follow up experiments are presented.

5.1 Follow up work on P(VDF-TrFE-CTFE)

5.1.1 Φ scans

In the previous chapter we proposed that changes in XRD spectra arose from the rotation of crystallites and the (110) diffraction peak increasing as the (200) is shrinking. This can be verified experimentally by measuring different orientations, as illustrated in figure 5.1.

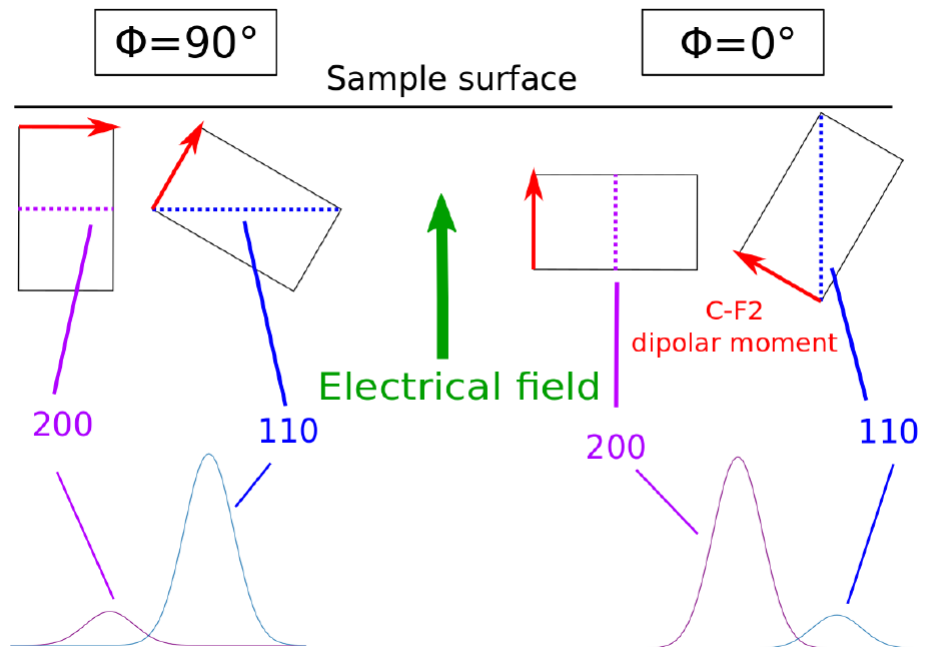


Figure 5.1: Schematic representation of the expected difference between a measurement at $\Phi = 0^\circ$ and $\Phi = 90^\circ$

In chapter 4, all XRD acquisitions were conducted with a $\Phi = 90^\circ$ value of 90° i.e all the crystallites contributing to the XRD spectra had their diffracting planes parallel to the sample

surface. At 0° on the other hand, the diffraction planes contributing to the XRD pattern are perpendicular to the surface. In order to measure at a different Φ angle the sample should be rotated as described in [1]. Whether at 0° or 90° , the terpolymers undergo the same variations due to electrical field but the domains we actually observe are different in each case. Figure 5.1 illustrates the crystalline orientations contributing to the XRD patterns: left is for $\Phi = 90^\circ$ and right for $\Phi = 0^\circ$.

With the application of an electrical field, the CF2 dipolar moments represented by red arrows align at best in the field direction. As discussed in chapter 4, at $\Phi = 90^\circ$ the population of crystallites with their (200) planes in Bragg's condition is depleted while the (110) population increases. The situation is different for the crystallites observed with $\Phi = 0^\circ$. The domains with their (200) diffraction planes in Bragg's condition have their dipolar moment oriented exactly in the electrical field direction. Therefore, when an electrical field is applied the (200) peak should grow in intensity at the expense of the (110) peak.

If our XRD interpretations are correct, measurements at $\Phi = 0^\circ$ should yield results opposed to the $\Phi = 90^\circ$ acquisitions. With this approach it should be possible to validate or disprove our XRD spectra interpretation from the previous chapter. Building on that, complete Φ scans with and without bias should allow to map the global orientation of dipoles inside the material. This approach would require at least some mathematical modeling and knowing the structure factors of the (200) and (110) diffraction planes. Mechanically stretching the samples beforehand could help setting a proper environment to make this experiment successful, as it was done in [1].

5.1.2 Clamping effect

An interesting possibility brought up by the XRD study is to locate the strain inside the material. In the previous chapter we did not go further than a qualitative comparison but with enough care it is possible to quantify the strain inside and outside the crystalline phase. To that end two issues must be addressed, the first one is to properly account for the different crystallites orientations in the material. The second issue, which is the one discussed here, is the substrate clamping.

The cantilevers were made with PEN as substrate and the samples used in XRD analysis were printed on glass. Ideally both mechanical and XRD measurements would have been performed on the same material. However, as mentioned in chapter 4 we did not use PEN for the XRD study because of the very high background signal it generates (fig 4.2). If we hope to compare the macroscopic strain to the XRD samples strain we need to assess how the glass clamping impacts our measurements. To that end we conducted two XRD studies, one on a sample with PEKK substrate and another with a sample printed onto glass. PEKK as a substrate does not hinder XRD interpretation and, because it is softer than glass, we should be able to see how the substrate

rigidity affects the strain measurements. The results are displayed in 5.2.

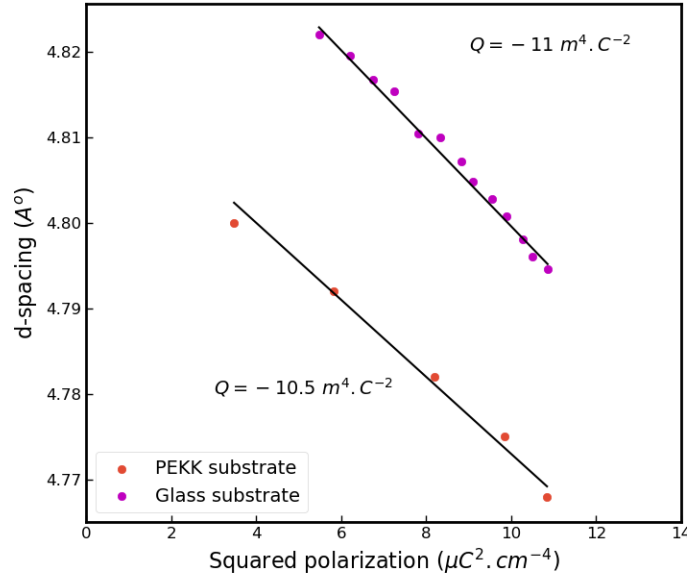


Figure 5.2: d-spacing with data from fig 4.14 as a function of squared polarization

In figure 5.2, the purple dots are the experimental values for the glass substrate and the red dots are for the PEKK substrate. Terpolymers are not piezoelectric but electrostrictive materials. That is why the d-spacing is plotted versus squared polarization. This allows for the extraction of an electrostrictive coefficient Q as per equation 3.9. The coefficients are identical in both cases and they reach values at $Q_{cryst} = 11m^4.C^{-2}$. This is of the same order as $Q_{macro} = 23m^4.C^{-2}$ extracted macroscopically in chapter 3, but as mentioned above the quantitative comparison between Q_{macro} and Q_{cryst} cannot be conducted yet.

It appears that the d-spacing values of both samples differ from 0.03\AA regardless of the electrical bias. This means that the substrate clamping affects the lattice dimensions during the fabrication process. However, it is not much of an issue because we are interested in the electrically induced variations (strain) and not in the absolute lattice parameters. As it turns out, the electrostrictive coefficients Q are almost identical in both cases. Therefore, the clamping does not affect the strain in the polymer thickness direction.

5.1.3 Macroscopic approach

To tackle the problem on different fronts, the understanding of strain can be studied from a macroscopic perspective. We briefly discussed in chapter 3 the notion of Maxwell stress and how

it is most likely contributing to strain in terpolymers. Despite its simple analytical expression, the influence of Maxwell strain is not quantified properly and varies from one study to another. A possible way to estimate its contribution would be to measure separately the electrostriction coefficient, free of the Maxwell effect. This can be done through capacitance measurements of a mechanically stressed sample, using equation 5.1 [2]. As there are no charged electrodes, the Maxwell strain is not present and only the other contributions are extracted.

$$Q_i = \frac{\partial(\frac{1}{\epsilon})}{\partial T} \quad (5.1)$$

Q_i = intrinsic electrostrictive coefficient
 ϵ permittivity
 T: Mechanical stress

We used equation 5.1 to get the intrinsic electrostrictive coefficient of a 2% CTFE terpolymer. The study was performed on a standard cantilever and fig 5.3 illustrates the measurement principle along with the results.

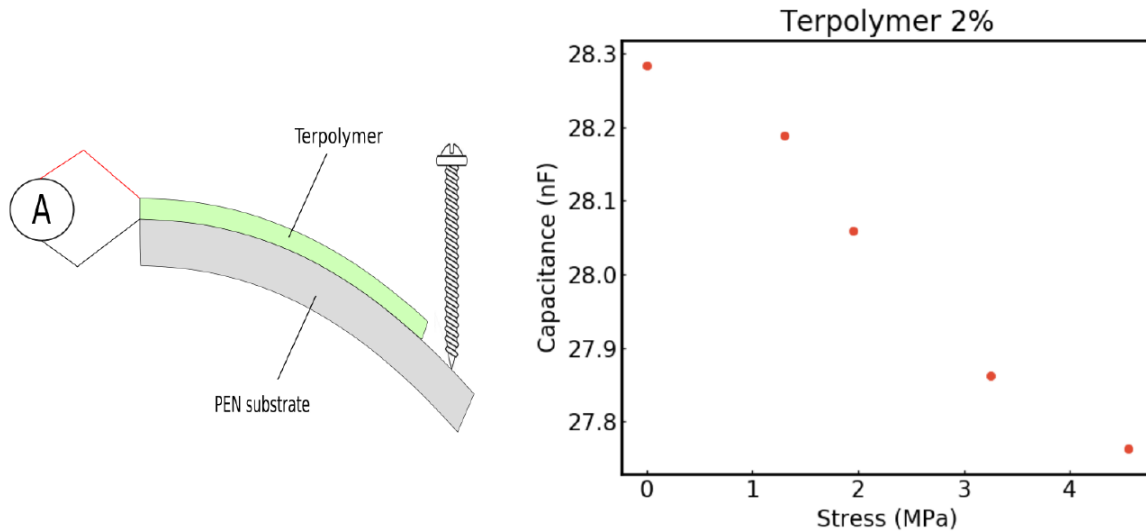


Figure 5.3: Capacitance measurements of a 2% CTFE terpolymer as a function of bending

Figure 5.3 left panel displays the measurement principle: the polymer is strained as the screw goes downward and the capacitance is measured at regular intervals. In order to estimate the terpolymer stress we assume that the cantilever bending is parabolic and consider an approximate value of 1 GPa for its Young's Modulus. The capacitance values versus terpolymer stress are reported in the right panel.

There is a significant dependence of the capacitance value to the applied stress. This is not a consequence of changes in the device geometry because a reduced thickness of the active layer would have resulted in an increase of the capacitance, not the other way around. Therefore we ascribe the capacitance variation to a change in permittivity and using equation 5.1, we get an intrinsic coefficient $Q_i \approx 6m^4.C^{-2}$. As the 2% CTFE terpolymer is a ferroelectric (cf chapter 2) material, a more meaningful value to characterize it is the piezoelectric coefficient. We calculate this intrinsic d_i using equation 3.13 which give a value of $-80.10^{-12}m.V^{-1}$ about twice as high as the actual piezoelectric coefficient.

Had the intrinsic d_i been lower than the one measured from electromechanical measurements, we could have ascribed the difference to Maxwell strain. Given the values we extracted, it is likely that the Maxwell contribution is negligible in 2% CTFE terpolymer. The higher intrinsic coefficient could have a physical significance or be the result of errors on the approximations we made of stress values. This is a preliminary experiment and a proper setup should apply a stress directly to avoid any uncertainty. We reproduced this experiment on a 8.3% CTFE terpolymer and the results are displayed in figure 5.4.

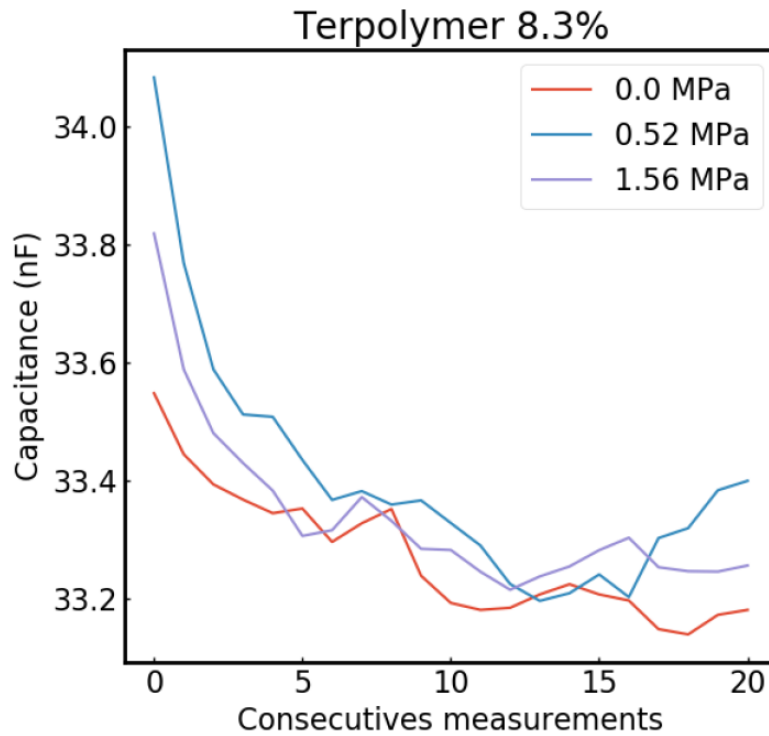


Figure 5.4: Capacitance measurements of a 2% CTFE terpolymer as a function of bending

As we can see in figure 5.4, the results obtained with 2% terpolymer could not be reproduced on the relaxor terpolymer because the capacitance measurements are not stable in time

(one acquisition every minute). Despite identical screw displacements, the stress values displayed in figure 5.4 are lower than in figure 5.3 because of the reduced rigidity of the 8.3% CTFE terpolymer. However, the coefficient Q is supposed to be higher and therefore we expected to see the same stress induced change. Although the variations are supposed to be of the same order as in the 2% terpolymer, it is difficult to extract any value because of the measurement instability.

The lack of significant variations could be interpreted as a dominant contribution of Maxwell strain, but drawing any definitive conclusion would require a properly calibrated setup, as we mentioned before. Regarding the temporal dependence of capacitance measurements, a solution could be to apply a periodic solicitation coupled with a Fourier analysis to isolate the effect of stress.

5.2 Other polymers

This study was focused on P(VDF-TrFE-CTFE), its performances as actuator and its electromechanical behavior. However, it is only one PVDF derivatives among numerous others. With the groundwork and characterization protocol already laid out in this study, another direction to pursue could be extending the comparison to different polymers.

The first material coming to mind is P(VDF-TrFE-CFE) whose structure is close to that of our terpolymers. Furthermore the state of the art is very similar to that P(VDF-TrFE-CTFE): - It is also used in actuation devices [3] or patents [4] with little regard to its performances compared to other compositions and polymers.

- Its electrical properties are well documented but the reports on its strain cycles are scarcer, especially for low CFE contents.
- The understanding of strain mechanisms is not fully understood and a conformation change is expected to play a significant role.

Figure 5.5 displays the comparison between 60.4/30.5/9.1% (VDF/TrFE/CFE) and 61.4/30.3/8.3% (VDF/TrFE/CTFE) terpolymers.

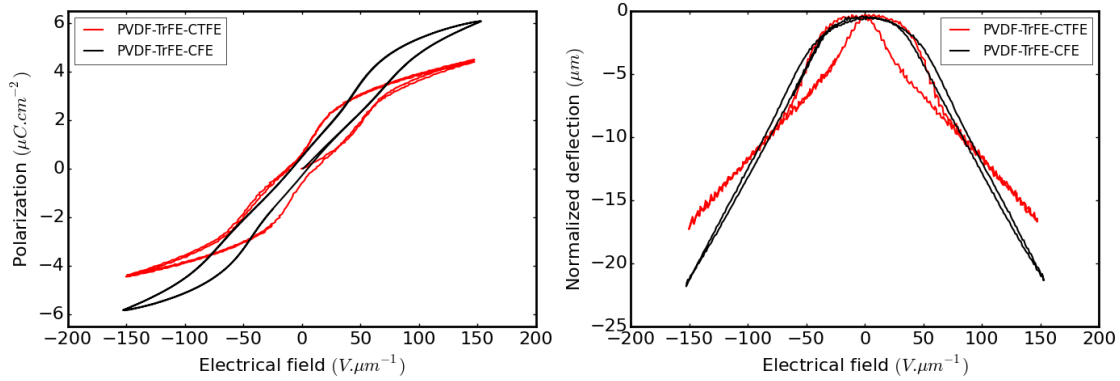


Figure 5.5: Comparison between two terpolymers, 60.4/30.5/9.1% (VDF/TrFE/CFE) and 61.4/30.3/8.3% (VDF/TrFE/CTFE). Left: Polarization cycle. Right: Strain cycle

Figure 5.5 left panel displays polarization cycles up to $150 MV.m^{-1}$. The CFE terpolymer reaches higher polarization values than the CTFE one, respectively $6\mu C.cm^{-2}$ and $4.5\mu C.cm^{-2}$. The cycle opening in CFE appears at higher fields and seems to be milder than with CTFE. This is also visible in the right panel with the strain hysteresis. An educated guess based on the conclusions from the previous chapter would be that a field induced phase transition also occurs in CFE terpolymer, but more gradually.

At high electrical fields the CFE terpolymer generates more stress than CTFE. If the conclusions from chapter 2 also apply to CFE, an intermediary composition with 4-5% CFE should perform even better. This is just an exemple but there are countless other PVDF derivatives, blends and composites.

5.3 Conclusion

Over the course of this work we shed some lights on the strain mechanisms of P(VDF-TrFE/CTFE). There are still many unknowns mechanisms and several paths can be pursued building on this study. First, the XRD acquisition could be continued with different Φ values to try and characterize the crystallites orientations. This would allow to check the validity of previous assumptions and help building a model of strain. The same goal can be tackled on a different front with an analysis of the intrinsic electrostriction. The equations of thermodynamic links the variation of permittivity versus stress to the electrostrictive coefficient M . This variation does not take into account mechanisms such as Maxwell strain and this separation can bring insightful information. On a different topic, the analyzes conducted on P(VDF-TrFE-CTFE) could be reproduced on similar materials, taking advantage of the framework provided here. A good starting point would be P(VDF-TrFE-CFE) a closely related polymer.

Bibliography

- [1] A. J. Bur, J. D. Barnes, and K. J. Wahlstrand, "A study of thermal depolarization of polyvinylidene fluoride using x-ray pole-figure observations," *Journal of Applied Physics*, vol. 59, no. 7, pp. 2345–2354, 1986.
- [2] T. Shaw, "The effect of stress on the dielectric properties of barium strontium titanate thin films," *Appl. Phys. Lett*, 1999.
- [3] L. Engel, S. Kruk, J. Shklovsky, Y. Shacham-Diamand, and S. Krylov, "A study toward the development of an electromechanical poly(vinylidene fluoride–trifluoroethylene–chlorofluoroethylene) buckling membrane actuator," *Journal of Micromechanics and Microengineering*, vol. 24, p. 125027, Dec. 2014.
- [4] F. Hakkens, "Deformable ultrasound array and system abstract."

General Conclusion

The first objective of this work was to assess the performances of P(VDF-TrFE-CTFE) terpolymers to act as active layer in thin film actuators. For this application the two figures of merit selected were the actuators deflection and the electromechanical coupling. These two quantities relate directly to the terpolymers stress and polarization response. The terpolymers with an intermediate CTFE ratio ($\approx 5\%$) turn out to be the best performing in terms of stress, 30% superior to copolymer at $100 \text{ V}\cdot\mu\text{m}^{-1}$. Regardless of the CTFE content, terpolymers coupling efficiency is about half that of copolymer. Therefore, the choice of a specific composition depend on the prioritizing order between performance and energy cost.

The necessity to perform such tedious characterizations come from the non-linear relationship between strain and electrical field (or squared electrical field). Because of it, P(VDF-TrFE-CTFE) cannot be simply characterized by a set of electromechanical coefficients. To evaluate the relevance of electrostrictive formalism applied to PVDF derivatives we studied the link between electrical field, polarization and strain. This study allowed us to propose a model of strain in terpolymers, accounting for both the changes in polarization and electrostrictive coefficient. As for the physical origin of the non-linearities, a likely candidate suggested by the literature was a field induced phase transition. parler copo

In order to correlate the electromechanical oddities to structural changes, we conducted in-situ XRD measurements on electrically biased samples. The electrical field has different effects on the XRD spectra such as domain orientation, lattice strain and phase transition. The first measurements were performed on copolymer where these effects could be isolated and discussed. We observed directly the presence of a field induced transition toward the ferroelectric phase past the Curie temperature.

The XRD interpretation out to be a more complex task in terpolymer were the different contributions were entangled. There is an ambiguity on the origin of pattern variations in terpolymer: whether we observe a conformation change toward a ferroelectric phase or a texturation effect due to the rotation of said phase. Still, the electromechanical changes are visible in the structure evolution, confirming that the crystalline phase is at the origin of macroscopic non-linearities.

There is still much to be done before fully understanding the origin of strain in PVDF-TrFE-CTFE. The possibilities brought by XRD measurements alone were barely exploited and should provide many other insightful results. Building on this study, another path to pursue could be extending the comparison of actuation performances to similar PVDF-TrFE derivatives, such as PVDF-TrFE-CFE.

Annex I: Vibration at higher frequencies

A major issue faced in our study was the actuation frequency limitation. Figure 1 illustrate that problematic with the comparison between a deflection at 1.5 Hz and at 12 Hz.

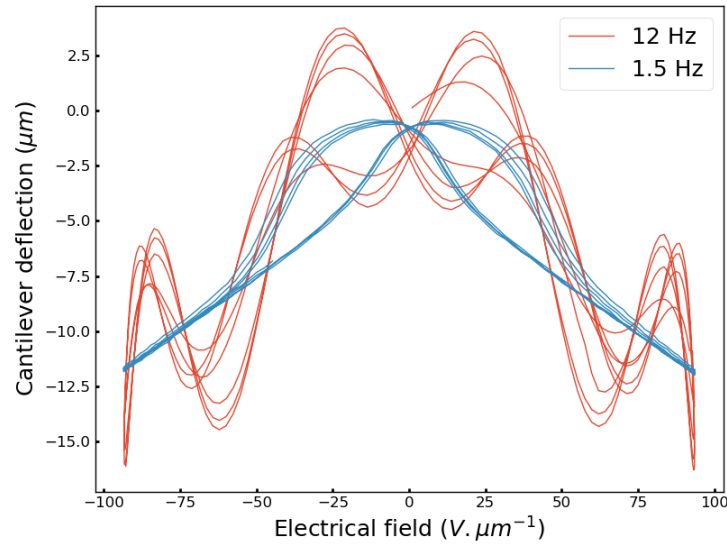


Figure 1: Deflection measurements of a cantilever at 12Hz and 1.5Hz

We observed cleaner modes with the synchrotron beamline interferometer, figure 2 . The sample was glued onto a glass substrate so we could measure the deformation properly up to 50 Hz. Above that value, new modes started to appear.

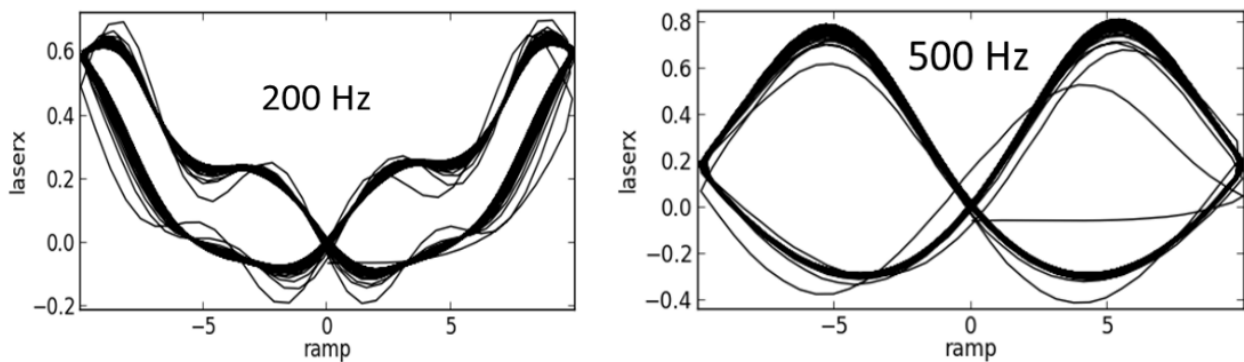


Figure 2: Deflection measurements at 200 and 500Hz of a glued round capacitance, measured with an interferometer

Annex II: Capacitance measurements in temperatures

This section presents the capacitance measurements made at high temperatures and used to discuss figures 3.19 and 3.26.

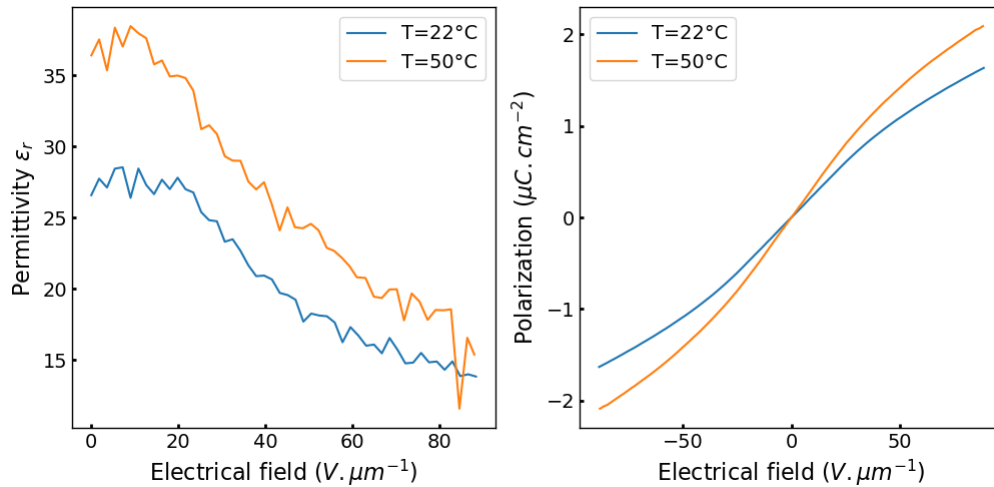


Figure 3: Capacitance measurements of the sample studied in figure 3.19

Figure 3 displays the capacitance measurements versus electrical field of the sample whose polarization cycles at $22^\circ C$ and $50^\circ C$ were compared. The difference between the two cycles was ascribed to the anti-ferroelectric cycle of phase transition but that cycle was somewhat tilted. This is due to the slightly higher dielectric polarisation at $50^\circ C$. Figure 4 displays the capacitance measurements we used to calculate the dielectric polarization in figure 3.26. Whether above or below the Curie temperature, the dependence of capacitance to the electrical field remains similar.

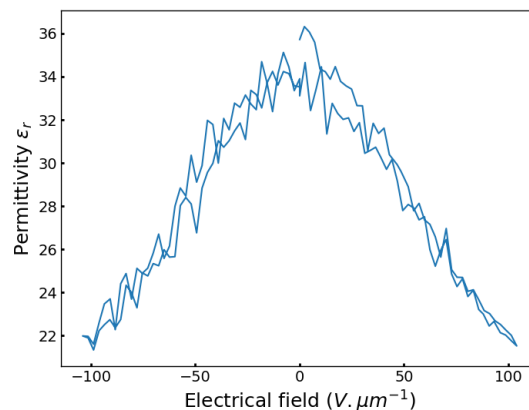


Figure 4: Capacitance measurements of the sample studied in figure 3.26

Annex III: Optical setup

The Bragg Brentano configuration is represented figure 5. The incident beam coming onto the substrate is not exactly parallel, which allows to scan a larger portion of the sample and get a more intense diffraction peak.

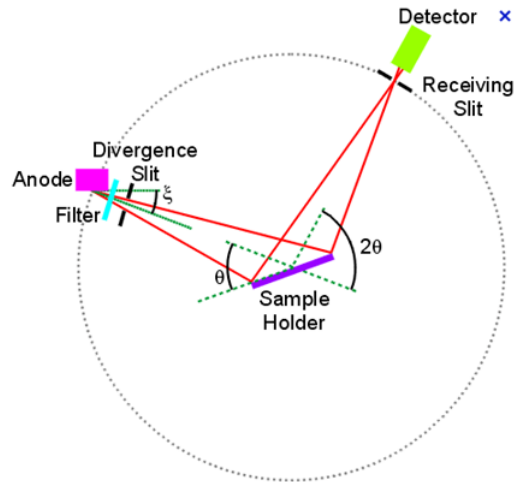


Figure 5: Bragg Brentano measurement principle

This optical configuration introduces an angular error as the incident θ value is not constant. This is corrected by the refocalization of the diffracted beam right on the detector. For that to function, the detector must be placed symmetrically to the tube with regard to the sample. That means the Φ angle defined in chapter has to be worth 90° and only the diffraction planes parallel to the sample surface can be acquired. In order to perform scans at $\Phi = 0^\circ$ as represented in figure 5.1, a different configuration has to be used (fig 6).

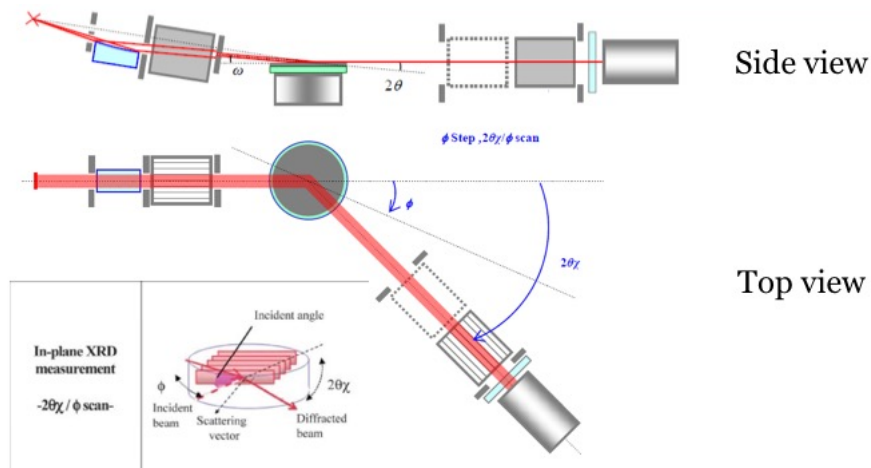


Figure 6: In plane measurements optical setup

Annex IV: XRD cycles and fitting algorithm

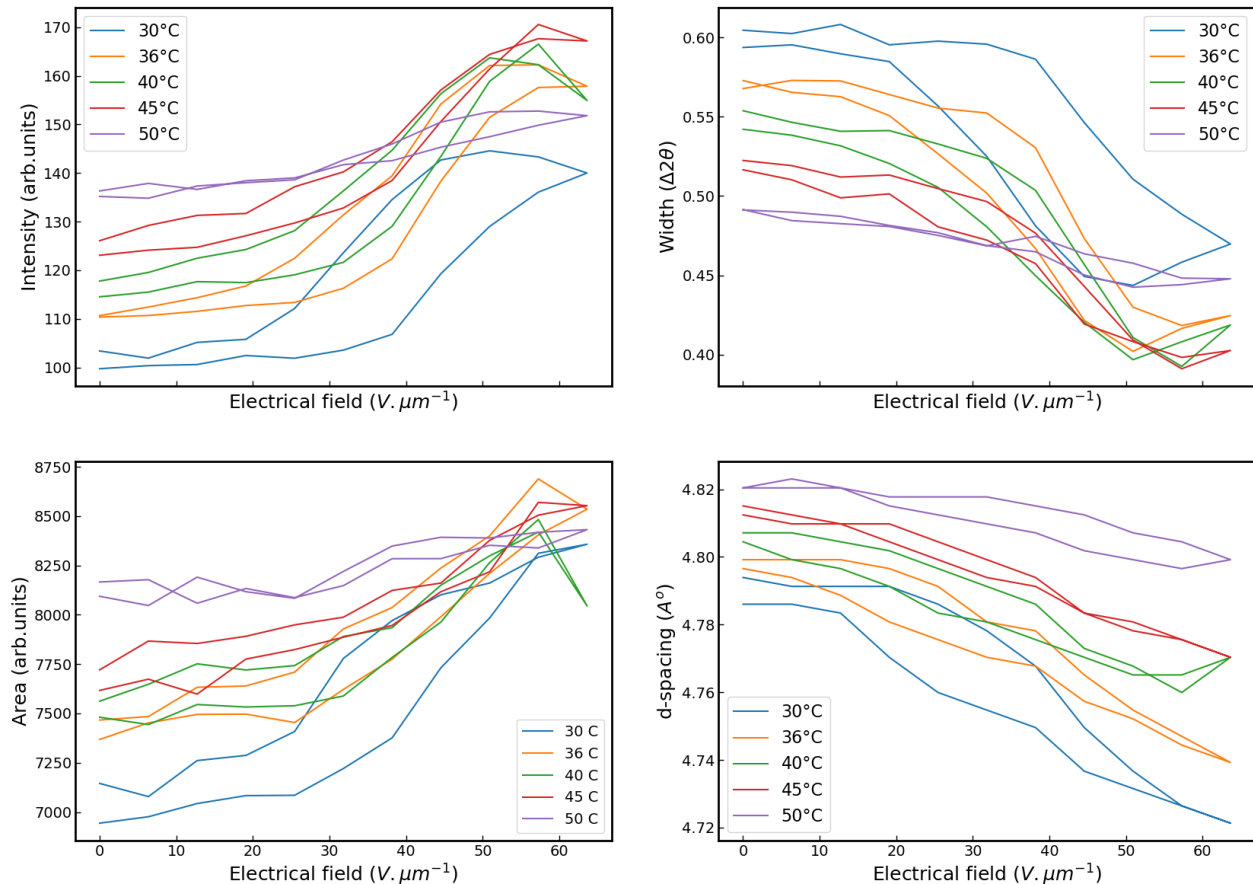


Figure 7: Complete dataset of the XRD temperature study. The 4 figures are the diffraction peak parameters: intensity, width, are and position.

Figure 7 displays the complete dataset of the temperature study from chapter 4. These are not the raw measurements but the diffraction peaks width, intensity, position and area. To obtain these values we used the python script hereafter.

Here are a few remarks on this code. It allow to perform an unlimited number of fits on a single run. The core function with the parameterized fitting algorithm comes from the minimize function of the lmfit package (Newville & al <http://doi.org/10.5281/zenodo.11813>). The data must be imported as two list of float for position and intensity, the function `getxrdml` is used to transform our xrdml files into floats. Only the function 1 and 3 are parameterized, 2 and 4 get their entry values from them. They account for the ka2 ray of copper.

```
from XRDML import getxrdml_scan
from lmfit import minimize, Parameters, Parameter, report_fit
```

```

from numpy import exp,sqrt,degrees,radians,sin,cos,pi,log10
import numpy as np

# ExtractPeak function
def ExtractPeak(x,y, a1,a2 , mod = 'absolute'):
    '''
    v0.3: N.V. 03-07-2015 -- extract peak from a 2 col (x,y)
    To D0 : mod relative, exception (too large scan in R mod...)
    -----
    Arguments
    x,y .....input np.array i.e. (2theta, I)
    a1,a2 .....(min, max) if mod = absolute (mod by default)
    a1,a2 .....(pos,R) if mod = relative
    '''
    if mod == 'relative':
        Resolution = x[1] - x[0] # regular step supposed
        i0 = int(np.floor( (a1 - x[0])/Resolution ))
        ii = int(np.floor(a2/(2.*Resolution) ))
        xp = x[i0-ii:i0+ii]
        yp = y[i0-ii:i0+ii]
        return (xp,yp)
    if mod == 'absolute':
        X = []
        Y = []
        for i in range(len(x)):
            if x[i]>a1 and x[i]<a2:
                X.append(x[i])
                Y.append(y[i])
        return (np.array(X),np.array(Y))

# ###
# Model
def PV(p,x):
    '''
    Pseudo-Voigt with eta(gaussian weight) = 0.5 without linear background
    - -----
    Arguments
    p = (a1,x01,fw1)
    '''
    v = abs(p[0]) * (0.5*np.exp(-(x-p[1])**2/((p[2]**2/(4*np.log(2)))))+
0.5*(1 / (((x-p[1])**2/(p[2]/2)**2) + 1 )))
    return v

def fcn2min(params, x, data):
    """ model 2 PV + Ka1,Ka2"""
    v = params.valuesdict()
    model = PV((v['amp1'],v['cen1'],v['fwhm1']),x) + PV((v['amp2'], v['cen2'],v['fwhm2']),x) + \
        PV((v['amp3'],v['cen3'],v['fwhm3']),x) + PV((v['amp4'], v['cen4'],v['fwhm4']),x) + \
        v['slope']*x+ v['background']
    return model - data

```

```

def MyModel(params,x):
    v = params.valuesdict()
    model = PV((v['amp1'],v['cen1'],v['fwhm1']),x) + PV((v['amp2'], v['cen2'],v['fwhm2']),x)+ \
        PV((v['amp3'],v['cen3'],v['fwhm3']),x) + PV((v['amp4'], v['cen4'],v['fwhm4']),x) + \
        v['slope']*x+ v['background']
    return model

v1 = np.arange(0,200,20)
v2 = np.arange(200,-20,-20)
Bias = np.concatenate((v1,v2))

temperature=30
nsave = 'terpo'+str(temperature)+'.txt'

Results = []

for ID in range(21):
    p = Parameters()
    #Only 1 and 3 need to be parmetrized, 2 and 4 are automatically rewritten as their Ka2 peaks
    #      (Name, Value, Vary, Min, Max, Expr)
    #      (Name, Value, Vary, Min, Max, Expr)
    p.add_many(('amp1' , 20 , True,6 , None, None),
               ('cen1' , 18.4 , True , 18.2, None, None),
               ('fwhm1', 0.36 , True, 0.3, 0.5, None),

               ('amp2' , 20 , True, None, None, '(amp1/2)'),
               ('cen2' , 18.4 , True, None, None,
                '2*degrees(arcsin(1.0024847494284688*sin(radians(cen1/2))))'),
               ('fwhm2', 0.3 , True, None, None,
                'fwhm1*1.0024847494284688*cos(radians(cen1/2))/cos(radians(cen2/2))'),

               ('amp3' , 40 , True, 6, None, None ),
               ('cen3' , 17.7 , True, 17.5, None, None ),
               ('fwhm3', 0.33 , True, 0.3, 0.5, None),

               ('amp4' , 10 , True, None, None, '(amp3/2)'),
               ('cen4' , 18.6 , True, None, None,
                '2*degrees(arcsin(1.0024847494284688*sin(radians(cen3/2))))'),
               ('fwhm4', 0.5 , True, None, None,
                'fwhm3*1.0024847494284688*cos(radians(cen3/2))/cos(radians(cen4/2))'),

               ('slope', -5, True, -6,-1, None),
               ('background', 262, True, None, None, None)
    )

    #Get experimental daa
    name = 'F:\\manuscrit\\data\\c4\\terpo temperature v2\\data\\'+str(temperature)+'-'+str(ID+1)+'.xrdml'
    bias=Bias[ID]
    x0,y0 = getxrdml_scan(name)

```

```
x,y = ExtractPeak(x0,y0,x0.min(),x0.max())

# do fit, here with leastsq model
result = minimize(fcn2min, p, args=(x, y))

p = result.params

# store results: amplitude, position and width of the PV functions.
# 1 and 3 are the fitting function,
# 2 and 4 are just the corresponding Ka2 peaks
tmpresults = [bias,p['amp1'].value, p['cen1'].value,p['fwhm1'].value,p['amp2'].value,
p['cen2'].value,p['fwhm2'].value,p['amp3'].value,p['cen3'].value,p['fwhm3'].value,
p['amp4'].value,p['cen4'].value,p['fwhm4'].value]
Results.append(tmpresults)

plt.show()

np.savetxt(nsave,np.array(Results),fmt='%.6f',header = '')
```